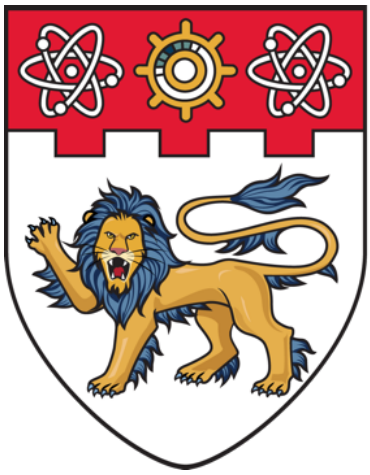

NANYANG TECHNOLOGICAL UNIVERSITY

SINGAPORE

MATHEMATICAL MODELLING OF BACTERIAL QUORUM SENSING AND BIOFILM EXTRACELLULAR POLYMERIC SUBSTANCES

ZHANG CHAODONG

INTERDISCIPLINARY GRADUATE SCHOOL

2017

MATHEMATICAL MODELLING OF BACTERIAL QS AND BIOFILM EPS ZHANG CHAODONG 2017

MATHEMATICAL MODELLING OF BACTERIAL QUORUM SENSING AND BIOFILM EXTRACELLULAR POLYMERIC SUBSTANCES

ZHANG CHAODONG

Interdisciplinary Graduate School
Nanyang Environment and Water Research
Institute @ NTU(NEWRI)

A thesis submitted to the Nanyang Technological University in partial fulfilment of the requirement for the degree of Doctor of Philosophy

2017

Acknowledgement

Firstly, I sincerely thank my main supervisor Prof. Yang Liang. We had many discussions on QS inhibition and population dynamics in biofilms. I have benefited a lot from his deep knowledge in microbiology, his support, feedback and encouragement. I would thank my co-supervisor Prof. Tan Soon Keat too, for his guidance to see the big picture, kind and effective support at my difficult times. My thanks also go to my mentor Prof. Liu Yu, who always gave valuable comments and suggestions during all my TAC meetings. My gratitude also goes to Prof. Su Haibin, without whom this thesis would not be possible. I also thank Ms July Fong for experimental validation of modelling results.

Secondly, I would like to thank Prof. Richard Webster, Prof. William Chen, IGS and NEWRI administrators Ellen and Hera for their kind support. I would also like to thank school of IGS, NTU and NEWRI institute for providing me research scholarships. They provide a platform for students and staffs to interact and share their research experience.

Last but not least, I would like to thank Dr. Aaron Bramson for his support of ABM models, technique help of netlogo and his suggestion to quantify space arrangement in biofilm. I would also like to thank Dr. Betty Fan and Dr. Zhang Ying for their guidance to help me present my research in written form. My gratitude also goes to my friends for sharing happiness and encouragement during my PhD study.

Contents

1 Introduction **17**

1.1 Background 17

1.2 Objectives 19

1.3 Overview 20

2 Literature Review **23**

2.1 Bacterial quorum sensing and biofilm EPS are critical in membrane biofouling 23

2.2 Biofilms and EPS 26

2.2.1 Biofilms, their development processes and impacts 26

2.2.2 Extracellular polymeric substances 29

2.2.3 EPS-regulated bacteria cooperation and aggregation in biofilms 30

2.2.4 Biofilm models 32

2.3 Bacterial quorum sensing 41

2.3.1 Architectures of bacterial QS 41

2.3.2 Parameters of QS network are mostly unknown and they are heterogeneous 44

2.3.3 QS inhibition by quorum quenching enzymes and quorum sensing inhibitors 46

2.3.4 Deterministic and stochastic models of cellular network . . 48

2.4 Quorum Sensing Models 51

2.5 Concluding remarks 53

3 Distinct QS network response topologies in parameter space and noise caused by parameter heterogeneity 55

3.1 Introduction 55

3.1.1 Quorum sensing network structure is well studied, but the kinetic parameters remain mostly unknown 55

3.1.2 QS network kinetic parameter values are heterogeneous among individual cells 59

3.2 Methods 60

3.2.1 Exploring *V.fischeri* QS network response in parameter space 60

3.2.2 Noise and QS switching behaviour by parameter heterogeneity 62

3.3 Results and Discussions 65

3.3.1 *V.fischeri* QS network baseline parameter values are fitted by experimental data from literature 65

3.3.2 QS network response curve topology is dependent on interaction strength 68

3.3.3 Noise by parameter heterogeneity is less than intrinsic noise when network is repressed, and greater than intrinsic noise when expressed 73

3.3.4 Parameter heterogeneity contributes significantly to QS network switching on threshold and time variation 76

3.4 Concluding remarks 80

4 Synergistic effects of quorum quenching enzyme and competitive binding quorum sensing inhibitor in inhibting *P.aeruginosa* QS circuit 83

4.1 Introduction 83

4.2 Materials and methods 86

4.2.1 las circuit 87

4.2.2 Quantify competitiveness of QSI to natural AHL 90

4.2.3 las and rhl circuits 91

4.3 Results 93

4.3.1 Vfr increased turning on speed of QS 93

4.3.2 Either QQ or QSI only could inhibit quorum sensing with low efficiency 94

4.3.3 Synergistic effects of combining QQ and QSI in inhibiting quorum sensing 95

4.3.4 G1 inhibits mutant with only rhl system more effectively than mutant with only las system 98

4.4 Discussions 101

4.5 Concluding remarks 102

5 Synergy of quorum quenching enzyme and ajoene analogue in inhibting *P.aeruginosa* quorum sensing 103

5.1 Introduction 103

5.2 Materials and Methods 105

5.3 Results and Discussions 108

5.3.1 Synergy of QQ and ajoene analogue in inhibiting las circuit 108

5.3.2 Synergy of QQ and ajoene analogue in inhibiting rhl circuit 109

5.4 Experimental proof of synergy between AiiA and ajoene analogues in inhibiting las circuit 111

5.5 Concluding remarks 112

6 Population dynamics of small colony variants in *Pseudomonas aeruginosa* biofilms 113

6.1 Introduction 113

6.2 Methods 116

6.3 Results 120

6.3.1 Substrate gradients in biofilm 120

6.3.2 Experimental morphology of Psl+Pel- and Psl-Pel+ reproduced by model 123

6.3.3 Psl++ mutant tends to aggregate when mixed with PAO1 . . 124

6.3.4 Percentage of Psl++ first increases and then decreases when mixed with PAO1 124

6.3.5 PAO1 out-competes Psl-Pel++ 127

6.4 Discussions 128

6.4.1 Incorporation of Psl and Pel in ABM biofilm model 128

6.4.2 Surface roughness produced by model are strongly dependent on shoving algorithm 129

6.4.3 Shear and erosion detachments contribute differentially to biofilm morphology and percentage of Psl++ mutant 129

6.5 Concluding remarks 131

7 Conclusion and future works **133**

7.1 Concluding remarks 133

7.2 Recommendation for future work 135

List of Figures

2.1 Biofilm development process 27

2.2 A general framework of mathematical biofilm models 34

2.3 Quorum Sensing network of *Vibrio fischeri* 44

2.4 Single and multiple stationary states of a one-component feedback loop 49

2.5 Stochastic single gene expression modeling results 50

3.1 The response curve of stationary P to outracellular AHL concentration A_e of *V.fischeri* quorum sensing network 67

3.2 $f(P)$ to P for different parameter sets 70

3.3 Relative fold changes of parameter sets 71

3.4 Single gene expression network 74

3.5 Comparison of population level protein Fanto Ratio and mRNA burst size with parameter heterogeneity 75

3.6 Distribution of *V.fisheri* Quorum Sensing network switch on threshold (A_T) 77

3.7 Normalized sensitivity indexes of each parameters used in *V.fisheri* quorum sensing network 79

3.8 Switching behaviors of deterministic and stochastic models of *V.fischeri* QS network 79

4.1 *P.aeruginosa* LasR/I QS circuit with QQ and QSI indicated in red. Dotted lines indicate the reactants still remains after the reactions, and solid lines indicate the reactants will disappear after the reactions. 86

4.2 Normalized GFP to G1 and AHL concentrations in *E.coli* lasB-gfp strain (from reference [1]). 90

4.3 *P.aeruginosa* network structure with both las and rhl circuits. 92

4.4 Time series concentration of LasR-AHL at different Vfr concentrations. V is the concentration of Vfr; $1-e^{-\beta V}$ is the probability that Vfr is bound to the promoter region of lasR gene. 94

4.5 QS dynamics when only QQ or QSI is added. (A): Simulation results of stationary AHL concentration to $\eta(QQ)$. (B): Simulation results of stationary AHL concentration to QI. (C): Experimental time series GFP adding only AiiA. (D): Experimental time series GFP adding only G1. 95

4.6 QS dynamics when QQ and QSI are combined. (A): Simulation results of stationary AHL concentration to $\eta(QQ)$ under different QI concentrations. (B): Simulation results of stationary AHL concentration to QSI concentration, with $\eta(QQ)$ assigned to different values. (C): Experimental time series GFP with $32\mu g/ml$ AiiA and different concentrations of G1 added. (D): Experimental time series GFP with $16\mu g/ml$ AiiA and different concentrations of G1 added. Cell volume fraction $\rho = 0.3$ for both (A) and (B). 97

4.7 Simulation QS states to QQ and QSI. (A): 3D stationary AHL concentration to $\eta(QQ)$ and SQI. (B): 2D map of QS on and off states to $\eta(QQ)$ and QSI. 97

4.8 Concentrations of lasR and rhlR mRNA in PAO1 and ΔlasR mutant to G1. r_1 represents lasR mRNA; r_2 represents rhlR mRNA; k_{RG1} and k_{RG2} represent the binding rates of G1 to LasR and RhlR proteins, indicating the inhibition effects of G1 to the two systems, respectively. (A): When G1 inhibits las system more effectively, G1 inhibits rhl system similarly in PAO1 and ΔlasR . (B): When G1 inhibits rhl system similarly as las system, G1 will inhibit rhl system a bit more effectively in ΔlasR than in PAO1. (C): When G1 inhibits rhl system more effectively, G1 will inhibit rhl more effectively in ΔlasR than in PAO1. 99

4.9 Concentration of lasR and rhlR mRNA in PAO1 and ΔlasR mutant to G1, when assuming the transcription rates of rhlR and rhlI is half the rates of lasR and lasI, respectively. 99

4.10 A simple logic OR gate model to describe the inhibition effects of G1 to las and rhl systems. 100

4.11 Experimental results showing that G1 has higher inhibition on system rhl than las in mutants with only respective system. (A) lasB-GFP of ΔlasIΔrhlI adding AHL. (B)lasB-GFP of ΔlasIΔrhlI adding AHL and G1. (C)rhlA-GFP of ΔlasIΔrhlI adding BHL. (D) rhlA-GFP of ΔlasIΔrhlI adding BHL and G1. 101

5.1 las and rhl QS circuits of *P.aeruginosa* with QQ and Ajoene analogue. 105

5.2 AHL concentration to $\eta_1(QQ)$ or Ajoene analogue (J) alone. 108

5.3 QS states of lasR/I circuit in *P.aeruginosa* to QQ and Ajoene analogue concentrations. (A) AHL concentration to $\eta_1(QQ)$ at different. (B) AHL concentration to J at different $\eta_1(QQ)$ values. (C) 3D plot of AHL concentration to $\eta_1(QQ)$ and J. (D) 2D on and off states to $\eta_1(QQ)$ and J. 109

5.4 QS states of rhlR/I circuit in *P.aeruginosa* to QQ and Ajoene analogue concentrations. (A) BHL concentration to $\eta_2(QQ)$ at different. (B) BHL concentration to J at different $\eta_2(QQ)$ values. (C) 3D plot of BHL concentration to $\eta_2(QQ)$ and J. (D) 2D on and off states to $\eta_2(QQ)$ and J. 110

5.5 Inhibition effect of using QQ alone or ajoene analogues alone. (A): LasR-GFP to time at different AiiA concentrations. (B) LasR-GFP to time at different ajoene analogue H9 concentrations. (C): LasR-GFP to time at different ajoene analogue JUL1224 concentrations. 111

5.6 Inhibition effect of using both QQ alone and ajoene analogues. (A): LasR-GFP to time at different H9 concentrations with $32\mu g/ml$ AiiA. (B) LasR-GFP to time at different JUL1224 concentrations with 32 $\mu g/ml$ AiiA 112

6.1 Psl and Pel in the model. Psl is tightly bound with cells and Pel is slowly diffusible. Psl+ represents strains that produce normal amount of psl, like psl+pel- and wt. 116

6.2 Expansion ratio of Psl-, Psl+ and Psl++ cells. 117

6.3 Biofilm with thickness z_0, density ρ and maximum specific growth rate μ_{max}. The system is 1D and separated into 3 layers: biofilm layer, diffusion layer and bulk layer. There is only one rate-limiting substrate and the concentration at $z = 0$ is c_0 (biofilm interface). The substrate concentration at the bulk is c_b. 121

6.4 Morphologies of biofilm composed of Psl+Pel- (Blue) and Psl-Pel+(Yellow) mutants. (A) Experiments by Yang *et al*[2]. (B-G) Simulation morphologies with $K_{er} = 0.03, 0.06, 0.09, 0.12, 0.15, 0.18h^{-1}$, respectively. 123

6.5 Population ratio of Psl-Pel+ in mixed biofilm composed of Psl-Pel+ and Psl+Pel-. (A) Psl-Pel+ population ratio to time at different K_{er} values. (B) Psl-Pel+ population ratio to total population at different K_{er} values. (C) Psl-Pel+ population ratio to K_{er} at 28h. The solid line is the linear regression of these points. 124

6.6 Biofilm formed by Psl++Pel++ (red) and PAO1 (green) at different times. Arrows of the same color indicate the merge of Psl++Pel++ colonies. In this simulation, $K_{spsl++0} = 0.5K_{s0}$. 125

6.7 Percentage of Psl++ to time in biofilm composed of Psl++ and PAO1 (A): Biofilm composed of Psl++Pel++ and PAO1 with $K_{spsl++0} = 0.5K_{s0}$. (B): Biofilm composed of Psl++Pel++ and PAO1 with $K_{spsl++0} = 0.25K_{s0}$. (C): Biofilm composed of Psl++Pel- and PAO1 with $K_{spsl++0} = 0.5K_{s0}$. (D): Biofilm composed of Psl++Pel- and PAO1 with $K_{spsl++0} = 0.25K_{s0}$. 126

6.8 Population to time of biofilm composed by Psl++Pel++ and PAO1. In this simulation, $K_{spsl++0} = 0.5K_{s0}$. (A): Population of PAO1. (B): Population of Psl++Pel++. (C): Total population. 126

6.9 Population to time of biofilm composed of Psl-Pel++ and PAO1. (A): Population of PAO1. (B): Population of Psl-Pel++. (C): Total Population. 127

6.10 Morphologies of psl-pel++ and PAO1 (psl+pel+) mixed biofilm at different time of simulation. 128

6.11 Percentage of Psl++Pel- when mixed with PAO1 when only shear detachment (A) or only erosion detachment (B) is implemented. . . 130

6.12 Morphologies of biofilm when only erosion detachment is implemented. (A): $f_c = 3.5$. (B): $f_c = 1$. 131

7.1 Collective motion of *Serratia marcescens*. (A): Velocity field of bacteria. green, <20$\mu m/s$; pink, 20-40 $\mu m/s$; red, >40$\mu m/s$. (B): Average speed to bacteria to bacteria surface coverage ρ. Image is from reference[3]. 135

7.2 (A): Schematic drawing to show that nearby aligned bacteria cells swim faster than isolated cells. (B):Steric interaction of two *M.xanthus* cells leads to velocity alignment. figure B is from reference [4]. . . . 136

List of Tables

2.1 Parameters in Chapter 2 24

3.1 Parameters in Chapter 3 56

3.2 Components of *V.ficscheri* QS network and their symbols 60

3.3 Reactions of *V.fischeri* Quorum Sensing Network 61

3.4 Principles to fit parameters of *V.fischeri* QS network 66

3.5 Parameters and their values of *V.fisheri* QS network 69

3.6 Fanto Ratio of LuxR number predicted by different models 76

4.1 Parameters in Chapter 4 84

4.2 Reactions of *P.aeruginosa* LasR/I Quorum Sensing Circuit 87

4.3 Fitted Parameters of *P.aeruginosa* LasR/I Quorum Sensing Circuit . 89

5.1 Parameters in Chapter 5 104

6.1 Parameters in Chapter 6 114

6.2 Parameters used in the model 119

7.1 Parameters in Chapter 7 134

List of Abbreviations

ABM Agent Based Model

AHL N-Acyl Homoserine Lactone

BHL C4-HSL in *P.aeruginosa*

CA Cellular Automaton

EPS Extracellular Polymeric Substance

GFP Green Fluorescent Protein

HSL Homoserine Lactone

IBM Individual Based Model

ODD Overview, Design Concepts, and Details

ODE Ordinary Differential Equation

QQ Quorum Quenching Enzyme

QS Quorum Sensing

QSI,QI Quorum Sensing Inhibitor

Summary

Biofilms are surface-attached microbial communities embedded in their self-generated extracellular polymeric substance (EPS). Biofilm formation is one of the main causes of membrane biofouling, which represents a major challenge in the application of membrane technology to water treatment. Bacterial cell-to-cell communication mechanism quorum sensing (QS) plays an important role in regulating biofilm physiology and EPS synthesis. QS architectures are well studied; however the kinetic parameters are mostly unknown and they are heterogeneous among individual cells. Quorum quenching enzymes (QQ) and QS inhibitors (QSI) can inhibit QS, but their combined effects have not been studied yet. EPS production in biofilms determines cell interactions like cooperation and aggregation. Studying the population dynamics affected by EPS production helps to better understand biofilm development. Using cellular network deterministic and stochastic models, QS response curve topology was found dependent on network parameter values. Noise caused by parameter heterogeneity is comparable with network intrinsic noise. Synergy of QQ and QSI in inhibiting QS were proved by models (and have been validated by experiments). Population dynamics of EPS over producing small colony variants (SCVs) of *P.aeruginosa* in biofilm with wild type PAO1 was modelled using individual based modelling methods based on two kinds of EPS, i.e., Psl and Pel. The model predicted auto-aggregative property of SCV mutant and that although SCV is more stable under shear, it cannot out compete PAO1. This thesis contributed to a better understanding of QS network, proposed more effective ways of inhibiting QS, and modelled how EPS affects the dynamics of biofilm population dynamics and physiology. The outcome of this thesis contributes to the knowledge of biofouling control.

Chapter 1

Introduction

1.1 Background

Water scarcity and pollution were expected to be two of the most serious concerns of the 21^{st} century [5, 6, 7]. Waste water treatment and recycling are promising ways to alleviate water scarcity and pollution [8, 9]. In recent years, biofilms have been gaining popularity as a key component of waste water treatment technologies, such as moving bed membrane bioreactors and biofilm-assisted membrane bioreactors [10, 11]. It was reported that biofilm reactors are more efficient in removing phosphorus and nitrogen than traditional activated sludge bioreactors. Biofilms have heterogeneous structures where the surface cell layer is aerobic and can consume carbon, while the deep layer inside is anaerobic and suitable for phosphorus-accumulating organisms to accumulate phosphorus. In addition, the higher nitrogen removal efficiency is due to the multi-functional capacities and cooperation in biofilms. For example, during simultaneous nitrification and denitrification, the complex configuration of biofilms provides suitable niches for both nitrifying and denitrifying bacteria [11, 12, 13].

Although bacteria are essential in waste water bioreactors, biofilms and their ex-

tracellular polymeric substances (EPS) cause membrane biofouling in membrane reactors[14]. Biofouling is caused by the growth of bacteria embedded in EPS maxtrix on membrane surface, which will reduce the wastewater treatment efficiency by increasing the flow pressure and reducing the wastewater flux through the membrane [15]. Biofouling is one of the most serious problems in the application of membrane technology to wastewater treatment[16]. Thus, it is critical to prevent unnecessary biofouling processes.

Strong correlation between bacterial quorum sensing (QS) and membrane biofouling have been observed and inhibiting QS can alleveate biofouling [17, 18]. QS was shown to meditate biofouling through regulating biofilm physiology and EPS production [19, 20]. Better understanding of bacterial QS and how to inhibit it will imporve current measures to control biofouling.

The structure of bacterial QS networks of some bacteria are well studied [21]. However, the kinetic parameters are mostly unknown, which limits mathematical models to accurately predict QS responses. On the other hand, even if the kinetic parameters are not known, they are, like parameters in other cellular networks, heterogeneous among individual cells[22, 23]. It is necessary to explore QS responses within a reasonable parameter space and analyse the noise in QS network caused by parameter heterogeneity to better understand QS networks. Deterministic and stochastic cellular network models can be used to study this problem.

Natural and synthetic quorum quenching enzymes (QQ) degrade QS signal and quorum sensing inhibitors (QSI) interfere with the QS signalling pathway [24]. QSIs inhibit QS with different mechanisms. G1, ajoene and ajoene analogues are QSIs of *P.aeruginosa*. G1 binds with receptor proteins, competing with natural QS signals [1]; ajoene and its analogues inhibit QS at translational level [25, 26]. Whether QQ and QSI combined have additive, synergistic or antagonistic effect has not been studied. Since QQ and competitive binding QSI interrupt different positive feedback loops in QS network their combined effects might be promising. The combined

effect of QQ and QSI like ajoene analogue on QS also needs to be studied.

Since biofilm physiologies - in particular EPS secretion - directly cause membrane biofouling, it is important to study the dynamics of biofilm development. EPS secretion is essentially altruistic behaviour: individual cells secrete and share their organic matter to benefit the group [27, 28]. Cell aggregation is a common phenomenon in biofilms [29, 30]. EPS was shown to be related to cell aggregation [31]. Psl and Pel are two kinds of EPS produced by *P.aeruginosa*. It was shown that Psl tends to aggregate cells but Pel tends to expand the biofilm [32]. An individual based model (IBM, also called agent based model or ABM) [33] can be used to study the dynamics of cells in biofilms[34]. More specifically, the incorporation of Psl and Pel in IBM can be used to study the population dynamics of small colony variants (SCVs) [35] and *P.aeruginosa* PAO1 in biofilms based on Psl and Pel properties.

1.2 Objectives

QS, biofilm physiology and EPS are significant factors in regulating the biofouling process. This thesis attempts to bridge the knowledge gap of unknown QS network kinetic parameters by exploring possible QS responses in a reasonable parameter space. Even unknown, parameters in QS network are heterogeneous. This thesis will analyse amplitude of variation in QS behaviour contributed by parameter heterogeneity by comparing with intrinsic noise, which is easy to calculate. QQ, QSI can inhibit QS at some level and thus alleviate biofouling. This thesis also tries to study whether QQ and QSI combined have a synergistic effect in inhibiting QS and if so, potentially provide a effective way to quench QS and control biofouling.

As biofilms and EPS directly cause membrane biofouling, IBM will be used to study their dynamics, specifically, to incorporate Psl and Pel of *P.aeruginosa* to study the population dynamics and biofilm morphologies of SCV and PAO1 biofilm.

The outlined objectives of the work in this thesis are:

- To explore responses of QS network in a reasonable parameter space.
- To analyse the noise of QS network caused by parameter heterogeneity.
- To investigate whether QQ and competitive binding QSI have additive, synergistic or antagonistic effect in inhibiting QS.
- To investigate whether QQ and ajoene analogue have additive, synergistic or antagonistic effect in inhibiting QS.
- To incorporate Psl and Pel into IBM to model the population dynamics and morphology of biofilm formed by *P.aeruginosa* SCV mutant and PAO1.

1.3 Overview

In chapter 2, firstly, the significance of QS, biofilm physiology and EPS in biofouling process was reviewed. Then,biofilm properties and models were reviewed. What can further be done to better understand and control QS, biofilm and EPS dynamics was discussed. Finally, QS structures, parameter heterogeneity, QQ and QSI inhibiting quorum sensing and cellular network models were reviewed.

In chapter 3, firstly *V.fisheri* QS network model was built and parameters were fitted from experimental results in literature. Then the parameter space was explored and four response curve topologies were found, which showed that how the network responses, like whether multi-stationary and hysteresis loop exist in the response curve, are dependent on both network structure and interaction strength. Furthermore, it was found in parameter regions that agree with literature, intrinsic noise is greater than noise by parameter heterogeneity when the network is repressed. And when network is expressed, noise by parameter heterogeneity is greater for both single gene expression network and *V.fisheri* QS network. Model combining intrinsic

noise and parameter heterogeneity better explained the trend of noise when QS is turned on in experiments. Finally, how parameter heterogeneity contribute to the variation of QS switching on threshold and time was explored.

Chapter 4 used mathematical model of QS network and found that QQ or competitive binding QSI alone can inhibit bacterial QS. When combined, strong synergy were identified between QQ and competitive binding QSI in inhibiting QS. This conclusion has been proved experimentally using AiiA as QQ and G1 as competitive binding QSI on *P.aeruginosa* LasR/I circuit. Additionally, previous study showed that in wild type PAO1 strains, G1 inhibits las circuit more effectively than rhl circuit [1]. The effect of G1 on RhlR/I circuit on *P.aeruginosa* were modelled and it was found, however, in mutants only containing functional las or rhl circuit, G1 inhibits the mutant with functional rhl more effectively. This result also agreed with experimental data.

Chapter 5 used mathematical network model and found that QQ and ajoene analogue, another kind of QSI, have synergy in inhibiting both las and rhl circuits in *P.aeruginosa*. The inhibiting mechanism of ajoene analogue is to block the translation of mRNAs involved in QS. It was found that ajoene analogue is more effective than G1 when used alone or combined with the QQ AiiA.

In chapter 6, specific properties of Psl and Pel concluded by studies in reference [2, 32] are incorporated in IBM. This model reproduced the experimental results in reference [2] and further predicted the auto-aggregation property of *P.aeruginosa* SCV and SCV cannot out compete PAO1 although it is more stable under shear, which agreed with existing experimental results from literature.

Chapter 7 summarized the study of QS inhibition and EPS biofilm interaction contributes to biofouling control.Then a recommendation on future work of bacteria collective motion was presented. This recommendation has a clear picture of hypothesis with strong literature support that steric and hydrodynamic interactions lead to bacteria velocity alignment and the average speed of aligned bacteria cells is increased

through hydrodynamic interaction. Three methods adapted from literature to model hydrodynamic interaction were proposed.

Chapter 2

Literature Review

2.1 Bacterial quorum sensing and biofilm EPS are critical in membrane biofouling

Bacteria are intensively used in waste water treatment, from activated sludge treatment [36] to various membrane reactors. Bacteria are used to remove the organic carbon in waste water during the secondary stage of treatment and remove nitrogen and phosphorus during the tertiary stage treatment. Heterotrophic or facultative bacteria feed on organic waste in waste water. In traditional activated sludge treatment processes, these bacteria form microbial flocs which are subsequently removed [37]. Ammonia is treated by nitrifiers and denitrifiers. Nitrifiers include Ammonia Oxidizing Bacteria or Archaea which oxidize ammonia into nitrite, and Nitrite Oxidizing Bacteria or Archaea which oxidize nitrite into nitrate. Denitrifiers convert nitrate into nitrogen gas. The dominant nitrifiers in waste water treatment plants are *Nitrosomonas spp.* [38] *Nitrosospira spp.* and *Nitrospira spp.* [39]. Biofilm assisted reactors have been gaining popularity since 1990s, like moving bed, trickling filter, granular filter and high rate plastic media filter biofilm reactors. Compared to conventional suspended reactors, biofilm reactors have higher quality effluent, lower

Table 2.1: Parameters in Chapter 2

Symbol	Definition
Sh	Sherwood number
d	Mass transfer coefficient at biofilm bulk interface
D_i	Diffusion coefficient of substrate i
H	Diffusion layer length
c_b	Bulk concentration
c_f	Concentration at biofilm water interface
Y	Yield coefficient
σ_{ji}	Vector describing overlap of two cells
$\vec{d}_i$	Vector describing movement of cell i during shoving
μ	Cell specific growth rate
μ_{max}	Cell maximum specific growth rate
K_S	Half-saturation constant of substrate S
A	An arbitrary cellular component that regulates itself
$f(A)$	Production rate of A regulated by itself
d_A	Degradation rate of an arbitrary component A
r	mRNA concentration
R	Protein concentration
k_r	mRNA production rate
d_r	mRNA degradation rate
k_R	Protein production rate per mRNA
d_R	Protein degradation rate
η_r	White noise of mRNA production rate
η_R	White noise of protein production rate
$\delta(\tau)$	Delta function
σ_R^2	Temporal variation of protein concentration
$\langle R \rangle$	Temporal mean of protein concentration

footprint, lower net sludge production, are more resistant to environmental change and are easier to control [14, 40]. It was shown that moving bed biofilm reactor achieved the same removal rate with only 1/3 of biomass concentration compared with suspended reactors [12].

While bacteria are critical in the waste water bioreactors, biofilms and their extracellular polymeric substances (EPS) cause membrane biofouling in membrane reactors[14]. Biofouling is caused by growth of bacteria embedded in EPS maxtrix on membrane surface, which will reduce the wastewater treatment efficiency by increasing the flow pressure and reduce the wastewater flux through the membrane. Biofouling is one of the most serious problems of applying membrane technology in waste water treatment[16]. Thus, it is critical to prevent unnecessary biofouling processes.

Strong correlation exists between quorum sensing (QS) signal N-Acyl homoserine lactone (AHL) and membrane biofouling [17]. In one work, AHL was detected in biofilm formed on membrane surface at a lab scale membrane reactor. And biofouling was reduced by applying quorum quenching(QQ) enzyme porcine kidney acylase I. Biofilm structure was shown to affect the rate of biofouling. Sufficient oxygen produced biofilms with high porosity, less EPS and thus with lower biofouling rate[19]. QS can meditate biofilm structure and it was shown that interrupting QS result in biofilm with higher permeability[20].

Bacterial QS, biofilm physiologies and EPS are critical in membrane biofouling process. Understanding and controlling QS and biofilm EPS contribute to alleviate membrane biofouling.

2.2 Biofilms and EPS

EPS and the embedded bacteria cells form biofilms which directly cause biofouling [14, 16]. It is critical to better understand biofilm and EPS dynamics in order to better understand biofouling processes. QS controls biofouling probably by meditating biofilm physiology and EPS[17, 19, 20].

2.2.1 Biofilms, their development processes and impacts

In nature, most of the bacterial cells live in communities or biofilms, often attached to surfaces, including biotic surfaces such as tissues, dental plaques and abiotic surfaces like air water interface, water pipes, food, culinary facilities, leaves and medical devices [41, 42]. As the definition of biofilm has a blurry boundary, floating colonies like microbial flocs and particles in Activated Sludge Water Treatment Reactors and Particle-Based Reactors can also be categorized as biofilms[43, 44]. Biofilms usually contain more than 95% water, and present porous structures which enhance mass transfer of nutrients, metabolic wastes and signals [45]. Common biofilms in nature consist of multiple species instead single species. Logically, their are more kinds of biofilms than bacterial species.

Typical biofilm development includes five main steps: initial attachment, irreversible attachment, vertical growth, maturation and dispersal as shown in figure 2.1. During initial attachment, bacteria cells temporally attach to surfaces or existing biofilms. This binding is transient and bacteria may again move away. Rhamnolipid biosurfactants can meditate this kind of temporal attachment[46]. Gradually, bacteria change their phenotypes and tighten the binding to the surface. The binding becomes permanent or irreversible. Specific adhesins promote the irreversible attachment [42]. After irreversible attachment, bacteria population will increase and biofilms become mature. Mature biofilms often have heterogeneous structures, resistant to antimicrobial agents or antibiotics, secret EPS and quorum sensing signals [47]. The final stage

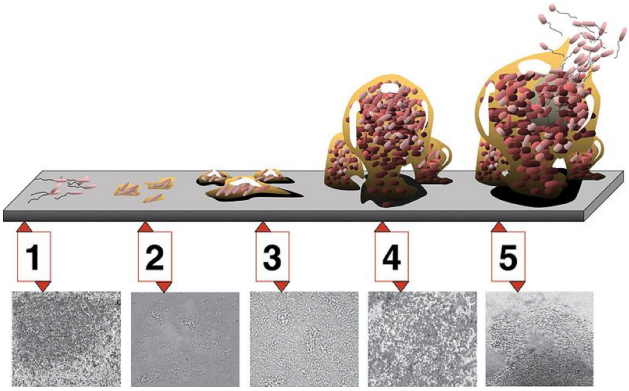

Figure 2.1: Biofilm development process. 1: Initial attachment, bacteria transiently attach to surface. This attachment will gradually evolve into irreversible attachment. 2: Irreversible attachment. 3: Vertical development. 4: Maturation. During this stage, cells in biofilm present very different phynotypes compared to cells in planktonic state. 5: Dispersal, a portion of the cells leave the biofim. (Image from reference [49],Image Credit: D.Davis).

of biofilm development is dispersal. During dispersal, bacteria cells become motile again, individually or as groups, and leave the biofilm. Bacteria dispersal enhances the survival of the species [48].

In biofilms, cells of the same species present various phenotypes. The main causes of this heterogeneity are chemical gradients, adjust to local environment, stochastic gene expression and genetic variation[50]. As cells aggregate inside biofilms, the reaction rates (consumption and production) will be large enough to create chemical gradients. Growth nutrients have highest concentration at the top of biofilms; metabolic wastes or signals have higher concentrations at the bottom and metabolic intermediate products accumulate at the middle of biofilms [50]. Bacteria change their phenotypes to adapt to the local environments, consisting of chemical concentrations, temperature, other cells, etc. Biofilms have well-formed structure with water channels. The local environment of cells vary greatly in different parts of biofilms. Stochastic gene expression also contributes to heterogeneity of biofilms. Cells of the same species or even two daughter cells produced by the same mother cell can have distinct growth rates and phenotypes [51]. This is very likely due to stochastic gene expression because the genetics and local environments of the two cells are

nearly the same. During biofilm development, bacteria genetics might also change due to mutation or plasmid transfer [52]. In summary, chemical gradients, varying local environment, cell adaptation, stochastic gene expression and genetic variance contribute to the heterogeneous properties of biofilms[50].

Cells in biofilm are 10–1000 times resistant to antibiotics and antimicrobial agents than cells in planktonic environment. The reasons are that: antibiotics fail to penetrate biofilm and kill all cells; cells in biofilms have reduced growth rate, which are more resistant to antibiotics. For example, antibiotics kill bacteria by interfering with their DNA replication [53], and cells in biofilm have longer division circle and are more resistant; Cells changes their phenotypes inside biofilm, which might increase their resistance[54].

Apart from biofouling, biofilms have other great impacts. Bacteria can form biofilms on medical devices which will impact the success of operations and contamination of patients. *P.aeruginosa*, *K. pneumoniae*, *S.epidermidis*, *S.aureus*, *C.albicans* and *E.faecalis* are often found to form biofilms on Central Venous Catheter [55]. Biofilms can also accumulate on Mechanical Heart Valve and Urinary Catheter [55, 56]. Biofilm can cause pathogenesis. *Pseudomonas aeruginosa*, *Staphylococcus aureus* and *Haemophilus influenzae* often form biofilms on the inner lung surface of cystic fibrosis patients and cause infections [57]. Biofilms can also cause infections like Infective Endocarditis, chronic ear infection, chronic prostitis and periodontitis [56].

Biofilms have great impact on food safety. Biofilms may contain pathogenic and spoilage species that decrease food hygiene and deteriorate food [58]. Biofilms also contaminate food processing equipments which will transfer diseases [59]. Biofilms on food processing devices can also be transferred to food while processing food. They provide a reservoir for pathogenic species. Species contaminate food include *Yersinia enterocolitica*, *Escherichia coli* , *Campylobacter jejuni* , *L. monocytogenes*, *Salmonella*, etc. Biofilms formed on food and food processing equipments are hard

to clean and erase because of the adherent surface property and extracellular matrix produced by biofilms. Recently, quite abundant researches have been done on biofilms on food in order to reduce food risk caused by biofilms [58].

2.2.2 Extracellular polymeric substances

Extracellular polymeric substances or EPS are organics with high molecular weight that exist at the intercellular space of microbial cells [60]. EPS is comprised of polysaccharides (40–95%), extracellular proteins (1–60%), extracellular DNAs and RNAs (1–10%), lipids, surfactants and humic substances [61]. The molecules are mainly secreted by microbial cells, produced from cell lysis, absorbed from the environment and shed from cell surface [60]. EPS is an important feature of bacterial biofilms, and phenotypic separations on EPS production have been observed [61].

There are many functional groups like carbonxyl, sulfhydryl and hydroxyl groups in EPS that can adsorb organic or inorganic compounds. The adsorbed substance can influence the structure of EPS and bacteria aggregates. For example, biofilm structure is maintained by EPS binding Ca^{2+} and Mg^{2+} [62]. EPS maintains the structures and stability of flocs, granules and biofilms by polymer bridging and depletion attraction [63, 64, 31]. EPS can be degraded by its own producers or other bacteria to serve as food and energy source [65]. Due to the various composition of EPS, it usually contains hydrophobic part and hydrophilic part. This affect the interactions of EPS and water. The hydrophobic part can absorb organic wastes[66]. EPS enhances the resistance of biofilm to antibiotics by adsorption , limiting transportation and forming aggregates that are difficult to penetrate [54]. The production of EPS by bacteria cells is affected by substrate type and concentration, the growth phase of bacteria and external conditions like concentration of metal ions [63].

More specifically, *P.aeruginosa* PAO1 biofilms produce 3 kinds of EPS: Alginate, Psl and Pel[2]. Alginate is rich in mannuronic and guluronic acid residues but not

important for biofilm structure[67]. Reference [32] concluded that Psl appears at early stages of biofilm and cross link cell and EPS matrix, making biofilm more elastic. Psl was shown to be tightly bound with bacteria cells. Pel is viscous and deformable. Pel appears at later stages of biofilm, reduces biofilm cross-linking and enhances biofilm dispersal.

2.2.3 EPS-regulated bacteria cooperation and aggregation in biofilms

EPS production is essentially altruistic behaviour of bacteria cells. Altruism is defined as the the strategy that individuals benefit the group at their own cost, and if all the individuals adopt the same strategy, the total benefit of the group will be positive. Bacteria secret EPS at the cost of their own fitness. EPS is responsible for bacterial adhesion to solid surface and can provide safe harbour for bacteria[27], assist in the adsorption of organic molecules and inorganic ions, enhance genetic information exchange and serve as food source in time of starvation[28]. Bacterium *Agrobacterium tumefaciens* infect Ti plasmid to plant to transform plant cells to produce opine at a cost. When the plant cells are transformed, the opine produced will benefit the bacteria group[68]. Bacteria produce extracellular enzymes to degrade complex organic compounds to serve as food for the group [69, 70].

For QS controlled altruistic phenotypes, QS is a good strategy to ensure all or none individual exhibit altruistic behaviour and thus prevent unbeneficial cost when cell density is low. For example, *Bacillus subtlis* and *Myxococcus xanthus* use QS to control sporulation [71]. Bacteria cells also live in micro-colonies to keep moisture, reduce solvent toxicity [29] and resist substrate inhibition. Usually a subpopulation of bacteria present altruistic characteristics. The remaining cells benefit from the altruism and present cheater-like traits. For example in some cases, only a portion of population secret EPS. *B. subtilis* can degrade extracellular proteins by secreting protease subtilisin E. But only a minority of cell secret this protease and benefit the whole group [72]. *S. Typhimurium* which infects the gut differentiates into two

phenotypes. The first type causes gut inflammation and benefit the second type and allow the second type to compete with other microbes [73].

As phenotypic separation benefits bacteria survival at changing environments and enhance division of labor, phenotypic separation into altruistic and cheater-like types can reduce cooperation cost at favorable conditions and benefit from cooperation at unfavorable conditions. EPS was shown to be secreted by only a portion of cells in biofilms, which can potentially benefit the species. It is already shown that bacteria can adapt their phenotypes in response to the change of the environment. However, the number of possible environments is so large or the environment is changing so quickly that mere strategy of changing phenotypes when the environment changes is not possible [73]. It was also hypothesized quick switching species needs more maintenance energy than slow switching species [33]. Thus fast adaption rate might not be advantageous in slow varying environment than the strategy of phenotypic separation. It is also possible that sensing-and-response type and phenotypic separation type are different evolutionary pathways for bacteria.

Cell aggregation in biofilms were often observed [29]. Aggregation brings altruistic cells closely together and thus promote altruism. However, aggregation also increase kinship competition for space and nutrient. Whether aggregation benefit or harm altruism is an interesting question. Bacterial aggregation tendency is the affinity of cells stay close to each other. It affects structure inside biofilms as well as biofilm formation. The abilities to form various defence clusters are different for various bacterial strains [29]. There is a wide range of colony sizes. Small colonies contain only hundreds of cells and large colonies have sizes of milimeters or centimeters. The shapes and inner structures of aggregates are various, even for the same species in the same environment [30]. Bacterial aggregations appear in biofilms was well as floating environment, such as activated sludge. Various image analysis tools and algorithms are available for detecting and study cell clusters [74, 75].

The current knowledge of mechanisms of bacterial aggregation is far from conclu-

sive. But there are some known mechanisms and factors that can influence bacterial aggregation. Bacterial aggregation is related to EPS production. Mutants of changed EPS production resulted in changed aggregation properties. Some bacterial species produce EPS that can drive cell aggregation through depletion attraction or polymer bridging. In depletion attraction process, polymers, often secreted by the bacteria, tend to avoid the bacteria and thus drive bacterial cells to aggregate together. Depletion attraction phenomenon exists in succinoglycan and *Sinorhizobium meliloti*, xanthan and *S.meliloti* and succinoglycan and *E.coli*. In depletion attraction, the larger the cell density, the less polymer is required. This is opposite with the polymer bridging mechanism [31]. Tendency to form aggregates is strongly related to the cell surface properties [76, 77]. Cell cultures influence the ability of cell aggregation. Organic or inorganic molecules such as zinc, lysozyme and salivary agglutinin can induce cell aggregation [78].

The mechanisms of bacteria altruism and aggregation are relatively independent. But aggregation has significant effect on bacteria altruism. *P.aeruginosa* SCVs produce excessive amount Psl and Pel, a kind of altruistic behaviour, and form tight aggregates [79]. Studying aggregation effect on altruism will contribute to how altruistic behaviour, like secreting EPS affect biofilm population dynamics and physiology.

2.2.4 Biofilm models

The most common biofilm model framework contains 3 domains: biofilm domain, diffusion domain and bulk domain as in figure 2.2. Biofilm domain is where the immobile biomass is located. Substrate is subject to diffusion and reaction (consumption and production by bacteria) here. Substrate is considered homogeneous in the bulk domain, but may vary with time. Substrates diffuse between the bulk and biofilm through the diffusion domain.

The diffusion layer is a workaround of mass transfer of substrates between bulk and

biofilm [33, 34, 80, 81]. The length of diffusion layer is determined by reactor configuration. It can be empirically calculated from the Sherwood number *Sh*.

$$Sh = \frac{k_L d}{D_i} \tag{2.1}$$

where k_L is the mass transfer coefficient at the bulk biofilm interface. D_i is the diffusion coefficient and d is character length related to reactor geometry. *Harald et. al* summarized the empirical equations of Sherwood number of vairous reactors in reference [82]. After obtaining *Sh*, the diffusion layer length can be calculated from equation 2.2. Diffusion layer length is irrelevant to substrate diffusion coefficient and is the same for different substrates.

$$H = \frac{d}{Sh} \tag{2.2}$$

The principle of setting the diffusion layer length H is to keep the mass transfer coefficient at the interface of biofilm and bulk constant. For simplicity, many models set H to around $100\mu m$ [82, 34, 83].

For still water, diffusion layer length H can be experimentally measured. When the substrate reaches steady state, according to equation 2.4, in diffusion layer, we have $\frac{dc}{dz} = \text{const} = \frac{c_b - c_f}{H}$. Thus, the diffusion layer length can be calculated from equation 2.3.

$$H = \frac{c_b - c_f}{(dc/dz)_w} \tag{2.3}$$

where c_b is the bulk substrate concentration; c_f is the substrate concentration at the water biofilm interface; $(dc/dz)_w$ is the gradient of substrate in the diffusion layer. These parameters can be experimentally measured and thus the diffusion layer length H can be calculated.

According to how biomass is represented, biofilm models can be briefly separated into 3 categories: continuous model, cellular automaton model and agent based model.

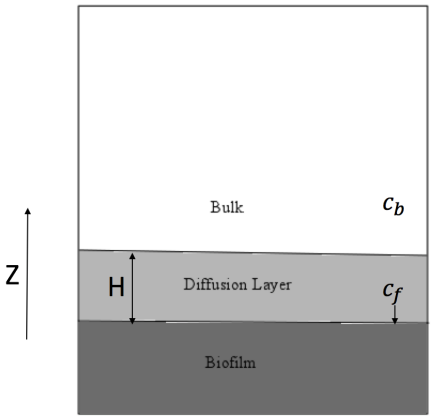

Figure 2.2: A general framework of mathematical biofilm models. The system consists of 3 domains: the biofilm domain, diffusion layer domain and bulk domain. Biomass is included in biofilm domain. Substrate concentration in biomass domain is determined by diffusion and reaction (consumption or production by bacteria). The substrate concentration in diffusion layer domain is solely controlled by substrate diffusion. Substrates diffuse from the bulk domain into biofilm domain (or reversed) through the diffusion layer domain. Substrates are considered spatially homogeneous in the bulk, but may vary with time.

Continuous models: Continuous models treat biomass as continuous substance and represent biomass by its density $\rho(\vec{r})$. The first set of biofilm models were 1-dimensional continuous models [81, 84]. Diffusion-reaction equation 2.4 determines the substrate concentration in the biofilm domain.

$$\frac{\partial c_i}{\partial t} = D_i \frac{\partial^2 c_i}{\partial z^2} + r_i \tag{2.4}$$

where c_i is the i^{th} substrate concentration; D_i is the diffusion coefficient and r_i is the reaction rate of the substrate. For nutrients consumed by the bacteria, the reaction rate is shown in equation 2.5.

$$r = -\frac{1}{Y}\mu_{max}\frac{c}{K_c + c}\rho \tag{2.5}$$

Y is the yield efficient, meaning the amount of biomass produced per unit amount of substrate consumed; ρ is the biomass density; K_c is half-saturation constant of growth rate and μ_{max} is the maximum specific growth rate of biomass.

Continuous models can be multi-dimensional, can contain multiple species and substrates [85, 86]. Continuous biofilm models show that sharp substrate gradient exists

inside the biofilm. Simulation results in reference [87] showed that oxygen can penetrate no further than 200 μm inside biofilm. There are also models that incorporate fluid flows and convection mass transportation in multi-dimensional biofilm models. Stress of biofilm caused by flow was investigated by a 2D continuous model in reference[88]. Biofilm can also be treated as fluid [89, 90] and biofilm structure is solved by solving multi-fluid equations. AQUASIM [91] is a software package for continuous 1D biofilm model. It was usually used to simulate biofilm water treatment reactors. AQUASIM also provides the mechanisms of biofilm detachment and attachment.

Continuous modes are proper to study biofilms of large spatial scale but not local heterogeneity. Because continuous models represent biomass by its density $\rho(\vec{r})$, which is averaged at a scale much larger than (say 10 times) average cell cell distance. Usually bacteria cell size is around $1\mu m$. Even if cells closely attach to each other, biomass density is averaged from spatial scale of $10\mu m$. So continuous models are not proper to study biomass distribution within $10\mu m$ and are usually used to study systems larger than several hundred microns.

Cellular automaton models In Cellular Automaton (CA) Models of biofilms, space is divided into discrete squares (2D) or cubes (3D). Solid components like biomass and EPS are represented by density in each grid. Fluids and soluble substrates are represented by continuous fields[92, 82]. Biomass grows and increases its density in a grid. When biomass density exceeds the threshold, the excess amount will be transferred to neighboring grids, or another grid if all neighboring grids are full.

The CA model built by Cristian et al. is described here, as it is one of the earliest biofilm CA models which included most modelling features [92]. A grid contains dimensionless substrate concentration S, biomass density C and other solid components $\vec{c}$ like bacteria and gel. The grid size can be small enough such that one bacteria cell can occupy multiple grids, or can be large enough that one grid contains many bacteria cells.

The substrate concentration is still determined by equation 2.4. In CA model, it is implemented in equation 2.6, where x_i is the i^{th} axis; $r_S(S,C)$ is the production/consumption rate of S and dl is the grade size and D_S is the diffusion coefficient.

$$\frac{\partial S}{\partial t} = \frac{D_s}{dl^2} \sum_i \frac{\partial S}{\partial x_i^2} + r_S(S,C) \tag{2.6}$$

The biomass concentration is updated according to growth equation 2.7, where R_C is the growth rate of biomass.

$$\frac{\partial C}{\partial t} = R_C(S,C) \tag{2.7}$$

When biomass in a grid reaches the maximum value, it will be split into two parts, one part of biomass stays in the original grid and another part is placed in a neighbouring grid that is not fully occupied. When no such candidate exists, it will recursively find a neighbouring grid of its neighbouring grid which is not fully occupied and place the biomass there. After initialization, the system continues runs the following steps until time limit or total biomass limit is reached.

1. Calculate substrate concentrations according to diffusion reaction equation 2.6.
2. Calculate biomass concentration according to growth equation 2.7.
3. Redistribute biomass.

CA models were used to study the relationship between nutrient concentration and biofilm surface roughness. It was found that, high substrate concentration produced smooth biofilms and low substrate concentration produces rough biofilms[92]. Simulation results of a CA model in reference [93] showed that accumulation of damage is the most probable mechanism of cell death in biofilms. CA models represent biomass and solid components by their densities in each grids. It is more realistic than continuous model in studying the spatial heterogeneity of biofilms. But it is not proper to study single cell heterogeneity or when the focus is at small scale where only a small amount of cells are involved.

Agent based model or individual based model Agent based model (ABM), also called individual based model (IBM), of biofilms simulate individual cells separately. There is an standard ODD (Overview, Design concepts, and Details) protocol for ABM. It is appropriate to study biofilms with low cell density and study biofilm properties as emergents of single cell rules [94]. The basic components in ABM models are very similar to those in CA models. The substrates are treated similarly and calculated by diffusion reaction equation 2.4. When cells overlap due to growth and division, shoving algorithm is used to separate cells and push the biofilm forward. For cell i, suppose there are J_i cells overlapping with it, then during he shoving process, cell i is moved according to equation 2.8. m_i is the biomass of cell i; $\vec{\sigma}_{ji}$ is a vector pointing from the center of cell j to i with length equal with their overlap length; $\vec{d}_i$ is the distance cell i needs to move. In practice, many times of shoving steps are needed to eliminate overlap.

$$\vec{d}_i = \sum_{j=1}^{J_i} \frac{m_j}{m_i + m_j} \vec{\sigma}_{ji} \tag{2.8}$$

The most important features of ABM are cells are modelled more explicitly and cell-cell heterogeneity can be easily studied. Most ABMs use the same diffusion-reaction framework described in figure 2.2. And equation 2.10 or its variations are used as cell growth dynamics. Generally, models did not consider the variation of cell growth rate in the same conditions. Biomass can be composed of different components, such as active biomass, capsules and inert biomass.

ABM has been used to study various biofilm properties and dynamics. It was found that plasmid invasion is not limited when invasion speed does not depend on host growth rate [95]. ABM study also showed that bacteria and phage can form self-organized spatial structure to maintain their co-existence. And in co-evolution simulation, the parameters regarding resistance to phage inside and at the surface of biofilms tend to evolve into the region that enable bacteria phage co-existence [96]. ABM models can also couple with fluid flow. For example, reference [97] used 3D ABM models to show that flow can smooth biofilm surface without affecting the

active growth layer.

Recently the number of packages for ABM of biofilms are increasing and becoming more sophisticated. iDynoMiCS is a java based ABM for biofilms [33]. Its aim is to provide a common platform for ABM of biofilm and enable researchers with few programming skills to use it. It has been used in some studies[98, 96] and currently under further development by a group of international developers. But adding features not included in the package needs to change the source code. Netlogo is an ABM programming language [99]. It provides extensions to connect with other programs. Reference[100] used matlab as server to calculate diffusion-reaction equations for biofilm models. And cell growth and division are modelled in netlogo. Bsim[101] is an ABM tool to study biofilm group level properties from single cell behaviours. Based on Bsim, it is easy to build new models.

Cell growth and division models Cell growth and division processes are required by all types of biofilm models. As growth and division is are basic roles of bacteria cells in agent based model of biofilms, they will be reviewed here. Bacteria reproduce by binary fission. At certain stage of cell cycle, a Z-ring with solid structure in the middle of the cell is formed by protein FtsZ; genome replicates and cell divides into two daughter cells, usually of equal size [102]. Unlike cells of mammals and birds which always experience local environment in a narrow region, bacteria cells adapt to changing environment by adjusting their phenotypes. When cells are introduced into new a batch culture, there are four growth phases: lag phase, exponential phase, stationary phase and death phase. During the exponential phase, biomass grows exponentially according to equation 2.9 .

$$\frac{dx}{dt} = \mu x \tag{2.9}$$

x is the total biomass; μ is called specific growth rate. The specific growth rate and its dependence on rate limiting substrates can be experimentally measured using chemostat configuration. The relationship between μ and rate limiting substrate

concentration S can be expressed in equation 2.10.

$$\mu = \mu_{max} \frac{S}{K_S + S} \tag{2.10}$$

μ_{max} is called the maximum specific growth rate. K_S is the half-saturation constant of this substrate. When $S = K_S$, the specific growth rate μ is half of μ_{max} [103].
Equation 2.9 and 2.10 describe the growth behavior of the total biomass of a single cell. The growth patterns of different components in a single bacteria cell are different. For typical bacteria like *E.coli*, cell components can be separated into 3 categories: the cytoplasm, including cytoplasmic proteins, ions, water, small molecules and everything inside the membrane except the genome; the cell surface, including cell wall, membrane and molecules like proteins and sugars embedded; and the genome [104]. If the cell is under constant local environment, the cytoplasm grows exponentially all the time. Cell surface grows in this way such that the density of cytoplasm keeps constant. For spherical cells, cell surface grows exponentially with the cytoplasm; rod shaped cells grow by increasing its length and thus cannot grow exponentially because the shape has changed. Genome begins to replicate when cytoplasm reaches a certain amount per origin of replication. The time required for genome replication is approximately constant. The time between completion of genome replication and the end of cell division is also relatively constant [104]. Because the cytoplasm keeps growing during the starting of genome replication and ending of cell division, in culture with higher growth rate, the cell size is also larger. Most ABM models of biofilms set a division radius to the cell agent. When the radius of the cell reaches the division radius, it will split into two daughter cells. This rule is only proper in studying cell size independent properties of biofilms.

The cytoplasm occupies most of the cell dry weight. For example, in *E.coli*, the approximate dry weight percentages of cytoplasm, surface components and genome are 83%, 14% and 3% respectively [104]. It is reasonable to assume cells only contain one kind of biomass which grows exponentially. Some models also include inert biomass and capsule related to EPS secretion [33].

When a cell generates two daughter cells of equal size, the growth rates of the daughter cells, although in the same environment, are rarely the same. This is because of the inherent variability of their growth rates. The standard deviation of generation times of *S. Typhimurium* cells in a microcolony containing 20 to 25 total cells originated from a single ancestor cell is 50% of the mean generation time [51]. Most ABM models of biofilms did not consider the variability of generation time, but set different sizes of daughter cells to get rid of the artifacts of synchronized cell division [34, 33]. This is appropriate when studying biofilms properties weakly related to single cell growth rate variability.

Monod Equation 2.10 describes the simple dependence of microbial growth on a single substrate. G.C. Okpokwasili and others published a through review on the kinetic models of microbial growth in 2006 [105]. Some of them are listed below.

Some essential substrates can inhibit microbial growth when their concentrations are too high. Andrew's equation [106] 2.11 is widely used to describe substrate inhibition kinetics, where K_i is a constant related to substrate inhibition.

$$\mu = \mu_{max} \frac{S}{K_S + S + S^2/K_i} \tag{2.11}$$

A generalized model 2.12 also describes the inhibition kinetics.

$$\mu = \frac{\mu_{max}(1 - S/S_m)^n}{S + K_S - (1 - S/S_m)^m} \tag{2.12}$$

where S_m is the threshold substrate concentration above which growth stops. m and n are constants.

There are also some models for multi-substrates. When substrate S and P serve for different purposes, such as carbon and nitrogen sources, the kinetics can be expressed by equation 2.13.

$$\mu = \mu_{max} \frac{S}{K_S + S} \frac{P}{K_P + P} \tag{2.13}$$

When two substrates S_1 and S_2 serve as the same purpose, the kinetics can be ex-

pressed by equation 2.14 .

$$\frac{\mu}{\mu_{max}} = W_1 \frac{S_1}{K_1 + S_1} + W_2 \frac{S_2}{K_2 + S_2}. \tag{2.14}$$

where $W_1 = \frac{K_1/S_1}{K_1/S_1 + K_2/S_2}$ and $W_2 = \frac{K_2/S_2}{K_1/S_1 + K_2/S_2}$.

When S_1 and S_2 inhibits the utilization of each other, the kinetics can be expressed by equation 2.15.

$$\mu(S_1, S_2) = \mu_{max1} \frac{S_1}{K_1 + S_1 + \frac{K_1}{K_2} S_2} + \mu_{max2} \frac{S_2}{K_2 + S_2 + \frac{K_2}{K_1} S_1} \tag{2.15}$$

2.3 Bacterial quorum sensing

2.3.1 Architectures of bacterial QS

Bacterial cells communicate with each other through the broad definition of signals. Bacteria can response to mechanical signals: when bacteria cells transiently attach to a surface, it will gradually change its phenotype and transfer from transient attachment to permanent attachment [42]. Growth substrates can also be signals for biofilm dispersal for some species and formation for others. Glucose inhibits the initial state of biofilm formation of *Aeromonas hydrophila* [107] but promotes the biofilm formation of clinical isolates of *staphylococci* [108]. Bacterial communication through upregulation of low-weight secreted protein Ycel promotes the resistance to antibiotics of *Burkholderia cenocepacia* species [109]. Bacterium *Bacillus subtilis* can also communicate with electric signals like brain neurons through ion channels [110].

One of the most important bacterial communications is QS. Phenomenally, bacteria inside a community change their phenotypes only when the population density reaches certain threshold[111]. The structure of QS cellular network is well studied. The mechanism of quorum sensing is chemical signal communication between cells

of the same species. When cell density is low, single cell produces quorum sensing signals, also called auto-inducers at base rate. When the auto-inducer concentration reaches a threshold, a positive feedback loop of cellular network will activate cells to produce more auto-inducer, and other quorum sensing activated or inhibited genes are regulated [112].

Bacterium *Vibrio fischeri* become luminescent when cell population density reaches a threshold. The quorum sensing signal or auto-inducer of *V. fischeri* is N-(3-oxohexanoyl)-homoserine lactone, a kind of Acyl homoserine lactone(AHL). This AHL can freely diffuse in and out of cell membrane. Protein LuxI is the enzyme for producing this AHL. When AHL concentration is large enough, it will bind with the receptor protein LuxR. The binding product of LuxR and AHL will activate luxR and luxI genes and boost the production of AHL and LuxR. It will also activate luminescence genes and *V. fischeri* will present luminescent phenotype [113]. The scheme is illustrated in figure 2.3.

Some bacteria, like *P. aeruginosa* have multiple interconnected QS systems. The LasR/I and RhlR/I systems with quorum signals N-(3-oxododecanoyl) homoserine lactone (3O-C_{12}-HSL) and N-butyryl-homoserine lactone (C_4-HSL), respectively are very similar to LuxR/I network in *V. fischeri*. The difference is that the production of receptor RhlR is meditated by the LasR/I network [114, 115]. Besides las and rhl QS circuits, *P. aeruginosa* also has other two quorum sensing systems, IQS and PQS. These networks interact with each other and not only respond to population density but also other environmental conditions [116]. At least 6% genomes of *P. aeruginosa* were found to be controlled by QS [117].

LuxR/I quorum sensing system is the prototype of QS systems of gram-negative bacteria. QS signals produced by gram negative bacteria are acyl-HSLs (AHLs), containing an acyl group attached to a homoserine lactone (HSL) ring. Generally different species produce AHLs with different acyl groups. The HSL rings are the same [118]. AHLs are produced by LuxI homologues. The precursor of AHL is

S-adenosylmethionine. AHLs bind to LuxR homologues and the binding product will regulate target genes. A typical LuxR homologue has two binding domains for AHL and DNA promoter. Evidence showed that the AHL-binding domain blocks DNA-binding domain when the receptor is not bound to AHL. When binding with AHL, the DNA-binding domain of receptor protein is exposed and able to bind and regulate target genes, including the luxI homologue gene. The acyl side chain of AHL determines the specificity of binding process with the receptor protein [119].

Gram-positive bacteria have different prototypes. The main differences are that the auto-inducing signals of gram-positive bacteria are peptides, which cannot freely diffuse in and out of cell membrane but need to be actively transported by the bacteria; the binding of auto-inducing peptides and receptors occurs at the outer cell surface instead of cytoplasm [120].

Although QS signals are highly specific to their producing species, cross talks of QS exist between different species. Species *B.cepacia* can use the two QS signals produced by species *P.aeruginosa*, 3-oxo-C12-HSL and C4-HSL, to activate its QS circuit. These two species were often found co-cultured in the lungs of cystic fibrosis patients [121]. The signal of gram-positive species *Staphylococcus* can activate the receptor and target genes in species *Enterococcus faecalis* [122].

There is one QS signal that has been found in more than 50 species, including both gram-positive and gram-negative strains. This signal is called autoinducer-2 (AI2), produced by LuxS gene and originally detected in species *Vibrio harveyi* [123]. Species *P.gingivali* and *Streptococcus mutans* can form mixed biofilms in dental cavities. Deleting the luxS gene, which is responsible for producing AI2, of either species did not eliminated their abilities to form mixed biofilms. However, when LuxS genes in both species were deleted, they could not form mixed biofilms [124]. This is evidence that AI2 is involved in interspecies communication.

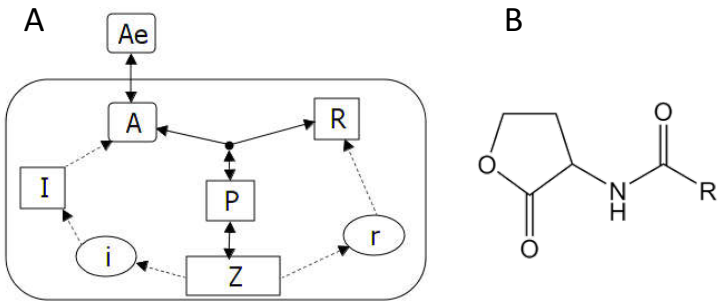

Figure 2.3: (A): Quorum Sensing network of *Vibrio fischeri*. *I* represents AHL enzyme LuxI; *i* is the mRNA of *I*; *R* is the receptor protein LuxR; *r* is the mRNA of *R*; *A* represents the cellular AHL; A_e represents extra-cellular AHL; *P* is the combination product of *R* and *A*; *Z* is the dimer of *P*. AHL can freely diffuse in and out of cell membrane. *Z* can activate luminescent genes and also increase the production of LuxR, LuxI and thus AHL, providing a positive feedback loop. (B): AHL molecule structure of general gram-negative quorum sensing signal. Different species differ in the R-group.

2.3.2 Parameters of QS network are mostly unknown and they are heterogeneous

Despite the fact that the structures of some QS networks are well studied, most of the kinetic parameter values are unknown as they are difficult to measure and rarely experimentally measured. The only experiment to roughly measure membrane permeability of AHL was performed in 1985 [125]. Some QS models analysed the qualitative properties of QS based on network structure [126] and others tried to quantitatively model QS but values of the same parameters mostly disagree in literature [127, 128, 129, 130, 131, 132]. Thus mathematical modelling to study QS network responses within reasonable parameter regions are necessary to understand bacterial QS.

On the other hand, even the QS network parameters are unknown, evidence shows that they are heterogeneous in individual cells even in identical environment. The fluorescence and QS turn on time of *V.fischeri* were different among individual cells in almost the same environment [22]. LuxR is the master regulator of *V.harveyi* QS and the luxR gene expression of *V.harveyi* is heterogeneous among individual cells

[133].

As QS is connected with other cellular components, stable difference of other cellular components can result in parameter heterogeneity of QS network. Bacteria with identical genetic codes can have different phenotypes in the same colony, or even in identical conditions. The next division time of two nearby daughter cells produced by division of one mother cell are rarely the same [51], although their genetic information and local environment are nearly identical.

Under starving condition, a subpopulation of bacterium *Bacillus subtilis* will form sporulation. The sporulating cells contain endospores that are readily visible under phase contrast microscopy while nonsporulating cells do not [134]. Sporulating cells are produced by asymmetric cell division. The larger one is the mother cell and the smaller one is called forespore, which is ultimately engulfed by the mother cell. The formation of endospore is not caused by genetic change because under favorable conditions, spores will quickly germinate and convert to ordinary cells [135]. Bacterium *Bacillus subtilis* also separate into two phenotypes during the middle of exponential growth phase. Part of the cells expressed swimming motility and the other were sessile. The sessile cells have long chains and motile cells present as single cells or cell doublets. The two phenotypes are controlled by the sigma factor σ^D and protein SwrA was shown to regulate the swimming behaviour in *Bacillus subtilis* [136]. The mechanism of phenotype separation is not clear yet.

Pseudomonas aeruginosa 47T2 is able to accumulate polyhydroxyalkanoates (PHA) in its cytoplasm. It was found that only a subpopulation of this species in waste frying oil cultures accumulate PHA and these cells differ in size and granulosity. The remaining population did not accumulate high amount of PHA [137]. High PHA accumulating strains could be selected, but it was not sure whether the phenotype type separation in PHA accumulation was due to genetic variation.

Myxococcus xanthus is able to produce β–galactosidase. Single cell expression was measured and it was found that in strain DK 4473 of this species, a subpopulation

does not produce β–galactosidase [138]. Surface charge of some strains of *Enterococcus faecalis* species is heterogeneous within the population [139], which affects biofilm formation with other bacterial species [140]. Later it was shown that endocarditis- and biofilm-associated pili (Ebp) are strongly correlated with the ζ-potential of *E. faecalis*. The strain *OG1RF* of *E. faecalis* has two distinct types of subpopulation with ζ-potentials $-38mV$ and $-26mV$. When the ebp operon EbpR or its structure genes ebpABC were deleted, the population became homogeneous in surface charge with ζ-potential $-38mV$ and when EbpR or ebpABC were over expressed. The population became homogeneous with ζ-potential $-26mV$ [141].

Non-genetic heterogeneity might also be caused by cell partition. During cell division, the distribution of mRNAs is approximately binomial [142]. These stable individual cell heterogeneities can directly or indirectly affect QS network.

Recently direct measurement of parameter heterogeneity of single gene expression network in yeast cells was performed in reference [23]. mRNA translation rate k_r approximately obeys Γ-distribution with coefficient of variance 0.5. Mathematical modelling of noise caused by parameter heterogeneity in QS network is important to understand the experimentally observed heterogeneity in QS networks [22, 133]. As intrinsic noise is the most studied it is easy to calculate [143], the magnitude of noise by parameter heterogeneity can be compared with intrinsic noise.

2.3.3 QS inhibition by quorum quenching enzymes and quorum sensing inhibitors

The ultimate goal of studying and understanding QS in this thesis is to inhibit QS to reduce biofouling. Recently, intensive studies are focusing on quorum quenching enzymes (QQ) that degrade QS AHLs by break AHL lactone ring or the acyl side chain and quorum sensing inhibitors (QSI) that interupt QS network components, like binding to signal receptor protein [144, 145]. It was found that both prokaryotes

and eukaryotes can secret QQ, including AHL-acylases, AHL-lactonase, decarboxylases and deaminase [144]. QQ can also be synthesized. A methyl anthrailate can inhibit the PQS circuit of *P.aeruginosa* [146]. Competitive-binding QSIs can be reversible or irreversible. Reversible competitive-binding QSIs bind to receptor protein in competition with natural AHL[147]. LasR-specific antiactivator can bind to LasR and inhibit its activity and it was found that this inhibition mechanism is to prevent the dimerization of LasR [148]. Irreversible competitive-binding QSIs bind to and then degrade or break receptor proteins like halogenated furanones [149].

There are also other QSIs that act in different mechanisms. Ajoene was shown to be able to inhibit the translation of mRNAs in QS circuits [26]. It is a kind of sulfur-containing compound that can reduce the key QS related virulence factors [25]. Analogues of ajeone were also found to have the capability to inhibit QS. One analogue replacing the allyl group with benzothiazole derivative was found to be more effective than ajoene in inhibiting QS and reducing virulence of *P.aeruginosa* [26]. The mechanism is that ajoene binds with small RNAs rsmY and rsmZ and inhibits their activities [25]. Small RNAs rsmY and rsmZ act in parallel and inhibit the regulator RsmA. RsmA inhibits the translation of mRNAs in QS circuits [150, 151]. The net effect is that ajoene and its analogue inhibit the translation of mRNAs in *P.aeruginosa* QS circuits.

Since QQ targets at AHL signal, competitive-binding QSI targets at receptor protein and QSI ajoene analogues target at the translation of mRNAs, their targets belong to different positive feedback loops. It is expected that QQ and QSIs combined have synergistic effects in inhibiting QS. Mathematical and experimental proofs are desired to test this hypothesis to see whether combining QQ and QSIs provide a promising method in inhibiting QS. Deterministic methods based on ordinary differential equations can be used to do the mathematical simulation.

2.3.4 Deterministic and stochastic models of cellular network

Cellular network models are usually used to study QS network and other cellular processes. Positive feedback loops can generate multi-stationary states [152]. But positive feedback itself is not sufficent to generate multi-stability. The network needs to present non-linear kinetics [153]. Negative feedback loop will result in a single state [154].

Using a simple example, that the cellular component A is regulated by itself: $\frac{dA}{dt} = f(A) - d_A A$, where $f(A)$ is the self-regulation function and d_A is the degradation rate of A. If $f(A)$ is positively regulated by itself, then $f'(A) > 0$ and vice versa. A stable stationary solution should satisfy equations 2.16. The solution that only satisfies the first equation is not stable.

$$\begin{cases} f(A_s) - d_A A_s & = 0 \\ f'(A_s) - d_A & < 0 \end{cases} \tag{2.16}$$

f_1, f_2 and $f_3$in figure 2.4 are 3 examples of self-regulation functions. It is clear that negative feedback loop (f_1) only has a single solution and positive feedback can have one or multiple stable stationary states. The network will have multi-stability when the line $f(A)$ crosses the line $d_A A$ from left to right multiple times.

Practical cellular networks are more complex and contain many components. A simple practice is to look at the net effects of component A to itself. For example, in the toggle switch example where two components repress each other, multistable states exists when the strengths of two repressions are at the same level [153].

The definition of intrinsic noise is clear. Inside a bacterial cell whose volume is small, unlike mass chemical reactions, often the reactants have small copy numbers. Thus whether a specific reaction will occur or not is a random event. Even if every cell obey the same set of rules, the outcome will be different because of the biochemical stochasticity inherent to the cellular network [143].

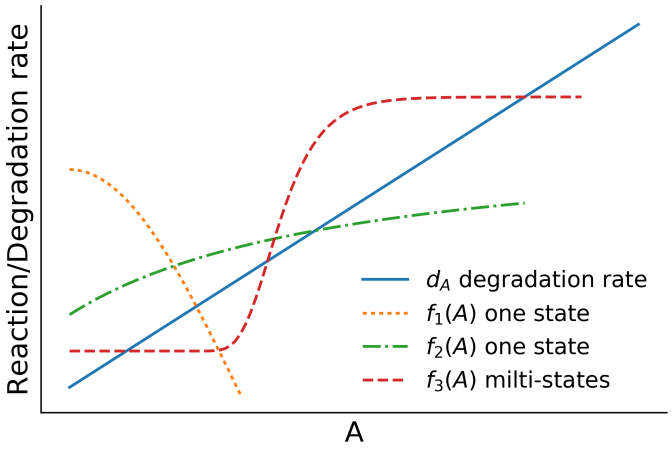

Figure 2.4: Single and multiple stationary states of a one-component feedback loop. The arbitrary component A is assumed to be regulated by itself: $\frac{dA}{dt} = f(A) - d_A A$, where $f(A)$ is the self-regulation function, and d_A is the degradation rate of A. Stationary solutions are the solutions of $f(A) - d_A A = 0$. (f_1): negative feedback loop. There is only one stationary state. (f_2): positive feedback loop. There is only one stationary state. (f_3): positive feedback loop. There are two stable stationary states, and one unstable stationary state.

Intrinsic noises can be simulated by stochastic chemical reaction models. A single gene expression model is shown in equation 2.17, where r represents the number of mRNA and R represents the number of protein, d_r and d_R are the degradation rates of mRNA and protein respectively, k_r is the mRNA production rate and k_R is the protein production rate by one mRNA.

$$\begin{cases} \frac{dr}{dt} & = k_r - d_r r \\ \frac{d_R}{dt} & = k_R r - d_R R \end{cases} \tag{2.17}$$

Using two sets of parameters in reference [155], $k_r = 0.01s^{-1}, d_r = 0.1s^{-1}, k_R = 1s^{-1}, d_R = 0.002s^{-1}$ and $k_r = 0.1s^{-1}, d_r = 0.1s^{-1}, k_R = 0.1s^{-1}, d_R = 0.002s^{-1}$, the results of r and R copy numbers are shown in figure 2.5. Average protein copy numbers R predicted by deterministic model $\frac{k_R k_r}{d_R d_r}$ are 50 for both sets of parameters. Average mRNA copy numbers $r = \frac{k_r}{d_r}$ are 0.1 and 1 respectively. Ozbudak *et al.* measured a single green fluorescent protein (GFP) gene expression of $10^4 - 10^5$ *Bacillus subtilis* cells of strains with varying transcriptional or translational rates [155], and found that population heterogeneity of GFP expression indicated by the Fanto Ratio

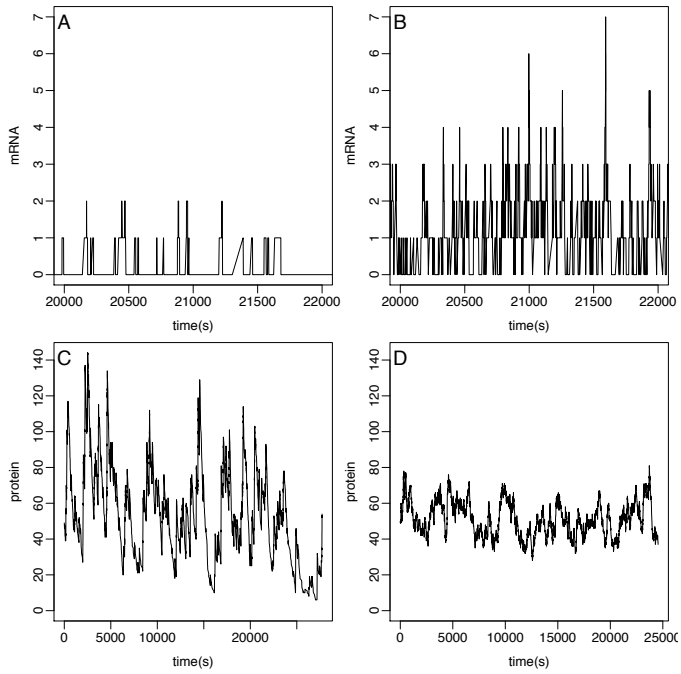

Figure 2.5: Stochastic single gene expression modeling results. A and C: mRNA and protein copy numbers using parameters: $k_r = 0.01s^{-1}, d_r = 0.1s^{-1}, k_R = 1s^{-1}$. B and D: mRNA and protein copy numbers using parameters: $k_r = 0.1s^{-1}, d_r = 0.1s^{-1}, k_R = 0.1s^{-1}, d_R = 0.002s^{-1}$

$\frac{\text{var}(R)}{\text{mean}(R)}$ increases quickly with translational rate and increases slowly with transcriptional rate. Ozbudak *et al.* used the stochastic model above to explain the experimental results. Gene expression intrinsic noise analysis shows that the burst size $b = \frac{k_R}{d_r}$, which is the average total protein produced by one mRNA in its lifetime, approximately equals the fanto ratio of protein R [155]. By introducing a white noise source, equation 2.17 becomes equation 2.18.

$$\begin{cases} \frac{dr}{dt} & = k_r - d_r r + \eta_r \\ \frac{d_R}{dt} & = k_R r - d_R R + \eta_R \end{cases} \tag{2.18}$$

where η_r and η_R are the white noise sources of mRNA and protein with $\langle \eta_i(t) \rangle = 0$ and $\langle \eta_i(t)\eta_j(t+\tau) \rangle = q_i \delta(\tau)$ (i and j represent r or R), where $\delta(\tau)$ is delta function. By Fourier-transforming analysis and considering that protein is more stable than mRNA, we can get equation 2.19, where σ_R^2 is the temporal variation of protein

concentration and $\langle R \rangle$ is the temporal mean of protein concentration.

$$\frac{\sigma_R^2}{\langle R \rangle} = 1 + \frac{k_R}{d_r + d_p} \approx 1 + b \tag{2.19}$$

Because intrinsic noise originates from the small number effects, cell size has great effect on intrinsic noise. Smaller size results in larger variance. Supposing in a eukarytic cell, a kind of protein can freely cross the nucleus membrane. Random noise is more significant to the nucleus protein concentration than the cytoplasm concentration [156].

Thus deterministic methods represented by ODEs can be used to explore QS network responses in parameter space and noise by parameter heterogeneity. Stochastic chemical reaction model can be used to calculate intrinsic noises of QS network to compare with noise caused by parameter heterogeneity.

2.4 Quorum Sensing Models

QS network belongs to cellular network. The core methods of QS network are intrinsic and stochastic models mentioned above. Some models included the environment geometry and individual cell heterogeneity. *V.fischeri* QS system is the earliest found QS system. James et al. developed a QS network model of *V.fischeri* based on ordinary differential equations using deterministic methods. This model treated the external AHL concentration as fixed values and proved that the QS network can have 3 stationary solutions, one of which is unstable at some range of external AHL values, indicating two distinct luminescence states of *V.fischeri* at this range of external AHL concentrations [157]. A deterministic model of the las QS system of *P.aeruginosa* was built by Jack et al. This work firstly considered a homogeneous environment where the stationary AHL concentration is a function of bacteria biomass density ρ. When biomass density ρ is small, QS network will be at off state. When biomass density ρ is intermediate, QS network will have multiple stationary states. And when ρ is large, QS network will be at on state. Secondly, this work considered a heteroge-

neous environment, similar conclusions were reached with a more complex model. This work basically proved that QS is biomass density dependent [126].

The parameters of models built by James et al. and Jack et al. were not deduced from experimental results, and were kind of arbitrarily decided. This was probably due to lack of experimental data to estimate the required parameters. Goryachev et al. used parameters estimated from literatures to build *V.fischeri* QS models with different levels of complexity. Deterministic method showed that multi-stationary states of QS exist whether the process of LuxR dimerization exists or not. However, LuxR dimerization is critical for the stability of multi-stationary states when noise exists, showed by stochastic methods, under certain parameter values [128]. A later work also used parameters estimated from literature to build the QS network model of *P.aeruginosa* that included all rhl, las and pqs systems [127]. In both models, the extracellular AHL was considered fixed.

Due to lack of experimental data, the estimation of similar parameters in literature differ greatly. The details will be shown in chapter 3. It is important to build a framework to combine different types of data from various experiments to fit the parameters of QS network. There is another issue that most models did not explicitly express. AHL is a kind of very stable molecule [131], and this poses a problem of modelling QS in a batch culture. QS network contains two positive feedback loops which means that in QS model of batch culture, larger concentrations of AHL will result in higher AHL production rate. When QS is activated, the AHL accumulating rate is accelerating and quickly its concentration will reach an impossible level. Some models fixed the external AHL to solve this problem, resembling continuous cultures, like references [157, 128, 127]. Some models used very large AHL degradation rates, like reference [126]. Batch culture is much easier to set up than continuous culture in laboratory. This problem needs to be handled properly when simulating QS in a batch culture to compare with experiments.

2.5 Concluding remarks

Bacterial QS, biofilm physiology and EPS are critical in biofouling process. Effective inhibiting QS can greatly reduce biofouling. The structures of QS are well studied but the parameters in QS network are mostly unknown, but they are heterogeneous in individual cells. Studying QS response in parameter space and analyse noise by parameter heterogeneity help to better understanding QS. An application is to study whether QQ and QSIs have synergistic effects in inhibiting QS. EPS production essentially affect interactions in biofilms like cooperation and aggregation of bacteria. IBM mathematical modelling on relationship of EPS and population dynamics helps better understanding biofilm processes. Specifically, Pel and Psl EPS produced by *P.aeruginosa* play distinct roles in biofilm. Incorporating them in biofilm models helps to validate the hypothesis of their properties and provides a specific example of how EPS affects population dynamics in biofilm.

Chapter 3

Distinct QS network response topologies in parameter space and noise caused by parameter heterogeneity

3.1 Introduction

3.1.1 Quorum sensing network structure is well studied, but the kinetic parameters remain mostly unknown

Some bacteria species are able to activate or repress certain set of target genes when population density reaches certain threshold. This density dependent sensing is called quorum sensing (QS). Quorum sensing networks of species like *V.fischeri* and *Pseudomonas aeruginosa* have been studied intensively and the structures are well known [158, 116]. *V.fischeri* QS network is the prototype of gram-negative bacteria. However, like other cellular rate parameters, not enough data exist to accurately

Table 3.1: Parameters in Chapter 3

Symbol	Definition
σ	AHL diffusion rate through membrane
k_{RA}	Combination rate of LuxR and AHL
d_P	Dissociation rate of LuxR-AHL monomer
i_0	Basal production rate of luxR mRNA
r_0	Basal production rate of luxI mRNA
k_r	LuxR production rate per mRNA per unit time
k_i	LuxI production rate per mRNA per unit time
K_r	Half-saturation constant of luxR activation by QS
V_r	Maximum luxR production rate
K_i	Half-saturation constant of luxI activation by QS
V_i	Maximum LuxI production rate
d_R	LuxR degradation rate
d_I	LuxI degradation rate
d_A	AHL natural decay rate
k_Z	Dimerization rate of LuxR-AHL monomer
d_Z	Dissociation rate of LuxR-AHL dimer
R	LuxR protein
A	Intracellular AHL
P	LuxR-AHL monomer
Z	LuxR-AHL dimer
I	LuxI protein
i	luxI mRNA
r	luxR mRNA
A_e	Outracellular AHL
V_A	Maximum production rate of AHL per cell
m_c	Molecule per cell
S_T	Sum of deviation score
$\vec{B}$	all parameters
$f(P)$	A function of P, solving f(P)=0 will get the stationary P values
cv	Coefficient of variation
γ	normalized forward sensitivity index
A_T	QS switch on AHL threshold concentration.

estimate the values of QS network values. Although some QS models tried to use appropriate parameters deduced from existing experiments, the values estimated by different authors differ greatly among each other, even scale agreement were not reached for many parameters.

For autoinducer diffusion rate through cell membrane σ, Iiterature showed that intracellular and outracellular AHL concentrations reach equilibrium within $20s$ [125]. If equilibrium is approximately reached when in intra and outracelluar concentrations reaches 10% of their initial difference, σ is estimated to be greater than $0.115s^{-1}$. This is the only experiment to roughly measure the autoinducer permeability through membrane yet [129]. Based solely on this experiment, there were different estimation of σ values:$0.17s^{-1}$ [127], 0.08–$0.4s^{-1}$ [128] and $0.05s^{-1}$ for σ[159].

The synthesis rate of AHL by enzyme LuxI was fitted [127] to be $6.7 \times 10^{-4}s^{-1}$. Another model [128] used $0.45s^{-1}$. An estimation of fully QS induced *Proteobacteria* produce AHL at the order of 150 copies per cell per second [129]. *Pseudomonas putida* IsoF was reported to maximumly produce 384 copies per cell per second [130]
.

No experiments have been conducted to estimate the combination rate of LuxR and AHL k_{RA}. Some estimated values were reported: 3.4×10^{-6} to $3.4 \times 10^{-5}nM^{-1}s^{-1}$[128], $1.67 \times 10^{-3}nM^{-1}s^{-1}$ [127].

d_P is the dissociation rate of LuxR-AHL monomer. Estimated values ranging from 3×10^{-3} to $10^{-2}s^{-1}$ [128] or $0.17s^{-1}$ [127] were reported.

The basal production rates of luxI and luxR mRNAs, i_0 and r_0, are the production rates without the dimer Z. In one work [128], i_0 and r_0 were estimated to be $1.5 \times 10^{-4}s^{-1}$ and $3 \times 10^{-4}s^{-1}$ respectively. In another work [127], $r_0 = 1.67 \times 10^{-4}s^{-1}$ and $i_0 = 4.2 \times 10^{-4}s^{-1}$, which were quite similar to the previous one.

k_r represents the number of LuxR molecules produced by 1 luxR mRNA per unit time. Its value was estimated to be $1.6 \times 10^{-2}s^{-1}$ [128] and $0.115s^{-1}$ [127]. k_i

represents the LuxI production rate by 1 luxI mRNA per unit time. Its value was similarly reported to be $1.6 \times 10^{-2} s^{-1}$ [128] and $0.115 s^{-1}$ [127].

The QS activation of luxR and luxI gene dynamics was also different in various works. Michaelis-Menten kinetics was used to describe gene transcription, with $K_r = 2.94nM$, $V_r = 1.4 \times 10^{-2} nM/s$, $K_i = 90nM$ and $V_i = 6 \times 10^{-3} nM/s$ [128] (table 3.1). In another work, linear dynamics was used to describe gene transcription, where transcription rate is proportional to dimer Z concentration [127] . When the cell is at QS on state, the LuxR-AHL dimer concentration is large enough to cause significant difference in these two kinetics.

The degradation rate of protein LuxR d_R was estimated to be $3.33 \times 10^{-5} s^{-1}$ [127] and $2 \times 10^{-4} s^{-1}$ [128]. The degradation rate of protein LuxI d_I was estimated to be $1.67 \times 10^{-4} s^{-1}$ [127] and $5 \times 10^{-5} s^{-1}$ [128].

AHLs were described as very stable compounds, their degradation rates d_A were at the order of 10^{-6} –$10^{-5} s^{-1}$ [131]. AHLs are also bio-degradable [160]. In the model of ref [128, 161], AHL degradation was completely ignored. Ref [127] used $1.67 \times 10^{-5} s^{-1}$ for d_A.

k_Z is the dimerization rate of LuxR-AHL monomer. Ref [128] estimated it to be 1×10^{-5} to $3 \times 10^{-5} nM^{-1} s^{-1}$. Ref [127] estimated it to be $8.3 \times 10^{-4} nM^{-1} s^{-1}$. d_Z is the dissociation rate of LuxR-AHL dimer. Ref [128] estimated it to be $0.01 s^{-1}$. Ref [127] estimated it to be $0.17 s^{-1}$. Ref [132] used the value $3.85 \times 10^{-4} s^{-1}$.

The value of $k_Z \frac{k_{RA}^2}{d_P^2}$ was estimated to be $8 \times 10^{-12} nM^{-3} s^{-1}$ [132],$1.21 \times 10^{-9} nM^{-3} s^{-1}$ [128], and $8 \times 10^{-8} nM^{-3} s^{-1}$ [127].

Clearly, wide parameter regions for QS network kinetics were provided in literature. Therefore it is necessary to research on how the network response within the regions to understand QS dynamics in depth.

3.1.2 QS network kinetic parameter values are heterogeneous among individual cells

Although QS network kinetic parameters are currently unknown, evidence from literature shows that they are heterogeneous among individual cells. Isogenic bacteria cells in nearly identical environment can vary significantly in their phenotypes [73, 72]. The examples of non-genetic population heterogeneity are vast. The next division time of two nearby daughter cells produced by division of one mother cell are rarely the same [51], although their genetic information and local environment are nearly the same. Non-genetic heterogeneity of QS network was also observed. In identical environment, the fluorescence and QS turn on time of *V.fischeri* were different among individual cells. LuxR is the master regulator of *V.harveyi* QS and the luxR gene expression of *V.harveyi* is heterogeneous among individual cells[133].

With the advancement of technology, direct measurement of cellular network kinetic parameters is possible. Single gene expression network kinetic parameters of eukaryotic yeast cells were measured [23] and the standard error to mean of every parameter is near 0.5. This is direct evidence that kinetic parameter values are heterogeneous among individual cells in identical environment.

Non-genetic population heterogeneity in bacteria is caused by noise and bi-stable or multi-stable states of cellular network[155, 162, 163, 134]. To better understand QS network properties, how does changing parameter values and parameter heterogeneity contribute to noise and switching behaviour of QS network should be studied.

As *Vibrio fischeri* QS is the earliest found QS network and is the prototype of QS for gram-negative bacteria [158], therefore is used to study how QS network response properties depend on parameter values and how parameter heterogeneity affect noise and switching behaviour of QS network.

Table 3.2: Components of *V.ficscheri* QS network and their symbols

symbol	component
R	LuxR protein
A	intracellular AHL
P	R-A
Z	dimer of P
I	LuxI protein
r	LuxR mRNA
i	LasI mRNA
A_e	outracelluar AHL

3.2 Methods

3.2.1 Exploring *V.fischeri* QS network response in parameter space

Figure 2.3A shows the network of *V.fischeri* QS network, and the components and corresponding symbols are shown in Table 3.2.

ODEs of each components can be obtained from reactions of *V.fischeri* QS network (Figure 2.3, Table 3.2 and 3.3) are shown in equations 3.1–3.7.

$$\frac{dP}{dt} = k_{RA}RA - d_P P + 2d_Z Z - 2k_Z P^2 \tag{3.1}$$

$$\frac{dZ}{dt} = k_Z P^2 - d_Z Z \tag{3.2}$$

$$\frac{dR}{dt} = d_P P - k_{RA}RA + k_r r - d_R R \tag{3.3}$$

$$\frac{dr}{dt} = r_0 + \frac{V_r Z}{K_r + Z} - d_r r \tag{3.4}$$

$$\frac{dA}{dt} = d_P P - k_{RA}RA + \frac{V_A I(P)}{K_A + I(P)} - d_A A + \sigma(A_e - A) \tag{3.5}$$

$$\frac{dI}{dt} = k_i i - d_I I \tag{3.6}$$

$$\frac{di}{dt} = i_0 + \frac{V_i Z}{K_i + Z} - d_i i \tag{3.7}$$

Table 3.3: Reactions of *V.fischeri* Quorum Sensing Network

Reaction	Description	Rate
$I \rightarrow I + A$	Translation of LuxI protein	$V_A I/(K_A + I)$
$A_e \rightarrow A_e + A$	QS signal diffuse into cell from outside	σA_e
$A \rightarrow null$	QS signal diffuse outside cell from inside	σA
$A \rightarrow null$	Decay of QS signal	$d_A A$
$R + A \rightarrow P$	Combination of receptor protein R and QS signal A	$k_{RA} RA$
$P \rightarrow R + A$	Dissociation of P	$d_P P$
$R \rightarrow null$	Decay of LuxR protein	$d_R R$
$r \rightarrow r + R$	Translation of LuxR mRNA	$k_r r$
$null \rightarrow r$	Transcription of LuxR	$r_0 + \frac{V_r Z}{K_r + Z}$
$r \rightarrow null$	Decay of LuxR mRNA	$d_r r$
$i \rightarrow i + I$	Translation of LuxI mRNA	$k_i i$
$I \rightarrow null$	Decay of LuxI protein	$d_I I$
$null \rightarrow i$	Transcription of LuxI	$i_0 + \frac{V_i Z}{K_i + Z}$
$i \rightarrow null$	Decay of LuxI mRNA	$d_i i$
$2P \rightarrow Z$	Dimerization of P	$K_Z P^2$
$Z \rightarrow 2P$	Dissociation of Z	$d_Z Z$

Since dimer (Z) of the complex of LuxR and AHL (P) can activate many target genes, and stationary concentrations of other components can easily represented by P, concentration of P in this model can represent the on and off state of the network. At first, stationary solutions can be obtained by letting the left side of equations (3.1–3.7) be zero, by setting outracelluar AHL concentration A_e as a constant boundary. When the network reaches stationary state, we can write the concentration of every component as a function of P, as in equations 3.8–3.13.

$$Z(P) = \frac{k_Z}{d_Z} P^2 \tag{3.8}$$

$$r(P) = \frac{r_0}{d_r} + \frac{1}{d_r} \frac{V_r Z}{K_r + Z} \tag{3.9}$$

$$R(P) = \frac{k_r}{d_R} r(P) \tag{3.10}$$

$$i(P) = \frac{i_0}{d_i} + \frac{1}{d_i} \frac{V_i Z}{K_i + Z} \tag{3.11}$$

$$I(P) = \frac{k_i}{d_I} i(P) \tag{3.12}$$

$$A(P) = \frac{d_P P}{k_{RA} R(P)} \tag{3.13}$$

From equation 3.5, and 3.8–3.13, the QS network components can be solved numerically. The stationary solutions of QS network were analytically analysed to find possible topologies of response curve first. Then repeated experiments with each kinetic parameters randomized were done to see whether different response curve topologies still exist.

3.2.2 Noise and QS switching behaviour by parameter heterogeneity

Noise caused parameter heterogeneity is compared with intrinsic noise. The former was calculated using deterministic methods and the latter using stochastic methods.

Deterministic methods

Cellular network is described by ODEs. Concentrations of components can be represented by $\vec{X} = \{X_1, X_2, \ldots, X_M\}$ where M is the number of components. Reactions can be represented by $R_1, R_2, \ldots, R_N$ where N is the number of reactions. Reaction R_i is determined by components concentrations $\vec{X}$ and environmental conditions $\vec{Y}$.

$$R_i = R_i(\vec{X}, \vec{Y}) \tag{3.14}$$

The ODE of each components can be represented in equation 3.15

$$\frac{dX_i}{dt} = \sum_{j=1}^{N} \alpha_{ij} R_j(\vec{X}, \vec{Y}) \tag{3.15}$$

where α_{ij} is the change of X_i concentration per unit of R_j reaction. Let the left side of equation 3.15 be zero, we will get the equations of the network stationary state.

Stochastic methods

When the number of molecules is small, chemical reactions are subject to stochasticity. The reaction rate might be faster or slower than the expected reaction rate in equation 3.14. The probability that one specific reaction i occurs within an infinitesimal time dt is $g_i(\vec{X}, \vec{Y})dt$, where the probability function $g_i(\vec{X}, \vec{Y})$ is a function of all the components $\vec{X}$ and environmental parameters $\vec{Y}$. Suppose Δt is a sufficiently small value. During Δt, the change of components concentrations $\vec{X}$ can be ignored. The expected amount of i^{th} reactions is $R_i \Delta t$. Dividing the Δt into N equal parts, each part is dt. When N is very large, we can ignore the probability that more than 2 reactions occur within time dt (O(dt^2)). The expected times of reaction i is $N g_i dt = g_i \Delta t$, which should be equal to $R_i \Delta t$. Thus we have equation 3.16.

$$g_i(\vec{X}, \vec{Y}) = R_i(\vec{X}, \vec{Y}) \tag{3.16}$$

For the next infinitesimal time dt, the probability that the j^{th} reaction will occur one time is $R_j(\vec{X})dt$. In τ time, the probability that no reaction occur can be calculated this way. Divide τ into $N (N \to \infty)$ equal parts, and each part is $dt = \frac{\tau}{N}$.

The probability that no reactions will occur is $(\prod_j (1-R_j dt))^N = \prod_j (1-R_j dt)^N$. $(1-R_j dt)^N = (1-R_j\frac{\tau}{N})^N = (1-\frac{R_j\tau}{N})^{\frac{N}{R_j\tau}R_j\tau}$ when $N\to\infty$, this equals to $e^{-R_j\tau}$. So the probability that no reactions occur within τ is $M(\tau) = e^{-\sum_j R_j\tau}$. Let T be the random variable that the first reaction occurs at $[T, T+dt]$. The probability that T is between $(t, t+dt)$ is $M(t)(1-M(dt)) = \sum_j R_j e^{-\sum_j R_j t} dt$. So the probability density of T is shown in equation 3.17.

$$f(t) = \sum_j R_j e^{-\sum_j R_j t} = \lambda e^{-\lambda t}, \text{ with } \lambda = \sum_j R_j \tag{3.17}$$

During stochastic simulation, we first randomly generate the time for next reaction according to equation 3.17. Then another random variable decide which reaction will occur, according the role that the probability of the i^{th} reaction is $\frac{R_i}{\lambda}$. And the perform the reaction and update the concentration of components $\vec{X}$.

The algorithm metioned above is the basic stochastic reaction algorithm (SSA). The advantage is that the simulation is accurate. The disadvantage is that for highly complex systems, this algorithm will be very slow. *V.fischeri* QS is only moderately complex, so this basic algorithm is sufficient. Other stochastic reaction algorithms include *Explicit τ-leaping*, *Implicit τ-leaping*, *Quasi-steady State Approximation* and *Total Quasi-steady State Approximation*. They are summarized in the review work of reference [164].

Noise caused by parameter heterogeneity was calculated using deterministic methods while randomizing network parameters, assuming they obey Γ-distribution[23] with coefficient of variance (sd/mean) 0.1. Intrinsic noise was calculated using stochastic methods with fixed parameter values. They are firstly compared in single gene expression network and then in *V.fischeri* QS network.

The switching threshold and switching time heterogeneity caused by parameter heterogeneity was calculated by deterministic methods with randomized parameters, similar with the methods calculating noise. Variance in switching time caused by intrinsic noise was calculated by stochastic methods.

3.3 Results and Discussions

3.3.1 *V.fischeri* QS network baseline parameter values are fitted by experimental data from literature

The principles below can be used to calibrate parameters of *V.fischeri* QS network.

1. The outracellular AHL concentration approximately equals stationary intracellular AHL concentration [125].
2. The AHL threshold should be around 30 – 100nM or 10-50 molecules / cell [133, 22].
3. When $A_e = 0$, the network should only have low stationary solution.
4. When unactivated, the mRNA concentrations of luxR and luxI are less than 15 copies per cell. When activated, they are more than 25 copies per cell [165].
5. When activated, the LuxR concentration exceeds 150 copies per cell [133].
6. Parameter values should agree with existing experimental measured values.

For the first principle, Kaplan et al. found that extra-cellular and intra-cellular AHL concentrations differ less than 15% within 20s [125]. If we assume the diffusion rate of AHL through membrane ranges from 0.05–0.5s^{-1} as estimated by references [128, 127, 159], it is incompatiable with the estimation when the cell is quorum sensing activated. At stationary state, according to equation 3.5, $\frac{A-A_e}{A_e} = \frac{V_A}{\sigma A_e}$. When a cell is QS activated at A_e around 50nM [133, 22], the difference between intra-cellular AHL concentration A and A_e will be more than 10 folds, which greatly deviates from the measurement of Kaplan et al. The solution of this incompatiability in this work is to firstly allow larger σ values than those in [128, 127, 159] and secondly also allow larger difference for A_e and A. The time for AHL to reach equilibrium was

Table 3.4: Principles to fit parameters of *V.fischeri* QS network

Principle	Deviation Score
Switch on threshold A_T should be between 10–50m_c	$\Theta(10-A_T)\frac{10-A_T}{10}+\Theta(A_T-50)\frac{A_T-50}{50}$*
Max component concentration c_{max} does not exceed 15 when $A_e=0$	$\Theta(c_{max}-15)\frac{c_{max}-15}{15}$
Minimum component concentration c_{min} should exceed 25 when $A_e=50$	$\Theta(25-c_{min})\frac{25-c_{min}}{25}$
Stationary R exceeds 150 when $A_e=50$	$\Theta(150-R)\frac{150-R}{150}$

* $\Theta(x)=1$ if $x\geq 0, =0$ if $x<0$

only roughly measured by Kaplan. And that is only measurement of membrane permeability of AHL to date. It is highly possible that AHL has higher permeability than estimated on this rough data. Also Kaplan's experimental configuration resembles the batch culture, and the model in this work assumes constant A_e concentration which resembles the continuous culture [166] and allows for larger difference between A and A_e because flow will continuously take out AHL from the culture. So AHL inside cell have larger transportation rate which results from larger concentration difference between A_e and A. Another solution would be to assume that cellular AHL concentration is always equivalent to that of extracellular concentration. But this assumption presumes infinity of membrane permeability and AHL diffusion rate, which are quite unrealistic, and also the positive feedback loop of LuxI becomes meaningless under this assumption. Thus the first solution was used.

Each principle is manually assigned a deviation score. If principle i is satisfied, then the i^{th} score s_i is 0. Otherwise s_i equals the percentage of deviation from the maximum/minimum value. For example, when the network is unactivated, the stationary luxR mRNA concentration of r cannot exceed $15m_c$. Suppose with certain parameters $r=18m_c$, the deviation score of this principle is $\frac{18-15}{15}=0.2$. All deviation scores are listed in table 3.4. The total score S_T is the sum deviation scores of each principle. Thus S_T is a positive function of all the parameters $\vec{B}$. Greedy algorithm is used: Every step the parameters are moved along the direction of total score gradient

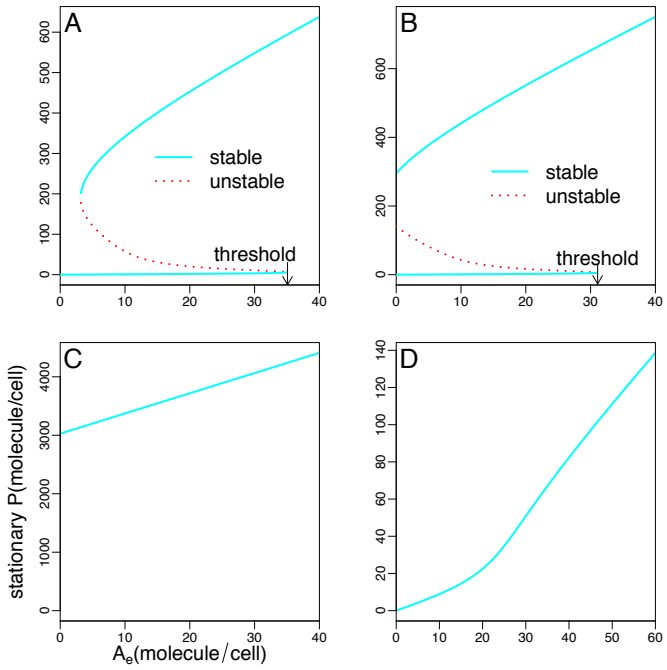

Figure 3.1: The response curve of stationary P to outracellular AHL concentration A_e of *V.fischeri* quorum sensing network. Figure A,B,C and D are produced with parameter sets A,B,C and D in table 3.5 respectively.

$\nabla S_T(\vec{B})$ until S_T is zero or very small. There is a large region of parameters that satisfies the principles mentioned above. One set of them is shown in table 3.5 (set A). This value set will be the baseline value in further analysis.

Apparently, current available data was not enough to fit most of the parameters in the LuxI/R quorum sensing network *V.fischeri*, although it is the earliest found QS network. When all the fitting principles are satisfied, there is still a wide space of possible parameter region. Accurate parameter measurement and quantitative experimental data can increase the accuracy of the *V.fischeri* QS model.

3.3.2 QS network response curve topology is dependent on interaction strength

Four response curves of stationary LuxR-AHL P to external AHL concentration A_e with different topologies were found in *V.fisheri* QS network as shown in figure 3.1.

Using fitted baseline values (set A in table 3.5) for each parameter, at a single extracellular AHL concentration A_e value, stationary P concentration has one or three solutions. When there are three solutions, one of them is unstable (figure 3.1 A). The stationary P concentration to extracellular AHL concentration A_e curve has a hysteresis loop. Supposing that initially $A_e = 0$ and the cell is at stationary state with lower P value. QS is off at this state. Slowly increasing the extracellular signal concentration only increases P at a small level. However, when A_e is increased above a threshold value, P will jump from low concentration to high concentration and QS will turn on. If initially the cell is at QS on state, slowly decreasing the signal will not turn QS off at the turn-on threshold but at some value lower beyond the turn-on threshold.

When parameter set B in table 3.5 is used, there are two stable solutions of stationary P when $A_e = 0$ (figure 3.1 B). When initially the network is at off state, slowly increasing A_e will turn on the network similarly with that using parameter set A. However,when the QS network is initially at on state, slowly decreasing A_e will not turn the network off even when A_e reaches 0.

When parameter set C in table 3.5 is used, there will be only one high stationary P solution for any A_e. That indicates the network will be always at on state regardless of the concentration of A_e.

When parameter set D in table 3.5 is used, the response curve becomes continuous (figure 3.1 D). There is only one stationary P solution for any A_e values. Pattern D is different from pattern C. Pattern D is that when A_e is small, stationary P is low and when A_e is large, stationary P is high. Also at small A_e, stationary P increases slowly

Table 3.5: Parameters and their values of *V.fisheri* QS network

Parameters	set A*	set B	set C	set D	unit	reference
σ	0.944	0.9252	0.5923	1.075	s^{-1}	[125, 129, 127, 159]
V_A	61.722	62.852	54.848	51.435	m_c/s*	[129, 130]
K_A	539.312	532.946	302.002	632.685	m_c	fitted
k_{RA}	9.49×10^{-5}	9.677×10^{-5}	1.085×10^{-4}	1.11×10^{-4}	$m_c^{-1}s^{-1}$	[128, 127]
d_P	0.006265	0.00614	0.003931	0.008302	s^{-1}	[128, 127]
r_0	1.85×10^{-4}	1.85×10^{-4}	3.172×10^{-4}	0.003108	m_c/s	[128, 127]
i_0	6.217×10^{-5}	6.217×10^{-5}	9.98×10^{-5}	7.949×10^{-5}	m_c/s	[128, 127]
d_r	4.286×10^{-4}	4.201×10^{-4}	2.69×10^{-4}	6.002×10^{-4}	m_c/s	[167, 168]
d_i	5.682×10^{-4}	5.615×10^{-4}	3.182×10^{-4}	2.634×10^{-4}	s^{-1}	[167, 168]
V_r	0.01776	0.01811	0.01424	0.006083	s^{-1}	[128]
V_i	0.06853	0.06933	0.06957	0.01778	m_c/s	[128]
K_r	1.403	1.401	0.6756	1.24	m_c	[128]
K_i	41.641	41.291	38.435	48.684	m_c	[128]
k_r	0.007794	0.007948	0.008906	0.009777	s^{-1}	[128, 127]
k_i	0.00715	0.007234	0.01143	0.00244	s^{-1}	[128, 127]
d_R	6.139×10^{-4}	6.017×10^{-4}	3.852×10^{-4}	8.114×10^{-4}	s^{-1}	[128, 127, 169]
d_I	8.294×10^{-4}	8.196×10^{-4}	4.644×10^{-4}	0.003845	s^{-1}	[128, 127, 169]
d_A	3.0×10^{-6}	3.0×10^{-6}	3.0×10^{-6}	4.216×10^{-6}	s^{-1}	[131]
k_Z	8.241×10^{-6}	8.322×10^{-6}	9.694×10^{-6}	8.292×10^{-6}	$m_c^{-1}s^{-1}$	[128, 127]
d_Z	0.0191	0.01891	0.011	0.01576	s^{-1}	[128]

* Parameter values in set A are the fitted parameters

m_c: molecules/cell

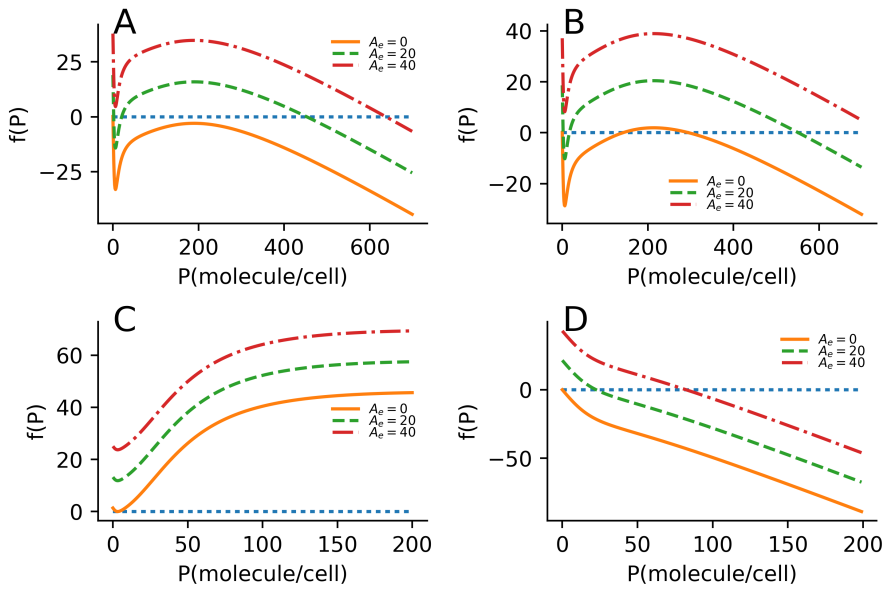

Figure 3.2: $f(P)$ to P for different parameter sets. Figure A,B,C and D are the results using parameter sets A,B,C and D in table 3.5 respectively. $f(P)$ is defined in equation 3.18. When parameter set C is used, only part of the $f(P)$ to P curve is shown in figure C. The unit of A_e is molecule/cell.

with A_e and at large A_e, stationary P increases quickly with A_e. The network can still be considered being turned on and off by extracellular AHL concentration A_e. But the hysteresis loop disappers compared to pattern A with baseline values.

From equations 3.8–3.13, stationary solution of the QS network can be solved by equation $f(P) = 0$ with $f(P)$ defined in equation 3.18.

$$f(P) = \frac{V_A I(P)}{K_A + I(P)} - d_A A(P) + \sigma(A_e - A(P)) = 0 \tag{3.18}$$

When parameter sets A, B or C are used, the curve of $f(P)$ to P has a local maximum $l_{max}(A_e)$ and a local minimum $l_{min}(A_e)$ (figure 3.2 A, B and C). Using parameter set A, $l_{max}(0) < 0$ and when $A_e = 0$, $f(P) = 0$ has one low solution. When A_e is intermediate, $f(P) = 0$ has 3 solutions, the middle of which is unstable. When $A_e = 40m_c$, $f(P) = 0$ only has one high solution. Thus the QS network is off when A_e is small, has multi-stable states when A_e is intermediate and is on when A_e is large, as in figure 3.1 A.

Using parameter set B, $l_{max}(0) > 0$ and $l_{min}(0) < 0$, $f(P) = 0$ has 3 solutions at

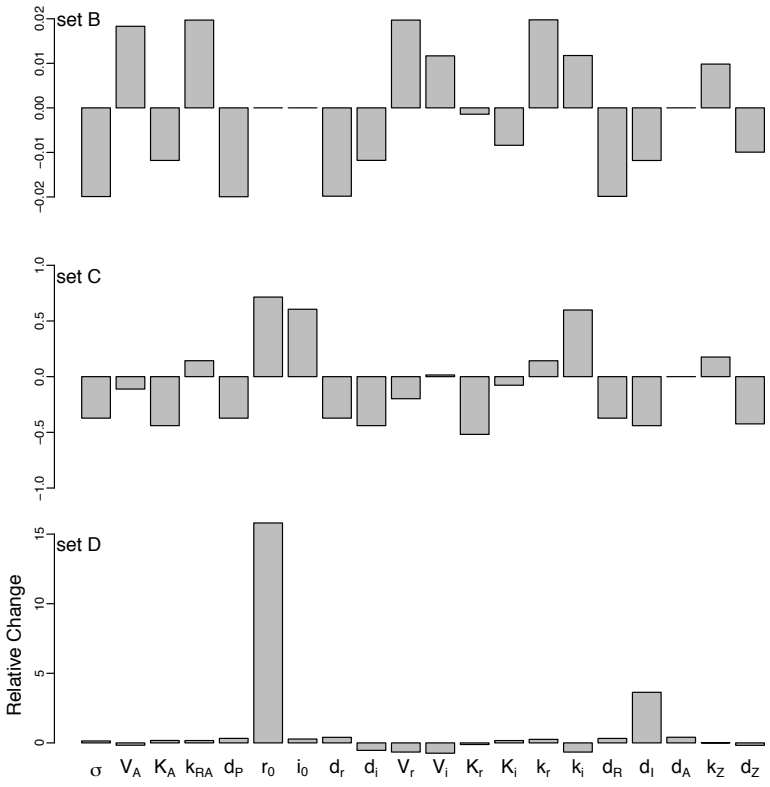

Figure 3.3: Relative fold changes of parameter sets B,C and D to set A.

$A_e = 0$, the middle of which is unstable. When $A_e = 40m_c$, $f(P) = 0$ will only have one high solution. Correspondingly, the QS network will have multi-stable states at $A_e = 0$. When A_e is large enough, the QS network is at on state.

When parameter set C is used, $l_{min}(0) > 0$, $f(P) = 0$ always has high solution, regardless of the value of A_e. Thus the QS network is only at on state.

With parameter set D, the topology of the curve of $f(P)$ to P changes. There is no local maximum and minimum (figure 3.2 D). The solution of $f(P) = 0$ is low when A_e is small and is high when A_e is large. But there is only one solution for any A_e. So the QS network can be turned on and off by A_e, only there is no multi-stable state.

Parameter set B was obtained by making $l_{max}(0) > 0$ and $l_{min}(0) < 0$. Parameter set C was obtained by making $l_{min} > 0$. In parameter set D, the local maximum of $f(P)$ disappeared, and $f'(P)$ was always negative (figure 3.2 D). From equation 3.18, we

know that $f'(P)$ is independent of A_e, thus if the parameter set makes $f'(P)$ at $A_e = 0$ negative, $f'(P)$ will always be negative. The maximum of $f'(P)$, f'_{max} can be treated as a function of parameters. Parameter set D was obtained by making $f'_{max} < 0$. The algorithm of obtaining parameter set B,C and D is similar with that of fitting parameter set A.

Relative fold changes of parameter sets B, C and D to set A are shown in figure 3.3. Comparing with parameter set B, which shifts the multi-stationary states to $A_e = 0$, none of the parameter deviates more than 2% of its baseline value in set A. Parameter set C has relatively larger average changes. But none of them exceeds 100%. Two parameters have significant changes in parameter set D, r_0 and d_I, which change 15 and 5 folds. Other parameters have relatively small changes.

V.fischeri quorum sensing network has two positive feedback loops: $R \to P \to Z \to r \to R$ and $I \to A \to P \to Z \to i \to I$. Deterministic model with fitted parameter set A predicts multi-stationary states at imtermediate levels of extracellular AHL. This is in agreement with literature that positive feedback loops can result in multi-stationary states [152, 153, 154].

Different parameter sets can even cause the change in the topology of stationary P to outra-cellular AHL A_e curve. It does not mean that wild type *V.fischeri* do have these four different response patterns found in this thesis. But it probably can be engineered to achieve this effect. It was shown in ref [170] that hysteresis loop can disappear for some parameter set in network consisting positive feedback. The bistability of glucose and lactose metabolic pathway in *E.coli* has been long studied. Lactose and similar molecules like thio-methylgalactoside (TMG) can induce the expression of lac operon. One of the genes in this operon laxY produces lactose permease which in turn enhance the transportation of TMG, thus producing a positive feedback loop. Operon lac is repressed at low TMG concentration (<3μm) and fully activated at high TMG concentration (>30μm). At intermediate TMG concentrations, the curve of lac operon expression and TMG concentration has a hysteresis loop, and in this

region, a single cell can have bistable phenotype. Mathematical model predicts that reducing the repression factor ρ can eliminate the hysteresis loop. This was experimentally proved by Ozbudak et al. by inserting plasmids with lac promoter, which competed the binding of repressor LacI and decreased the value of ρ. In strains with average 25 copies of this plasmid, the hysteresis loop disappeared [170]. In this work, a single value, the repression factor ρ was reduced around 30 folds (from 170 to 5). When the network was more complex and had more parameters,like the QS network of *V.fischeri*, much smaller changes in multiple parameters could result in the elimination of the hysteresis loop in the response curve. One result of decreasing the repression factor ρ is the increase of basal lac operon activity. That is because efficient repressor LacI exists at basal state is not enough. In the *V.fischeri* quorum sensing network model of this thesis, basal LuxR production r_0 increased most in parameter set D (15 folds), obtained by greedy algorithm, compared to paraemter set A. This means that, increasing the basal production rate of the key component in a positive feedback loop with multi-stationary states might eliminate the multi-stationary states.

3.3.3 Noise by parameter heterogeneity is less than intrinsic noise when network is repressed, and greater than intrinsic noise when expressed

In single gene expression network

Single gene expression network (figure 3.4 A) can be expressed by equations 2.17 [155]. where r represents mRNA and R represents protein. The half life time of mRNA is about minutes [171], hense the degradation rate of mRNA d_r is set to $0.001s^{-1}$ (5min half time). Considering that protein is more stable than mRNA[155], protein degradation rate is set to $d_R = 0.0001s^{-1}$. The translation rates of luxI and luxR mRNA in *V.fischeri* are around $0.01s^{-1}$ as fitted in this work. It was shown

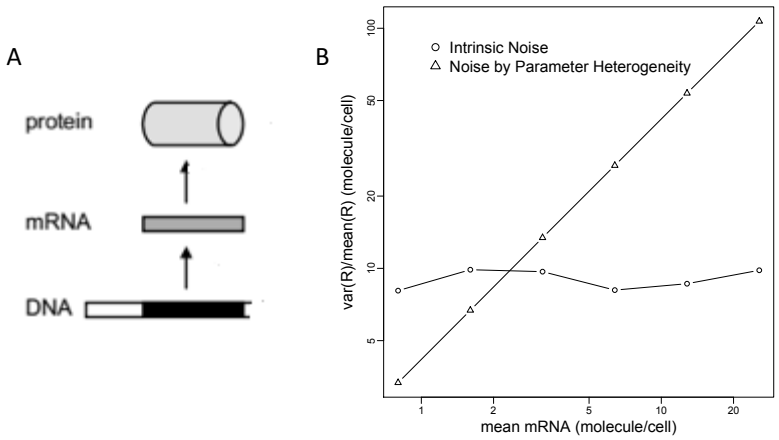

Figure 3.4: (A): Single gene expression network. (B): Noise by parameter heterogeneity and intrinsic noise in single gene expression network.

that the number of mRNA copies in *E.coli* is around 50 when expressed [172]. Considering *E.coli*'s cell volume is large, it is assumed that mean mRNA copy number of expressed gene is 20. Thus the set of parameter values are $k_r = 0.02s^{-1}, d_r = 0.001s^{-1}, k_R = 0.01s^{-1}, d_R = 0.0001s^{-1}$. It is assumed that they obey Γ distribution resembling the experimental results in reference [173] with coefficient of variation 0.1 while calculating noise caused by parameter heterogeneity. k_r was gradually decreased and the two noise were calculated, as shown in figure 3.4. Noise is represented by Fanto Ratio (variance/mean) of protein R.

Intrinsic noise barely changes with mean mRNA copy number but noise by parameter heterogeneity increases linearly with mRNA copy number. Thus when single gene expression network is repressed (mean mRNA ≤ 2), intrinsic noise is larger than noise by parameter heterogeneity. But when the gene is expressed (mean mRNA $\geq$ 10), noise by parameter heterogeneity will be larger than intrinsic noise.

Ozbudak *et al.* showed in single gene expression, the mRNA burst size (k_R/d_r, mean protein produced one mRNA) approximately equals to the time series Fanto Ratio of protein in a cell[155]. However, when parameter heterogeneity exists in the cell population, the population Fanto Ratio was not equal to the time series Fanto Ratio of a single cell[174] and thus is not equal to mRNA burst size, as shown in figure

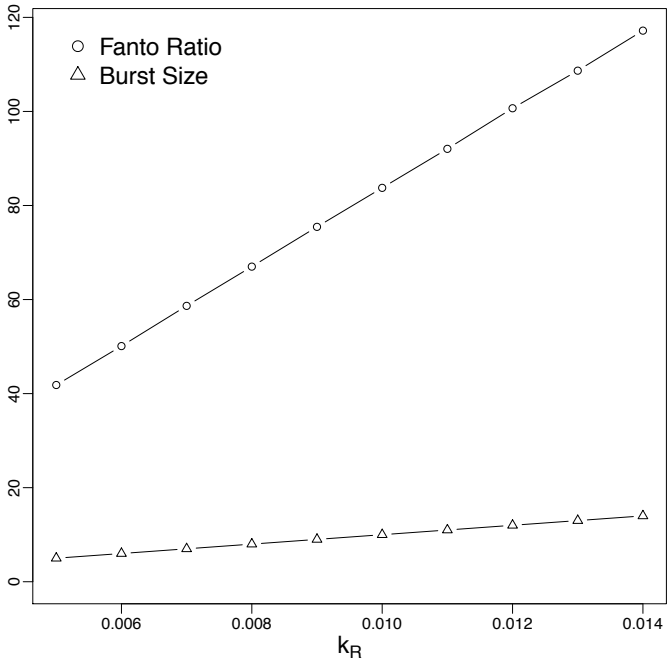

Figure 3.5: Comparison of population level protein Fanto Ratio and mRNA burst size in single gene expression network with parameter heterogeneity.

3.5.

In *V.fischeri* QS network

Teng *et al.* measured the copy number of the master regulator LuxR dimer in *V.harveyi* [133] and showed that the Fanto Ratio of LuxR is 12 at QS off state and increased to 50 at QS on state. Despite of a same name, LuxRs in *V.harveyi* and *V.fisheri* are not homologous. LuxR in *V.harveyi* is directly regulated by small mRNAs. However, they are both involved in the QS network of the two species and are repressed at low population density and expressed at high population density. The Fanto Ratio of LuxR in *V.fisheri* was calculated using stochastic methods and deterministic methods with parameter heterogeneity. The calculated data from *V.fisheri* QS network model will not be compared with the exact value of *V.harveyi* experimental data, but to see the trend of change in component Fanto Ratio from QS off to on state. The master regulator Z or P is not used because using fitted parameter set A, their values were

Table 3.6: Fanto Ratio of LuxR number predicted by different models

Fanto Ratio	QS off	QS on
Experiment of *V.harveyi*	12	50
Stochastic Model	8	1
Deterministic Model with Parameter Heterogeneity	0.2	22
Combined model	9	22

mostly 0 using stochastic modeling at QS off state. When the model includes stochastic methods, the sample size was 1000 and one sample was obtained by stopping the reaction when reaction time reaches $2 \times 10^4 s$ for QS off state and $1 \times 10^3 s$ for QS on state. As shown in table 3.6, simulations with only stochastic methods predict the Fanto Ratio of LuxR decreased from 8 to 1 when a cell was QS switched on. Using deterministic methods only with parameter variation, Fanto Ratio increased from 0.2 to 22. And combining the two sets of methods together, the model predicted that Fanto Ratio increased from 9 to 22, which fits the experimental trend best. Thus modelling and experimental data suggested that intrinsic noise dominates when QS is off and noise by parameter heterogeneity dominates when QS is on.

3.3.4 Parameter heterogeneity contributes significantly to QS network switching on threshold and time variation

For QS network with mutli-stationary states (parameter set A and B in table 3.5), the threshold value is the smallest A_e when the QS network has only high stationary solution for $f(P) = 0$ (equation 3.18). When the QS network has multi-stationary states, the curve of $f(P)$ to P has a local minimum l_{min} (figure 3.2 A and B) . The local minimum was calculated as a function of A_e, $l_{min} = l_{min}(A_e)$, and the solution of $l_{min}(A) = 0$ is the switching threshold of the QS network. The threshold can be solved numerically easily.

A sample of QS turning on threshold A_T with random parameters was obtained using

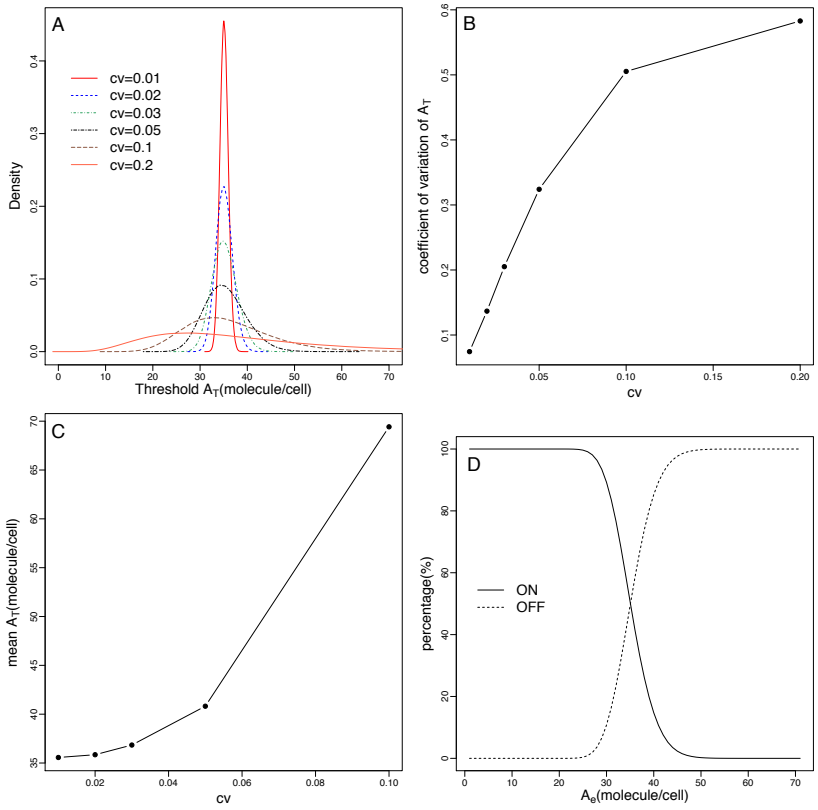

Figure 3.6: (A) Distribution of *V.fisheri* Quorum Sensing network switch on threshold (A_T). (B) Coefficient of variation (standard deviation / mean) of A_T. (C) Mean A_T at different parameter cv values. (D) Percentage of quorum sensing on and off to A_e with parameter $cv = 0.05$. Each parameters independently obeys Γ-distribution with mean equals its baseline value. The coefficient of variation (cv) is equal for all parameters. For a single value of cv, the sample size is 10^6.

values in parameter set A as the baseline values. The distribution of A_T was calculated by getting 10^6 samples. When parameters deviate from their baseline values, the switch on threshold A_T had a distribution shown in figure 3.6 A. When parameter cv increased, the shape of A_T density function became broader. Increasing parameter cv also increased the cv of A_T (figure 3.6 B). This meant that the mean A_T with the parameter distribution mentioned earlier is different from the A_T of a cell with mean parameter values (when $cv = 0$). This is in agreement with reference [173] that the behaviour of a cell with average parameters deviates from the average behavior of the population. The mean value of A_T also increases with cv (figure 3.6 C). The density distribution of A_T is non-Gaussian.

Parameter heterogeneity of individual cells caused the shift of QS switch on threshold. Thus , only a portion of the bacteria cells will be turned on at an appropriate homogeneous extracellular A_e concentration, and phenotypic separation was caused by the difference of turning on threshold. This was in agreement with experiment in reference [22].

Sensitivity analysis enables the understanding of how much change of the threshold value caused by the change of each parameters. The normalized forward sensitivity index [175] is used here as in equation 3.19.

$$\gamma_i = \frac{\partial A_T}{\partial b_i}\frac{b_i}{A_T} \tag{3.19}$$

A_T is the switch on threshold value of *V.fisheri* QS network when all parameter values were set to their corresponding baseline values; b_i is the baseline value of the i^{th} parameter used in the quorum sensing model. The normalized forward sensitivity index showed the percent of threshold change caused by 1 percent change of parameter near its baseline value. Assuming all parameters obey Γ-distribution with the same coefficient of variation (cv).The normalized sensitivity index is shown in figure 3.7. It was clear that the normalized forward sensitivity indexes of every parameter is less than 1.2. The indexes of k_{RA}, d_P, r_0, d_r,V_r,K_r,d_R,k_r ,k_Z, and d_Z are between 0.5 and 1.2. Those of the others are minimized. The result means that a small change of any parameter will not result in big difference of the turn on threshold of *V.fisheri* QS network. However, simultaneously variation of all the parameters might have more significant effects.

Switching time heterogeneity of *V.fischeri* can be caused by both parameter heterogeneity and intrinsic noise. When *V.fischeri* QS network is initially at off state and ourtracellular AHL exceeds its turning on threshold, it requires some time to turn on. Switching behaviours with deterministic model and an instance of stochastic model are shown in figure 3.8. In modelling analysis, it is assumed that initially the cell is at quorum sensing off state, and the component concentrations are equal to the stationary concentrations when $A_e = 0$. The ourtracellular AHL is assumed to be $100m_c$.

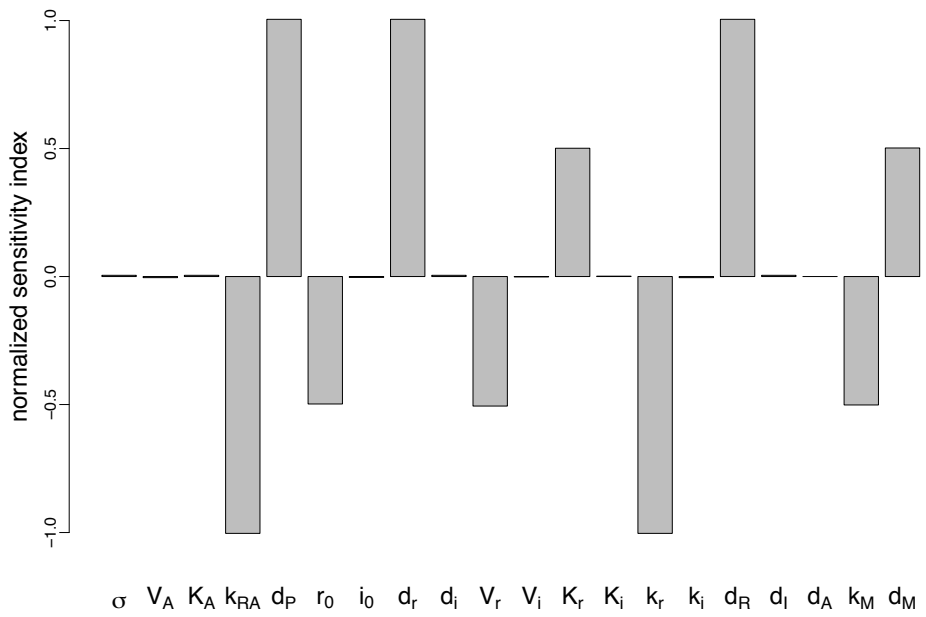

Figure 3.7: Normalized sensitivity indexes of each parameters used in *V.fisheri* QS network. The normalized sensitivity indexes are calculated using equation 3.19 and with the baseline parameter values (parameter set A)

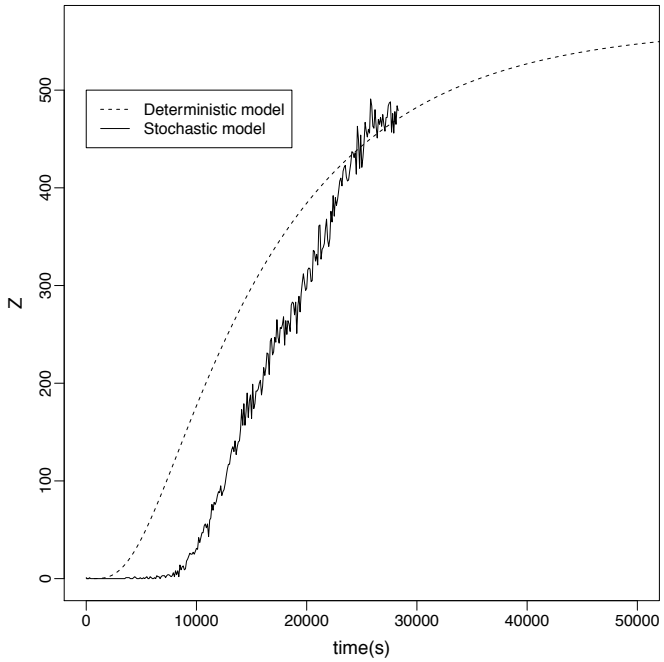

Figure 3.8: Switching behaviors of deterministic and stochastic models of *V.fischeri* QS network.

The network is treated as on when for every component, the difference to final concentration X_{100} is less than 0.1 of its initial difference ($X_{100} - X \leq 0.1(X_{100} - X_0)$). Using parameter set A, stochastic model predicted that the mean switching time is 32335s with standard deviation 6325s (from 22 samples). Assuming each parameters obeys Γ-distribution with *cv* 0.1, deterministic model predicts that the mean switching time is 35967s with standard deviation 9198s (from 10000 samples). Experimental results in reference [22] show that in *V.fischeri* QS network, when time ranges from 100-150 minutes, QS start to response to external AHL and after 150-250 minutes, QS will reach final on state. It is difficult to compute the contributions of intrinsic noise and parameter heterogeneity on the switching time heterogeneity from one-time experimental data. The simplest method is to measure the turning on time multiple times and see whether switching on times of the same cell have correlations.

3.4 Concluding remarks

QS is clearly correlated with biofouling. QS network structures are well studied, but parameters in QS kinetics are mostly unknown. The values of the same parameter used in literature strongly disagree with each other. It is necessary to analyse QS network properties within reasonable parameter region to improve the understanding of QS. On the other hand, literature shows that parameters of QS network are heterogeneous among individual cells even the environment is identical. This chapter analysed the noise caused by parameter heterogeneity in QS network by the comparison of it to QS network intrinsic noise and concluded that QS network response curve topology is dependent on both network structure and interaction strength. With the kinetic parameters aligned with literature, intrinsic noise is greater when gene is suppressed, while noise by parameter heterogeneity is greater when gene is expressed. This chapter provides a theoretical foundation of how QS network depends on interaction strength and deeper understanding of QS network noise caused by parameter

heterogeneity by comparing with intrinsic noise.

Chapter 4

Synergistic effects of quorum quenching enzyme and competitive binding quorum sensing inhibitor in inhibting *P.aeruginosa* QS circuit

4.1 Introduction

Bacterial quorum sensing(QS) can greatly impact microorganisms in waste water treatment plants [145]. Biofilm formation and dispersal were shown to be controlled by QS for species like *Pseudomonas aeruginosa* [176], *Staphylococcus aureus* [177] and *Vibrio cholerae* [178]. QS is also related to membrane biofouling in treatment plants and it was shown that quorum quenching(QQ) enzymes can reduce biofouling [179]. Thus controlling and inhibiting QS can greatly influence waste water treatment processes.

Substances that inhibit QS can be separated into two main groups. The first group is QQ enzymes, that target QS signals, and the second is the quorum inhibitors (QSIs),

Table 4.1: Parameters in Chapter 4

Symbol	Definition
V_A	Maximum production rate of AHL
d_A	Degradation rate of AHL
k_{RA}	Combination rate of LasR and AHL
d_P	Dissociation rate of LasR-AHL monomer
d_R	Degradation rate of LasR
k_r	Translation rate of LasR
r_0	Basal production rate of lasR mRNA
V_r	Maximum production rate of lasR mRNA by QS
β	Constant related to Vfr regulation
K_{r1}	Half-saturation constant of lasR production with Vfr
K_{r2}	Half-saturation constant of lasR production without Vfr
d_r	Degradation rate of lasR
k_i	Translation rate of lasI
d_I	Degradation rate of LasI
i_0	Basal production rate of lasI
d_i	Degradation rate of lasI
K_P	Dimerization rate of LasR-AHL
d_Z	Dissociation rate of LasR-AHL dimer
k_{RQ}	Combination rate of LasR and QSI
d_F	Dissociation rate of LasR-QSI
$\eta(QQ)$	Degradation rate of AHL by QQ
ρ	Cell volume fraction
V_b	Average cell volume
A_{max}	Maximum AHL concentration
G	G1
k_{RG}	Combination rate of LasR and G1

where interfere with QS components [144, 145]. QQ for AHL-based QS either degrades AHL lactone ring or the acyl side chain [144]. Competitive binding QSIs mimic natural AHL and bind to the receptor protein and compete with natural AHL for binding sites [147]. For example, LasR-specific antiactivator can bind to LasR and inhibit its activity. It was found that this inhibition mechanism is to prevent the dimerization of LasR [148].

The mechanisms and applications of these QS inhibitors remain to be studied. Furthermore, the combination effect of QQ and QSI has rarely been studied. Whether QQ and QSI interact with each other synergistically, act antagonistically or just have additive effects has not been proved. It is reasonable that they are synergistic because QQ targets at the signal AHL and QSI targets at the receptor, which interrupt the two positive feedback loops separately. Mathematical model and experiments are both needed to prove previously commented synergistic hypothesis.

One example of QQ is the AHL-lactonases, AiiA, which degrades AHL by hydrolysing its lactone ring [180]. As most gram-negative QS signals share the same lactone ring, theoretically, AiiA can degrade a wide range of AHLs. It has been experimentally shown that AiiA can degrade 3-oxo-C12-HSL and C4-HSL produced by *P.aeruginosa* las and rhl circuits, respectively. G1 as a QSI was found by structure-based virtual screening method. G1 is able to compete with natural AHL for the binding cite of LasR, therefore inhibit QS in *P.aeruginosa* PAO1. G1 was found to affect 46 proteins, including several virulence factors like elastase and chitinase [1].

The las and rhl QS circuits of *P.aeruginosa* interact with each other in a hierarchical manner, where the rhl circuit is under control of las curicuit. The most important feature is that LasR-AHL dimer directly controls the trancription of lasR gene [116]. In *P.aeruginosa* PAO1 strain, where both las and rhl circuits exist, G1 could only inhibit las system but cannot inhibit rhl system. However, when lasR was mutated, G1 can effectively inhibit rhl system [1]. The mechanism of this phenomenon needs to be studied and the inhibition effects on strains only containing las system or rhl

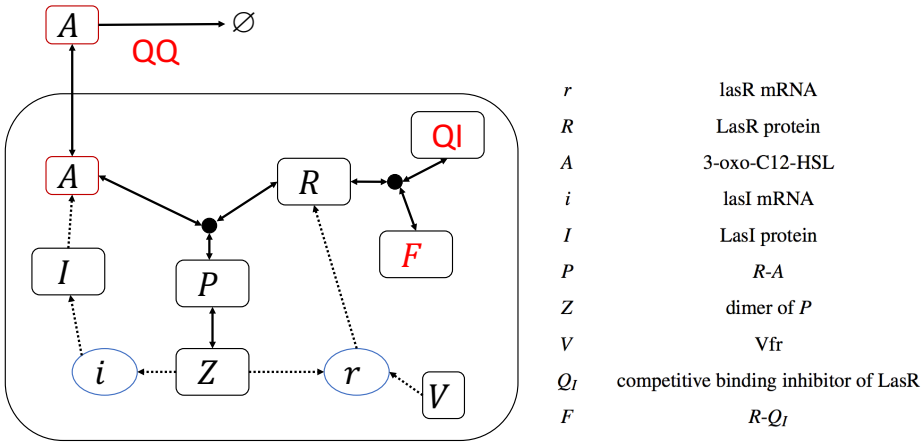

Figure 4.1: *P.aeruginosa* LasR/I QS circuit with QQ and QSI indicated in red. Dotted lines indicate the reactants still remains after the reactions, and solid lines indicate the reactants will disappear after the reactions.

system are of interest.

This work uses mathematical modelling of the *P.aeruginosa* LasR/I QS network in batch culture to investigate whether QQ and QSI have synergistic, antagonistic or additive effects on quenching QS. Then the effect of G1 on rhl system was specifically studied. The modelling results were then proved by experiments (conducted by Ms July Fong) using AiiA as QQ and G1 as QSI and some of the experimental results are also shown in this chapter for the purpose of comparison better understanding . The inhibiting effects of G1 on strains containing only las or rhl systems will be compared using modelling methods and followed by experimental validation.

4.2 Materials and methods

The LasR/I and RhlR/I QS circuits of *P.aeruginosa* are shown in figure 4.1. QQ and QSI are written as Q_Q and Q_I where necessary to avoid confusion. QSI binds to LasR similarly to AHL, however, AHL can stabilize LasR[148] but QSI cannot.

Table 4.2: Reactions of *P.aeruginosa* LasR/I Quorum Sensing Circuit

Reaction	Description	Rate
$I \rightarrow I + A$	Production of A	$\frac{V_A I}{k_A + I}$
$A \rightarrow null$	natural decay of A	$d_A A$
$R + A \rightarrow P$	Combination of R and A	$k_{RA} RA$
$P \rightarrow R + A$	Dissociation of P	$d_P P$
$R \rightarrow null$	Decay of LasR protein	$d_R R$
$r \rightarrow r + R$	Translation of lasR mRNA	$k_r r$
$null \rightarrow r$	transcription of lasR	$r_0 + V_r Z(\frac{1-e^{-\beta V}}{K_{r1}+Z} + \frac{e^{-\beta V}}{K_{r2}+Z})$
$r \rightarrow null$	Decay of lasR mRNA	$d_r r$
$i \rightarrow i + I$	Translation of lasR mRNA	$k_i i$
$I \rightarrow null$	Decay of LasI protein	$d_I I$
$null \rightarrow i$	Transcription of lasI	$i_0 + \frac{V_i Z}{K_i + Z}$
$i \rightarrow null$	Decay of lasI mRNA	$d_i i$
$2P \rightarrow Z$	Dimerization of P	$K_P P^2$
$Z \rightarrow 2P$	Dissociation of Z	$d_Z Z$
$R + Q_I \rightarrow F$	Combination of R and Q_I	$k_{RQ} R Q_I$
$F \rightarrow R + Q_I$	Dissociation of F	$d_F F$
$F \rightarrow Q$	Degradation of R in F	$d_R F$
$A \rightarrow null$	degradation of A by QQ enzyme	$\eta(Q_Q) A$

4.2.1 las circuit

P.aeruginosa QS networks have been intensively studied by experiments and models [181, 128, 127, 126, 182, 148, 183]. The reactions of LasR/I QS circuit are shown in table 4.2.

Since we are only interested in whether QQ and QSI have additive, synergistic or antagonistic effect in inhibiting QS, some complex features in the QS network can be simplified to make the model easier to implement and reduce computational cost. Models only tell the stationary concentrations of QS components given QQ and QSI with final cell volume fraction ρ of real growing cluture. Time for QS to turn on is much less than the time required for the growth of cell culture[22]. Successfully

inhibiting QS with fixed ρ is sufficient to inhibit QS in a growing culture where cell volume fraction finally reaches ρ. Cell heterogeneity is ignored and every cell is synchronized. AHL diffuses so fast that it is homogeneous inside and outside cells[125]. Vfr is assumed to be some large enough constant unless otherwsie indicated, as Vfr is normally expressed in experimental strains. The interactions of LasR/I QS circuit with other cellular components, such as the binding of 3-oxo-12HSL to RhlR[126], are ignored. QSI concentration is considered a constant because its concentration is sufficiently large. A maximum concentration of AHL A_{max} is set in the model to avoid extremely large concentration of AHL, while not affecting the question interested in.

The ordinary differential equations of each components are listed in equations 4.1 to 4.8. Stationary QS components are solved by letting the left side of these equations be 0.

$$\frac{dA}{dt} = \rho \frac{V_A I}{K_A + I} + \rho d_P P - \rho k_{RA} R A - d_A A - (1-\rho)\eta(Q_Q)A \tag{4.1}$$

$$\frac{dR}{dt} = k_r r + d_P P - k_{RA} R A - d_R R + d_F F - k_{RQ} R Q_I \tag{4.2}$$

$$\frac{dF}{dt} = k_{RQ} R Q_I - d_F F - d_R F \tag{4.3}$$

$$\frac{dr}{dt} = \frac{r_0}{V_b} + \frac{V_r Z}{V_b}\left(\frac{1-e^{-\beta V}}{K_{r_1} + Z} + \frac{e^{-\beta V}}{K_{r_2} + Z}\right) - d_r r \tag{4.4}$$

$$\frac{dP}{dt} = k_{RA} R A - d_P P + 2 d_Z Z - 2 k_Z P^2 \tag{4.5}$$

$$\frac{dZ}{dt} = k_Z P^2 - d_Z Z \tag{4.6}$$

$$\frac{di}{dt} = \frac{i_0}{V_b} + \frac{V_i}{V_b}\frac{Z}{K_i + Z} - d_i i \tag{4.7}$$

$$\frac{dI}{dt} = k_i i - d_I I \tag{4.8}$$

Most of the parameter values of *P.aerigunisa* LasR/I QS circuit are not known. They were firstly estimated from literature and then fitted to allow switching behaviour of the QS network, which was observed in experiments[22, 184]. These fitted parameters are shown in table 4.3.

Table 4.3: Fitted Parameters of *P.aeruginosa* LasR/I Quorum Sensing Circuit

Parameter	Value	Unit	References
V_b	1.37	μm^3	[185]
V_A	181.476	nM/s	[129, 130]
K_A	1585.6	nM	fitted
k_{RA}	3.2×10^{-5}	$nM^{-1}s^{-1}$	[128, 127]
d_P	6.265×10^{-3}	s^{-1}	[128, 127]
r_0/V_b	2.24×10^{-4}	nM/s	[128, 127]
i_0/V_b	7.52×10^{-5}	nM/s	[128, 127]
d_r	4.286×10^{-4}	s^{-1}	[167, 168]
d_i	5.682×10^{-4}	s^{-1}	[167, 168]
V_r/V_b	0.021	nM/s	[128]
V_i/V_b	0.083	nM/s	[128]
K_{r_1}	4.125	nM	[128]
K_{r_2}	50	nM	[128]
K_i	122.43	nM	[128]
k_r	7.794×10^{-3}	s^{-1}	[128, 127]
k_i	7.15×10^{-3}	s^{-1}	[128, 127]
d_R	6.139×10^{-4}	s^{-1}	[128, 127, 169]
d_I	8.294×10^{-4}	s^{-1}	[128, 127, 169]
d_A	3.23×10^{-6}	s^{-1}	[131]
k_Z	2.803×10^{-6}	$nM^{-1}s^{-1}$	[128, 127]
d_Z	0.0191	s^{-1}	[128]
k_{RQ}	3.23×10^{-5}	$nM^{-1}s^{-1}$	use K_{RA}
d_F	6.265×10^{-3}	s^{-1}	use d_P
A_{max}	20	μM	assumed

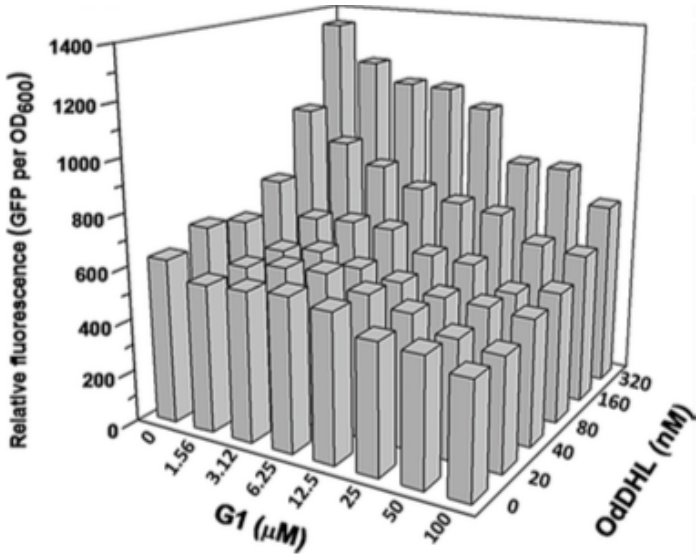

Figure 4.2: Normalized GFP to G1 and AHL concentrations in *E.coli* lasB-gfp strain (from reference [1]).

4.2.2 Quantify competitiveness of QSI to natural AHL

The competitiveness of QSI to natural AHL in binding receptor protein is hard to quantify. Because it is not only related to the binding rate, but also the dissociation rate of the binding product. Furthermore, the fact that AHL stabilize receptor protein adds to the complexity of quantification. On the other hand, experiments cannot directly measure the binding rates of QSI and AHL to receptor protein and the dissociation rates of the binding products. However, experiments can control the concentrations of QSI and AHL and measure the expression of target genes by the green fluorescent protein (GFP) (normalized by OD). For example, in *E.coli* lasB-gfp strain, where lasR-lasB-gfp genes were inserted as plasmids, GFP values were measured under various different concentrations of G1 and AHL [1].

A simple model is proposed to estimate the competitiveness of QSI to natural AHL from experiment data. In this model, it is assumed that lasR, lasB and gfp genes are activated by the same promoter LasR-AHL. Measured normalized GFP value is proportional to protein concentration, which is proportional to gfp mRNA concentration

and which in turn is proportional to lasR mRNA. Thus the model can be described by equations 4.9 to 4.12 regarding the components of lasR mRNA (r), LasR protein (R), AHL (A), LasR-AHL (P), G1 (G) and normalized GFP (GFP). Here a simple Monad kinetics was used the describe the relationship of transcription rate of r to P.

$$\frac{dr}{dt} = r_0 + V_r \frac{P}{K_r + P} - d_r r \tag{4.9}$$

$$\frac{dR}{dt} = d_P P - k_{RA} RA - d_R R + d_F F - k_{RG} RG \tag{4.10}$$

$$\frac{dP}{dt} = -d_P P + k_{RA} A \tag{4.11}$$

$$\frac{dF}{dt} = k_{RG} - d_F F - d_R F \tag{4.12}$$

where K_r is half saturation rate of P; d_r is the degradation rate of lasR mRNA and d_F is the dissociation rate of LasR-G1. Other parameters have the same meaning as those shown in table 4.2.

With this model, the stationary components can be written as equation 4.13.

$$[GFP] = \frac{k_2 k_f}{K_r} + \frac{k_2 \theta k_f}{k_4 K_r} + \frac{k_1 k_3}{k_r K_r} A[GFP] - \frac{\theta}{k_r} G[GFP] - \frac{k_3}{k_r K_r k_f} A[GFP]^2 \tag{4.13}$$

where $k_1 = \frac{r_0}{d_r} + \frac{V_r}{d_r}$, $k_2 = \frac{r_0}{d_r} K_r$, $k_3 = \frac{k_r}{d_R}$, $k_r = \frac{d_P}{k_{RA}}$, $[GFP] = k_f r$ and θ is shown in equation 4.14.

$$\theta = \frac{FA}{PG} = \frac{k_{RG} d_P}{k_{RA}(d_F + d_R)} \tag{4.14}$$

θ represents the ratio concentration of F caused by unit concentration of G to the concentration of P caused by per unit of A and thus can represent the competitiveness of G to A in binding with R. θ was estimated from equation 4.13 with multi-linear regression using experimental measured data $[GFP]$, A and G.

4.2.3 las and rhl circuits

Figure 4.3 shows *P.aeruginosa* QS network with both las and rhl systems. Components in las system are represented by subscript 1 which can be indicated by table

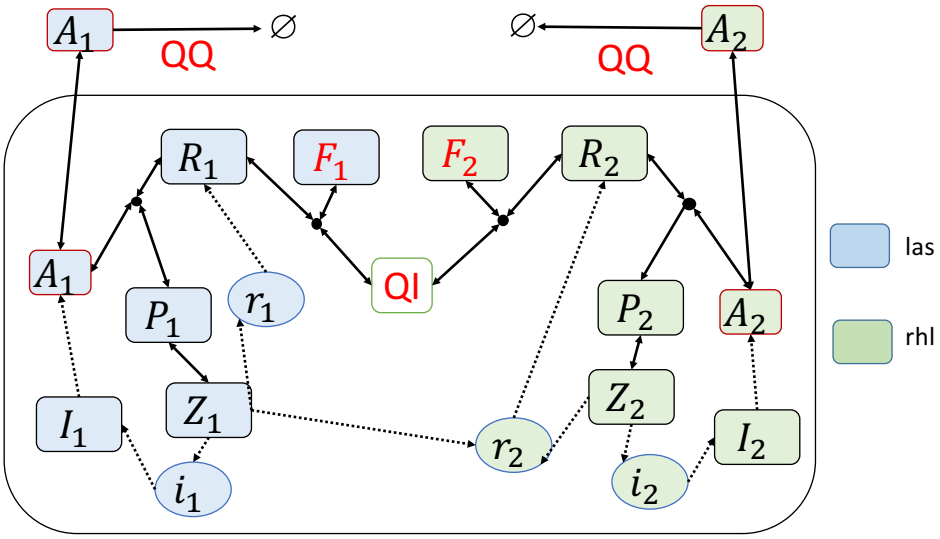

Figure 4.3: *P.aeruginosa* network structure with both las and rhl circuits.

4.2. Components in rhl system are represented similarly with subscript 2. i_2 and r_2 represent rhlI and rhlR mRNAs; I_2 and R_2 represent RhlI and RhlR proteins; A_2 represents C4-HSL or BHL; P_2 represents the binding product of RhlR and C4-HSL and Z_2 represents the dimer of P_2. F_1 and F_2 represent R_1-$G1$ and R_2-G1. The degradation rates of QQ to A_1 and A_2 are $\eta_1(QQ)$ and $\eta_2(QQ)$ respectively.

Only the most important interaction of las and rhl system was included in the model: Z_2 positively regulates the transcription of r_2. Here it is assumed that Z_1 and Z_2 bind to the same promoter of rhlR gene and act equivalently. As a result, the transcription rate of rhlR increased by Z_1 and Z_2 is $V_{r2}\frac{Z_1+Z_2}{K_{r2}+Z_1+Z_2}$. The other reactions and kinetic parameter values of rhl system are assumed to be the same as their corresponding parameter values in las system, for simplicity.

4.3 Results

4.3.1 Vfr increased turning on speed of QS

Vfr was shown to be able to directly bind the to promoter region of lasR and activate the transcription of lasR gene [181]. Let V be the concentration of Vfr and $\gamma(V)$ be the probability that Vfr is bound to the promoter region of lasR gene. Then we have equation 4.15 to solve $\gamma(V)$.

$$1-\gamma(V_1+V_2)=(1-\gamma(V_1))(1-\gamma(V_2)) \tag{4.15}$$

Thus we can get the binding probability $\gamma(V)$ expressed in equation 4.16.

$$\gamma(V)=1-e^{-\beta(V)} \tag{4.16}$$

Experimental data shows that Vfr will not affect the final QS status [181], thus it is assumed that Vfr promotes the binding of LasR-AHL dimer and lasR promoter represented by different half saturation constants of LasR-AHL which is shown in table 4.2.

The regulation of Vfr is complex with many unknown factors. In this model the concentration of Vfr was assumed to time invariant to show how Vfr affect the QS of *P.aeruginosa*. The time series concentration of LasR-AHL (P) at different Vfr concentrations are shown in figure 4.4. Vfr increases the speed of turning on QS but will not affect the final concentrations of LasR-AHL and other QS related components. This is in agreement with the work in reference [183].

As the focus of this work is the combined effect of QQ enzyme and QSI, in the further analysis of the *P.aeruginosa* QS model, Vfr is considered sufficient and the activation of lasR gene by LasR-AHL dimer (equation 4.4) becomes normal Monod Kinetics.

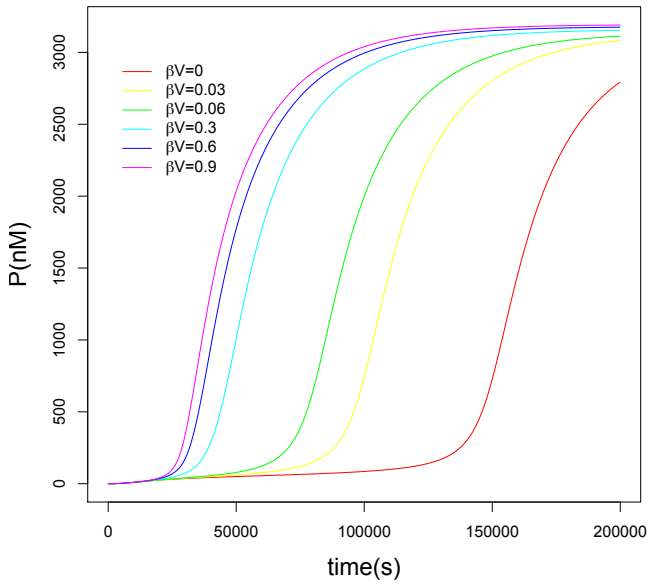

Figure 4.4: Time series concentration of LasR-AHL at different Vfr concentrations. V is the concentration of Vfr; $1-e^{-\beta V}$ is the probability that Vfr is bound to the promoter region of lasR gene.

4.3.2 Either QQ or QSI only could inhibit quorum sensing with low efficiency

When only QQ was added, simulation results in figure 4.5A show distinct on and off states of QS. When QQ concentration is low and $\eta(QQ)$ is small, stationary AHL concentration is very high. But when $\eta(QQ)$ exceeded a threshold, stationary AHL concentration suddenly decreased to an insignificant value. Similar switching behaviours have been observed in the simulation response curves of QS components to population size[186], cell volume fraction[126] or to external AHL concentration[128]. Switching behaviours of QS network have also been observed experimentally at individual cell level[22, 184]. Experimental results of time series GFP when adding AiiA alone (figure 4.5C) also showed inhibiting behaviour. But switching behaviour was not observed. The final GFP value (time = 15h) gradually decreased when increasing AiiA.

Simulation results of adding only QSI (figure4.5B) show similar switching behaviour.

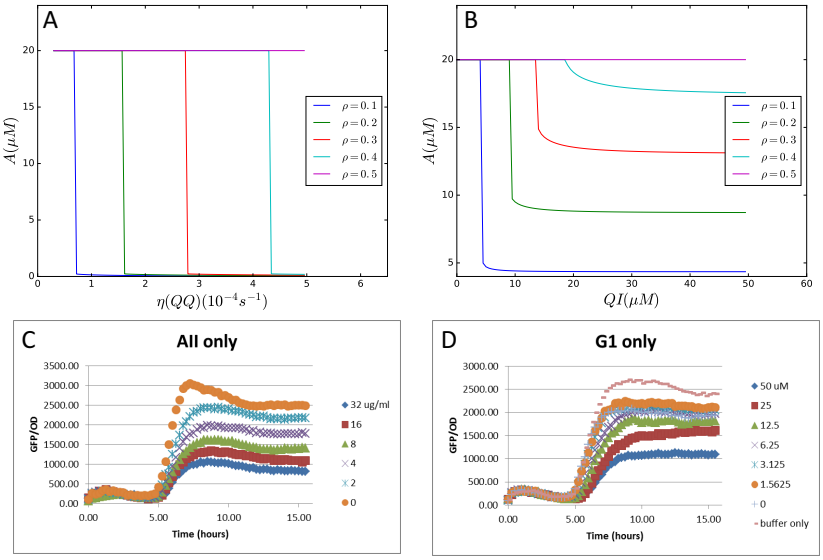

Figure 4.5: QS dynamics when only QQ or QSI is added. (A): Simulation results of stationary AHL concentration to $\eta(QQ)$. (B): Simulation results of stationary AHL concentration to QI. (C): Experimental time series GFP adding only AiiA. (D): Experimental time series GFP adding only G1.

However, stationary AHL concentrations are higher with sufficient QSI and the slope at the switching point is less steep, compared with simulation results of adding QQ alone at large ρ. Experimental results of adding G1 only are very similar with these of adding AiiA only. GFP gradually decreases with G1 and no switching behaviour was observed.

Both experimental and simulation results show that either QQ or QSI only can inhibit QS. In simulations, extremely high $\eta(QQ)$ or QSI concentration was needed to inhibit QS. In experiments, adding only AiiA or G1 can reduce GFP, but the remaining GFP values are still high (more than 1/3 of its original value).

4.3.3 Synergistic effects of combining QQ and QSI in inhibiting quorum sensing

Figure 4.6A shows the simulation results of stationary AHL to $\eta(QQ)$ curves at different QSI concentrations. When adding QSI alone, $15\mu M$ QSI is required to in-

hibit QS (figure 4.5B). However, when $0.5\mu M$ QSI is added, the minimum $\eta(QQ)$ required to inhibit QS reduced from $2.7 \times 10^{-4}s^{-1}$ to $0.8 \times 10^{-4}s^{-1}$. Thus, small amount of QSI can significantly enhance the inhibiting effect of QQ. Similarly, stationary AHL to QSI curves at different $\eta(QQ)$ values in figure 4.6B show that small $\eta(QQ)$ value can significantly enhance the inhibiting effect of QSI.

In experiments, different concentrations of G1 are mixed with 32 and 16 $\mu g/ml$ AiiA and the time series GFP data is shown in figure 4.6C and 4.6D respectively. Comparison with adding G1 or AiiA alone indicated that combining these two substances can result in much lower final GFP values and QS is inhibited more completely. Adding AiiA greatly enhanced the inhibiting effect of G1.

Both simulations and experiments showed strong synergistic effects between QQ and QSI in inhibiting QS. The synergy was quantitatively significant by examples: In simulations, $0.5\mu M$ QSI and $\eta(QQ) = 1 \times 10^{-4}s^{-1}$ could prevent QS from turning on, but neither 1 μM QSI alone nor $\eta(QQ) = 2 \times 10^{-4}s^{-1}$ alone had this capacity. In experiments, the final GFP value of the culture adding $16\mu g/ml$ AiiA and 12.5 μM G1 was twice lower than the final GFP adding $32\mu g/ml$ AiiA only and 3 times lower than the final GFP adding $25\mu M$ G1 only.

The simulation results of stationary AHL to QQ and QSI is plotted in 3D shown in figure 4.7A. A clear boundary of QS on and off states is observed which is shown in figure 4.7B. This curve is U-shaped which means that QQ and QSI have synergistic effect in inhibiting QS [187]. In this work $\eta(QQ)$ was assumed to be proportional to QQ. When Michaelis–Menten equation is used to describe the enzymatic dynamics[188] , stronger synergy between QQ and QSI is expected and the conclusion of simulation will remain the same.

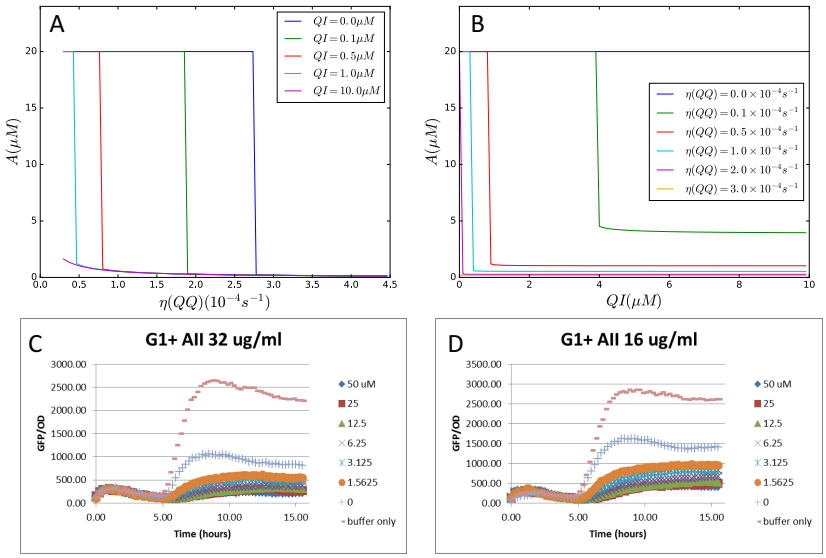

Figure 4.6: QS dynamics when QQ and QSI are combined. (A): Simulation results of stationary AHL concentration to $\eta(QQ)$ under different QI concentrations. (B): Simulation results of stationary AHL concentration to QSI concentration, with $\eta(QQ)$ assigned to different values. (C): Experimental time series GFP with $32\mu g/ml$ AiiA and different concentrations of G1 added. (D): Experimental time series GFP with $16\mu g/ml$ AiiA and different concentrations of G1 added. Cell volume fraction $\rho = 0.3$ for both (A) and (B).

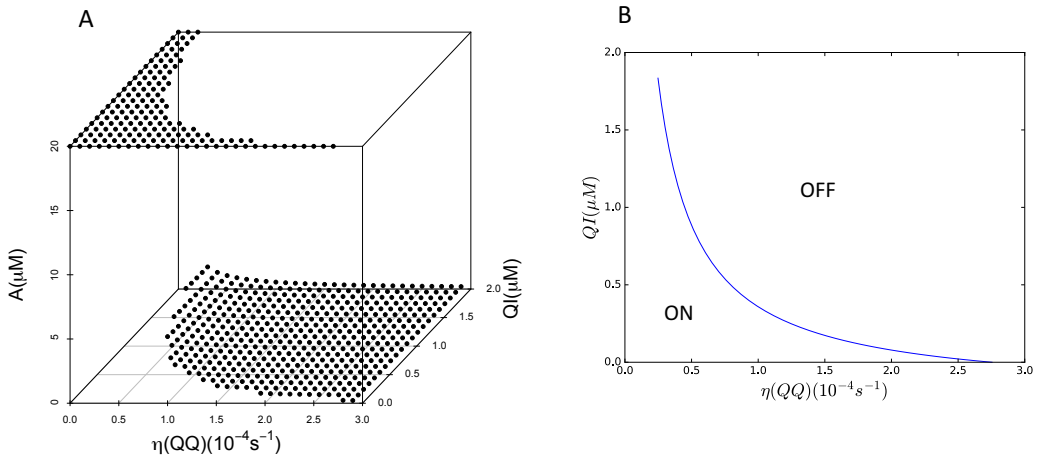

Figure 4.7: Simulation QS states to QQ and QSI. (A): 3D stationary AHL concentration to $\eta(QQ)$ and SQI. (B): 2D map of QS on and off states to $\eta(QQ)$ and QSI.

4.3.4 G1 inhibits mutant with only rhl system more effectively than mutant with only las system

To study the effect of G1 on mutants with only functioning las or rhls system, in the simulation the inhibition effect on rhl system was changed by using different values for k_{RG2}, the binding rate between RhlR and G1, and then compare the inhibition effect of G1 to rhl system in PAO1 and lasR mutant (Δ lasR). As it is assumed that rhl system does not control las system, the inhibition effect of G1 to las is the same in PAO1 and mutant containing only functional las system.

Firstly, the transcriptional rates of rhlR and rhlI were assumed to be the same as the transcriptional rates of lasR and lasI, that is $r_{20} = r_{10}, V_{r2} = V_{r1}, i_{20} = i_{10}, V_{i2} = V_{i1}$. Under this assumption, the binding rates of G1 to LasR and RhlR (k_{RG2} and k_{RG1}) represent the inhibition effects of G1 to las and rhl systems, respectively. When $k_{RG2} = k_{RG1}$, the inhibition effect of G1 to las is equal to the inhibition effect of G1 to rhl in lasR mutant, as shown in figure 4.8 B. In this situation, G1 has slightly higher inhibition effect on rhl system in lasR mutant than PAO1. When G1 inhibits las system more effectively in mutants containing only one functional system, as shown in figure 4.8 A with $k_{RG2} = 0.5k_{RG1}$, G1 inhibits rhl system similarly in ΔlasR and PAO1. When G1 inhibits rhl system more effectively in mutants, as shown in figure 4.8C, G1 inhibits rhl system more effectively in ΔlasR than in PAO1, which agrees with experimental results [1].

Secondly, it was shown that the rhl system is activated later than the las system [117]. It is assumed that the transcription rates of rhl system is half the transcription rates of las sytem: $r_{20} = 0.5r_{10}, V_{r2} = 0.5V_{r1}, i_{20} = 0.5i_{10}, V_{i2} = 0.5V_{i1}$. Same results were predicted by the model, that when G1 inhibits las system more effectively than rhl system in respective mutants containing only one functional system, G1 will inhibit rhl system similarly in PAO1 and ΔlasR (figure 4.9 A), and when G1 inhibits rhl more effectively than las in respective mutants, G1 will inhibit rhl more effectively in ΔlasR than in PAO1 (figure 4.9). Another conclusion from this simulation is that

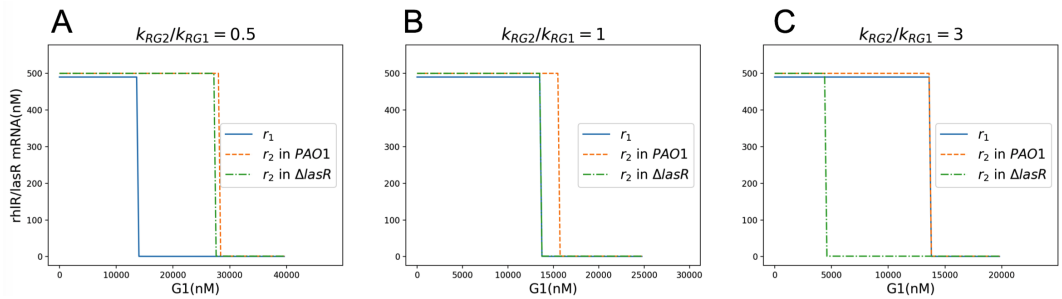

Figure 4.8: Concentrations of lasR and rhlR mRNA in PAO1 and ΔlasR mutant to G1. r_1 represents lasR mRNA; r_2 represents rhlR mRNA; k_{RG1} and k_{RG2} represent the binding rates of G1 to LasR and RhlR proteins, indicating the inhibition effects of G1 to the two systems, respectively. (A): When G1 inhibits las system more effectively, G1 inhibits rhl system similarly in PAO1 and ΔlasR . (B): When G1 inhibits rhl system similarly as las system, G1 will inhibit rhl system a bit more effectively in ΔlasR than in PAO1. (C): When G1 inhibits rhl system more effectively, G1 will inhibit rhl more effectively in ΔlasR than in PAO1.

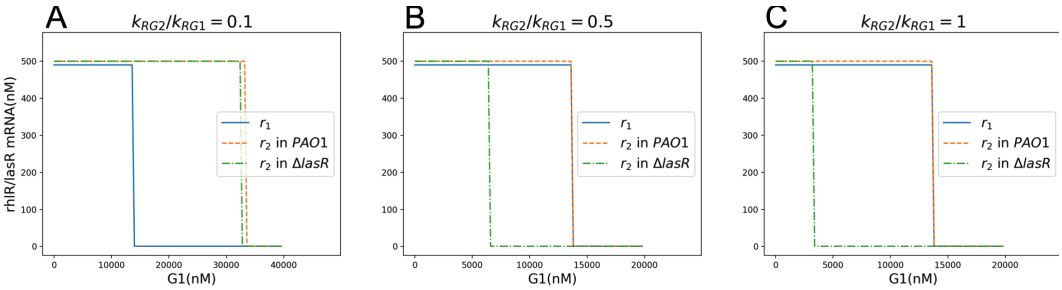

Figure 4.9: Concentration of lasR and rhlR mRNA in PAO1 and ΔlasR mutant to G1, when assuming the transcription rates of rhlR and rhlI is half the rates of lasR and lasI, respectively.

the inhibition effect of G1 is not only related to its competitiveness against natural AHL/BHL for competitor (equation 4.14), but also the kinetic rates with in the system like transcriptional rates.

The phenomenon in modelling results of figure 4.8 and 4.9 can be explained by a simple logic OR gate model as shown in figure 4.10. The transcription of rhlR is activated by both las and rhl system [116]. In lasR mutant, the minimum G1 requires to inhibit rhl system is c_1, and in rhlR mutant, the minimum G1 requires to inhibit las system is c_2. If $c_1 < c_2$, then, in PAO1 when the concentration of G1 is added to c_2, las system is still be active, which will activate rhlR, and thus rhl system will still be active. The concentration of G1 should be increased to c_2 to inhibit rhl system.

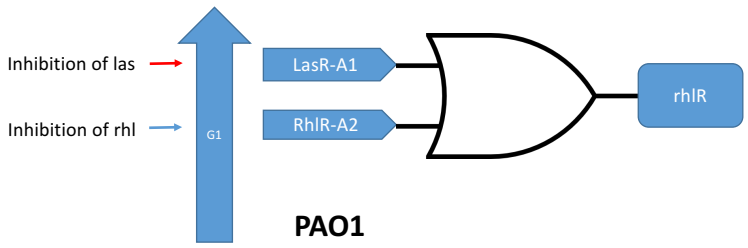

Figure 4.10: A simple logic OR gate model to describe the inhibition effects of G1 to las and rhl systems.

In ΔlasR mutant, when adding G1 with concentration c_1, the rhl system is already quenched. Thus G1 will inhibit rhl system more effectively in ΔlasR than in PAO1. According to the results in experiments [1] , it is more likely that G1 inhibits rhl system more effectively than las system in respective mutants.

The conclusion has been experimentally validated using ΔlasIΔrhlI double mutants as shown in figure 4.11. G1 can inhibit lasB-GFP only when added AHL concentration was smaller than $2.5\mu M$. When AHL exceeds this concentration, $50\mu M$ G1 has little effect in inhibiting las system. However, the inhibiting effect of $50\mu M$ G1 to rhl system was still significant when the concentration of BHL is $10\mu M$. Thus higher inhibition effect of G1 to rhl system was obvious.

In order to estimate the competitiveness of G1 to AHL or BHL in binding respective receptor, the binding rates of natural AHL/BHL with the corresponding receptor protein and the dissociation rates of the binding product need to be known (equation 4.13). According to references [128] and [127], $\frac{d_P}{k_{RA}}$ is at the scale of 100nM. Thus from experimental data using multi-linear regression of equation 4.13, the competitiveness of G1 to AHL in binding LasR is estimated to be $\theta_{las} \sim 10^{-3}$. The competitiveness of G1 to BHL is estimated to be $\theta_{rhl} \sim 10^{-2}$. G1 has higher competitiveness to BHL and inhibits rhl system more effectively in mutants. However, G1 inhibit las system more effectively in PAO1, due to the specific hierarchical structure of las and rhl system.

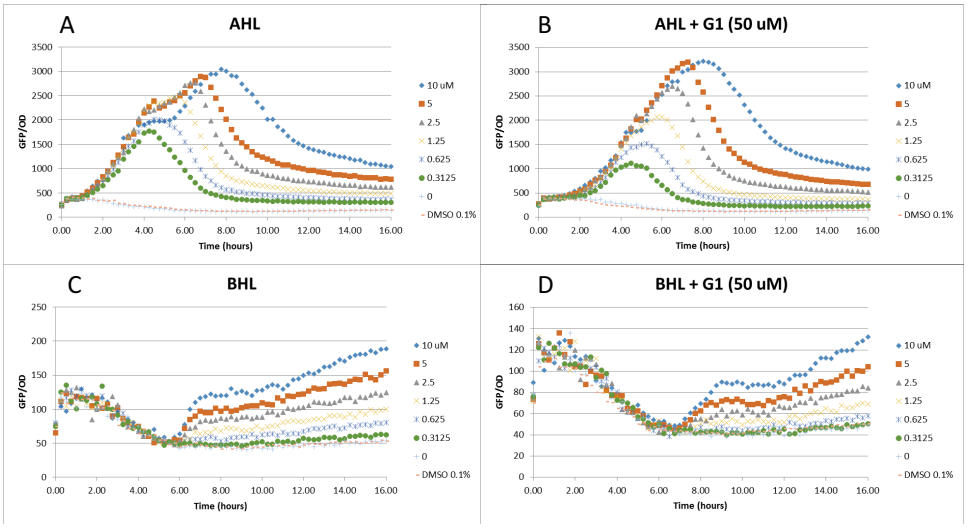

Figure 4.11: Experimental results showing that G1 has higher inhibition on system rhl than las in mutants with only respective system. (A) lasB-GFP of ΔlasIΔrhlI adding AHL. (B)lasB-GFP of ΔlasIΔrhlI adding AHL and G1. (C)rhlA-GFP of ΔlasIΔrhlI adding BHL. (D) rhlA-GFP of ΔlasIΔrhlI adding BHL and G1.

4.4 Discussions

Switching of QS circuit in the simulations was not observed in experiments. This is due to simplifications of the model, which assumes every cell is homogeneous and synchronized. However, bacterial cells are inherently heterogeneous [51], even when two cells produced by separation of the same mother cell[189]. Certain amount of QQ and QSI might be able to inhibit the QS of some cells but not others. Thus in the experiments measuring population level GFP, switching behaviour was not expected even if it exists in individual cells. In the work of reference[22] studying the heterogeneous response of *Vibrio fischeri* QS, switching behaviour was observed while tracking single cells but the population level fluorescence was a graded response. This is also the case in lactose utilization network in reference[170], where switching of the network was observed only in single cell but not at population level.

3-oxo-C12-HSL was shown to be able to stabilize LasR [148], but competitive binding QSI is not showing to have this ability. Thus when LasR is bound to AHL forming *P*, the LasR protein will not degrade and *P* can only be dissociated into LasR and

AHL. When LasR is bound to QSI forming F, the LasR protein will still be subject to degradation and thus not only F can dissociate into LasR and QSI but also F can change into QSI when the bound LasR is degraded. The fact that QSI cannot stabilize LasR is very important. Modelling results show that if QSI can stabilize LasR, then QSI only serves as buffer and make QS slower to turn on and turn off but will not affect the final stationary state.

4.5 Concluding remarks

Inhibiting QS is important to control water treatment processes like reducing membrane biofouling. In this work, mathematical modelling showed that QQ and competitive binding QSI have synergy in inhibiting QS. This conclusion has been validated by experiments. Experiments and modelling agreed with each other very well. Additionally, the results of both simulation and experimental showed that in mutants containing either functional las or rhl system, G1 inhibits the mutant with rhl system more effectively. However, in PAO1 containing both las and rhl system, G1 inhibits las more effectively due to the hierarchical structure of las and rhl QS circuits. This work has proposed a more effective way of inhibiting QS, and provided better understanding of QS network interaction with G1.

Chapter 5

Synergy of quorum quenching enzyme and ajoene analogue in inhibting *P.aeruginosa* quorum sensing

5.1 Introduction

As described in chapter 4, Quorum Quenching Enzyme (QQ) AiiA and competitive binding quorum sensing inhibitor (QSI) G1 have synergy in inhibiting *P.aerugisnoa* quorum seensing (QS). However, the drawback is that G1 is not very efficient. Its binding capability with receptor proteins is much lower than natural AHL/BHL. And because of its competitive binding inhibiting mechanism, G1 will hardly inhibit QS completely. A large concentration of G1 is needed in order to effectively inhibit QS in *P.aeruginosa* [1].

To overcome this disadvantage, some other QS inhibition substances with a different and more effective mechanism might be considered in combination with QQ. Ajoene

Table 5.1: Parameters in Chapter 5

Symbol	Definition
M_A	Cellular component RsmA
M_{YZ}	Cellular component RsmY and RsmZ
J	Ajoene analogue
M_J	Binding product of RsmYZ and Ajoene analogue
d_{YZ}	Degradation rate of M_{YZ}
d_J	Degradation rate of J
d_{MJ}	Dissociation rate of M_J
M_{YZ0}	Initial concentration of RsmYZ
σ_{YZ}	Related to RsmYZ dynamics
M_{A0}	Maximum concentration of RsmA
k_{r0}	Translation rate of mRNA without RsmA
k_r	Translation rate of mRNA with RsmA
b_1	Parameter b of las system as in chapter 4
b_2	Equivalent parameter b of rhl system

and its analogue can inhibit the translation of mRNAs in QS circuits [26]. Ajoene is a kind of sulfur-containing compound that can reduce the key QS related virulence factors [25]. One ajoene analogue replacing the allyl group with benzothiazole derivative was found to be more effective than ajoene in inhibiting QS and reducing virulence of *P.aeruginosa* [26]. The mechanism of inhibition is that ajoene binds with small RNAs rsmY and rsmZ and inhibits their activities [25]. Small RNAs rsmY and rsmZ act in parallel and inhibit the regulator RsmA. RsmA inhibits the translation of mRNAs in QS circuit [150, 151]. The net effect is that ajoene and its analogue inhibit the translation of mRNAs in *P.aeruginosa* QS circuits. Thus ajoene and its analogue are alternative candidates for G1 to inhibit QS in combination with QQ.

In this chapter, the combined effect of QQ and ajoene analogue was studied using mathematical modelling. The result was analysed and decide whether ajoene analogue is a better choice for competitive binding QSI G1 to inhibit *P.aeruginosa* QS.

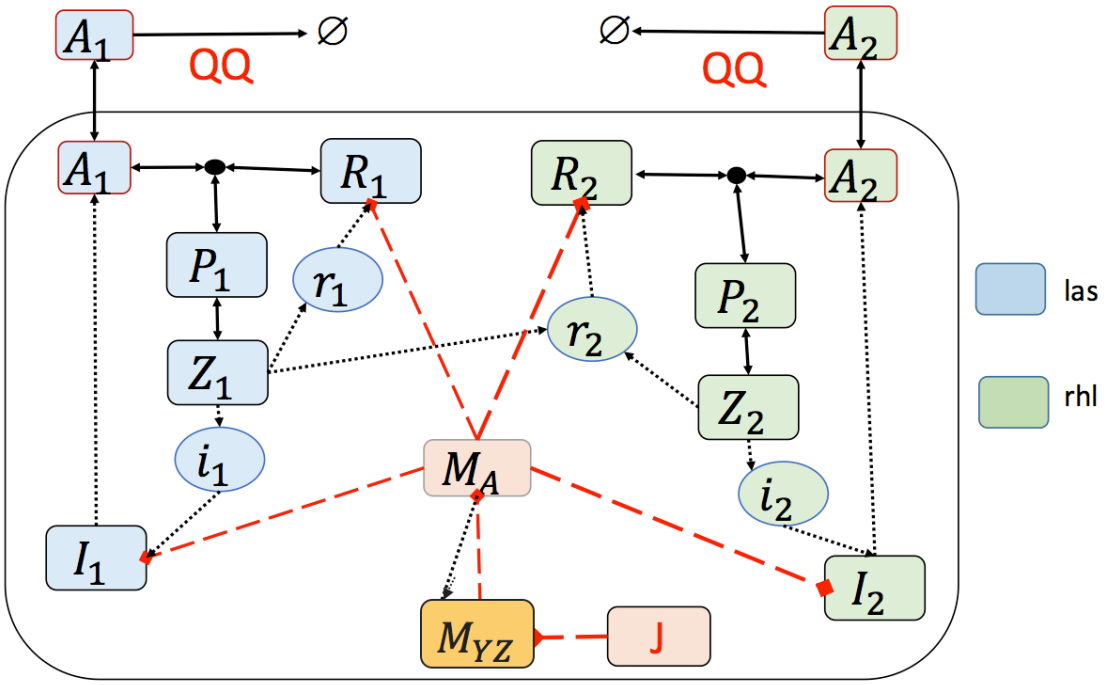

Figure 5.1: las and rhl QS circuits of *P.aeruginosa* with QQ and Ajoene analogue.

5.2 Materials and Methods

The network of *P.aeruginosa* las and rhl system with QQ, ajoene analogue and the substream network regulated by ajoene analogue is shown in figure 5.1. Ajeone analogue (J) inhibits the small RNAs rsmY and rsmZ. As rsmY and rsmZ act in parallel, they were treated as one component in this model and represented by M_{YZ}. rsmYZ binds to the regulator RsmA (M_A) and inhibits its activity. RsmA binds to the mRNAs involved in QS and inhibits their translations. Thus the overall effect of ajoene or its analogue is to inhibit the translation of lasR/I and rhlR/I mRNAs. The other components and their symbols are the same as those in chapter 4.

The binding product of of J and M_{YZ} is represented by M_J. The dynamics of M_J is shown in equation 5.1, where k_{MJ} is the binding rate of M_{YZ}, J and d_{YZ} is the degradation rate of M_{YZ}, d_J is the degradation rate of J and d_{MJ} is the dissociation

rate of M_J.

$$\frac{dM_J}{dt} = k_{MJ}M_{YZ}J - d_{YZ}M_J - d_JM_J - d_{MJ}M_J \tag{5.1}$$

As the concentration of J is large, it is assumed to be constant. Thus the effective concentration of M_{YZ} is described by equation 5.2.

$$M_{YZ} = M_{YZ0}\frac{1}{1+\frac{1}{d_{YZ}+d_J+d_{MJ}}J} = M_{YZ0}\frac{1}{1+\sigma_{YZ}J} \tag{5.2}$$

M_{YZ0} is the concentration of rsmYZ where no J is added. The inhibition of J to M_{YZ} can be described by one parameter σ_{YZ}. For simplicity, the inhibition effect of rsmYZ to RsmA is described by equation 5.3, where M_{A0} is the maximum concentration of RsmA. And the inhibition effect of RsmA to any mRNA r is described by equation 5.4. k_{r0} is the translation rate of the mRNA without RsmA, and k_r is the translation rate with the inhibition of RsmA.

$$M_A = M_{A0}\frac{1}{1+\sigma_{MA}M_{YZ}} \tag{5.3}$$

$$k_r = k_{r0}\frac{1}{1+\sigma_rM_A} \tag{5.4}$$

The reactions of QS components are the same as those in chapter 4, except that the translational rates are adapted by equation 5.4. The ordinary differential equations

of all components are represented by equation 5.5-5.18.

$$\frac{dA_1}{dt} = \rho \frac{V_{A1} I_1}{K_{A1} + I_1} + \rho d_{P1} P_1 - \rho k_{RA1} R_1 A_1 - d_{A1} A_1 - (1-\rho)\eta_1(QQ)A_1 \tag{5.5}$$

$$\frac{dR_1}{dt} = k_{r1} r_1 \frac{1}{1+\sigma_{R1} M_A} + d_{P1} P_1 - k_{RA1} R_1 A_1 - d_{R1} R_1 \tag{5.6}$$

$$\frac{dr_1}{dt} = \frac{r_{10}}{V_b} + \frac{V_{r1}}{V_b} \frac{Z_1}{K_{r1} + Z_1} - d_{r1} r_1 \tag{5.7}$$

$$\frac{dP_1}{dt} = k_{RA1} R_1 A_1 - d_{P1} P_1 + 2 d_{Z1} Z_1 - 2 k_{P1} P_1^2 \tag{5.8}$$

$$\frac{dZ_1}{dt} = k_{P1} P_1^2 - d_{Z1} Z_1 \tag{5.9}$$

$$\frac{di_1}{dt} = \frac{i_{10}}{V_b} + \frac{V_{i1}}{V_b} \frac{Z_1}{K_{i1} + Z_1} - d_{i1} i_1 \tag{5.10}$$

$$\frac{dI_1}{dt} = k_{i1} i_1 \frac{1}{1+\sigma_{I1} M_A} - d_{I1} I_1 \tag{5.11}$$

$$\frac{dA_2}{dt} = \rho \frac{V_{A2} I_2}{K_{A2} + I_2} - d_{A2} A_2 + \rho d_{P2} P_2 - \rho k_{RA2} R_2 A_2 - (1-\rho)\eta_2(QQ)A_2 \tag{5.12}$$

$$\frac{dR_2}{dt} = k_{r2} r_2 \frac{1}{1+\sigma_{R2} M_A} + d_{P2} P_2 - k_{RA2} R_2 A_2 - d_{R2} R_2 \tag{5.13}$$

$$\frac{dr_2}{dt} = \frac{r_{20}}{V_b} + \frac{V_{r2}}{V_b} \frac{Z_1 + Z_2}{K_{r2} + Z_1 + Z_2} - d_{r2} r_2 \tag{5.14}$$

$$\frac{dP_2}{dt} = k_{RA2} R_2 A_2 - d_{P2} P_2 - 2 k_{P2} P_2^2 + 2 d_{Z2} Z_2 \tag{5.15}$$

$$\frac{dZ_2}{dt} = k_{P2} P_2^2 - d_{Z2} Z_2 \tag{5.16}$$

$$\frac{di_2}{dt} = \frac{i_{20}}{V_b} + \frac{V_{i2}}{V_b} \frac{Z_2}{K_{i2} + Z_2} - d_{i2} i_2 \tag{5.17}$$

$$\frac{dI_2}{dt} = k_{i2} i_2 \frac{1}{1+\sigma_{I2} M_A} - d_{I2} I_2 \tag{5.18}$$

The copy number of one kind of sRNA in a bacterial cell was estimated to be 10000 [190]. In this model, the average cell volume of *P.aeruginosa* is $1.37 \mu m^3$, and thus 1 copy per cell is approximately equivalent to 1 nM. The estimation of the maximum concentration of sRNAs rsmYZ M_{YZ0} was estimated to be 10000nM. Similarly, regulator RsmA is a kind of protein and its concentration was estimated to be $2000 nM$ [191]. From experimental data in reference [26], σ_{YZ} σ_{MA}, σ_{R1}, σ_{I1}, σ_{R2} and σ_{I2} used values of 21.12, 0.011, 0.0069, 0.0069, 0.069 and 0.0051 nM^{-1}respectively. Other parameters were same as those in chapter 4. The final stationary concentrations of AHL/BHL in the batch culture were used to identify the QS states.

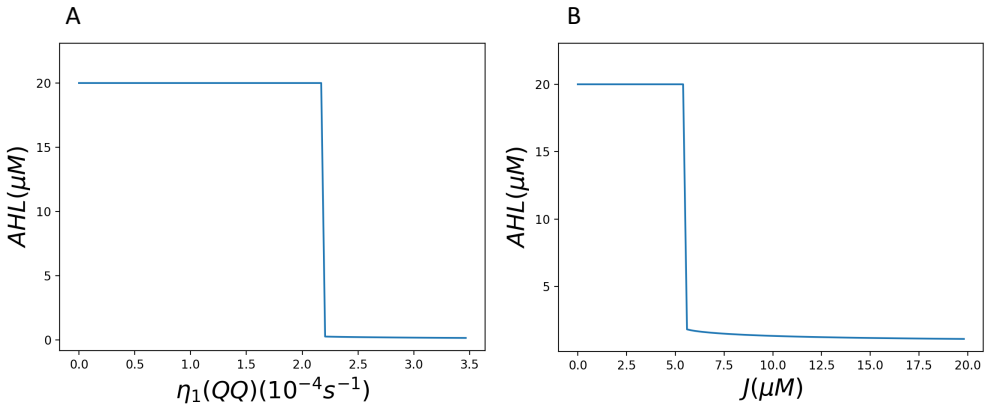

Figure 5.2: AHL concentration to $\eta_1(QQ)$ or Ajoene analogue (J) alone.

5.3 Results and Discussions

5.3.1 Synergy of QQ and ajoene analogue in inhibiting las circuit

When adding QQ alone, switching results were produced (figure 5.2A), same as that in chapter 4. $\eta_1(QQ)$ represents the degradation rate of QQ to AHL. Ajoene analogue alone can also inhibit quorum sensing (figure 5.2B) and it is comparatively more effective than competitive QSI G1 shown in chapter 4. It is intuitively reasonable because QSI binds with receptor proteins competitively with natural AHL, but the AHL can still function. Ajoene and its analogue inhibits the translation of mRNAs in QS system and thus inhibit QS more completely than competitive binding QSI.

When QQ and ajoene analogue J are combined, they strongly assist the inhibiting effect of each other. For example, $0.2\mu M$ J has little effect alone, however, when combined with QQ, it can halve the minimum $\eta_1(QQ)$ required to turn LasR/I circuit off, as shown in figure 5.3A. Similarly, adding QQ and making $\eta_1(QQ)$ $0.05 \times 10^{-4} s^{-1}$ has little effect alone, but when combined with J, the minimum J required to turn QS off is reduced more than twice as shown in fgure 5.3B. 3D plots of AHL concentration to $\eta_1(QQ)$ and J is plotted in figure 5.3C, a clear separation of on and off states was observed. The 2D on and off state is shown in figure 5.3D. The boundary between on and off states is "U"-shaped, similar to QQ and QSI, and thus QQ and J

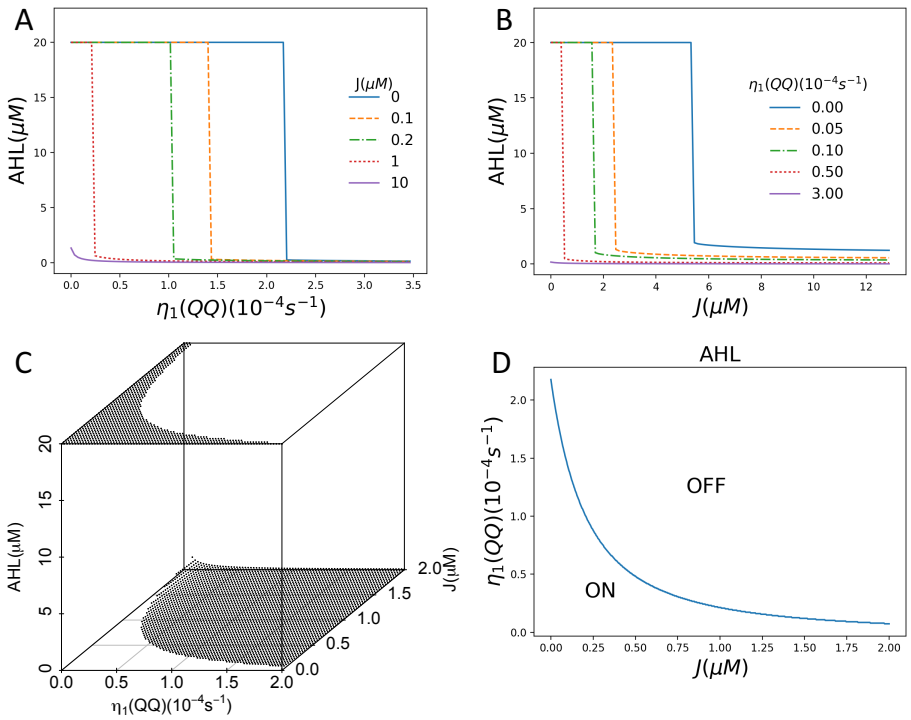

Figure 5.3: QS states of lasR/I circuit in *P.aeruginosa* to QQ and Ajoene analogue concentrations. (A) AHL concentration to $\eta_1(QQ)$ at different. (B) AHL concentration to J at different $\eta_1(QQ)$ values. (C) 3D plot of AHL concentration to $\eta_1(QQ)$ and J. (D) 2D on and off states to $\eta_1(QQ)$ and J.

also have synergy in inhibiting the las circuit of *P.aeruginosa* [187].

5.3.2 Synergy of QQ and ajoene analogue in inhibiting rhl circuit

Similar synergistic effect of QQ and Ajoene analogue in inhibiting rhl circuit has been observed in simulation as shown in figure 5.4. Small amount of J which has little effect on rhl system alone can greatly assist the inhibiting effect of QQ. And small value of $\eta_2(QQ)$ which is far from enough to turn rhl system off can significantly reduce the amount of J required to turn rhl system off. A clear boundary was also observed in the 3D plot of BHL concentration to $\eta_2(QQ)$ and J. The boundary was "U"-shaped as shown in figure 5.4D indicating that QQ and J have synergy in turning QS off.

QQ AiiA target at quorum sensing signals and degrade AHL and BHL in *P.aeruginosa*

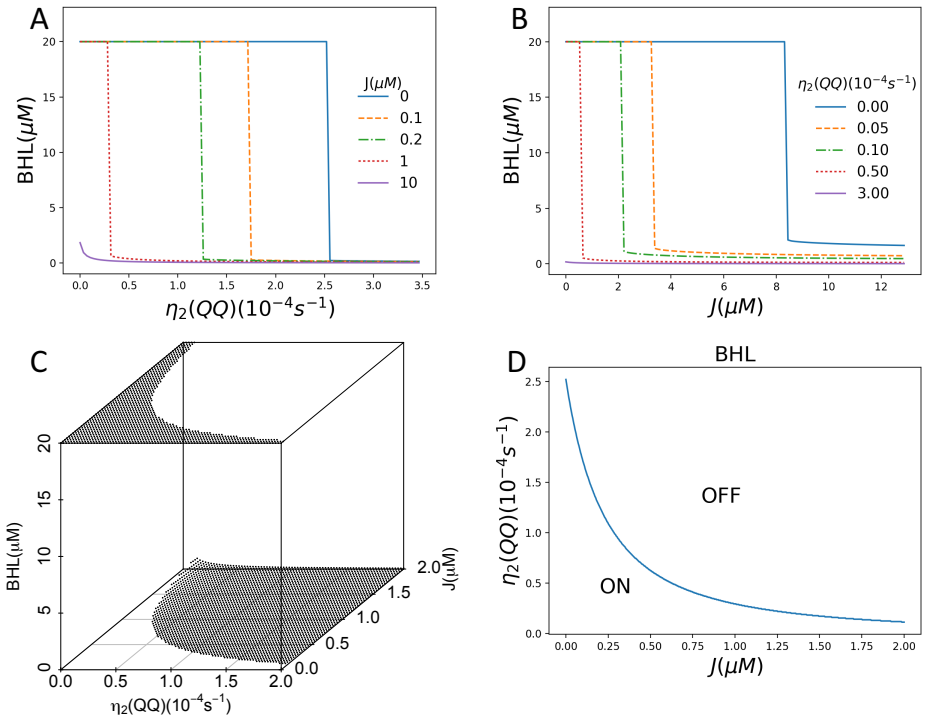

Figure 5.4: QS states of rhlR/I circuit in *P.aeruginosa* to QQ and Ajoene analogue concentrations. (A) BHL concentration to $\eta_2(QQ)$ at different. (B) BHL concentration to J at different $\eta_2(QQ)$ values. (C) 3D plot of BHL concentration to $\eta_2(QQ)$ and J. (D) 2D on and off states to $\eta_2(QQ)$ and J.

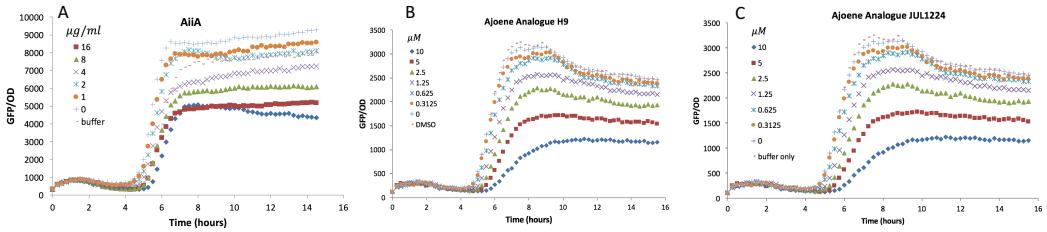

Figure 5.5: Inhibition effect of using QQ alone or ajoene analogues alone. (A): LasR-GFP to time at different AiiA concentrations. (B) LasR-GFP to time at different ajoene analogue H9 concentrations. (C): LasR-GFP to time at different ajoene analogue JUL1224 concentrations.

[192]. Ajoene and its analogues target the transcription process of lasR/I and rhlR/I mRNAs [25]. They inhibit QS under different mechanisms and have strong synergy when combined.

5.4 Experimental proof of synergy between AiiA and ajoene analogues in inhibiting las circuit

Experiments were done using AiiA as QQ and two ajoene analogues H9 and JUL1224 [26] (All the experiments were done by Ms July Fong. They are briefly discussed here of comparing purpose). As shown in chapter 4, AiiA only can inhibit las circuit at some level (figure 5.5 A). H9 and JUL1224 alone also have the capacity to inhibit las circuit, as shown in figure 5.5 B and C. When QQ and ajoene analogues are combined, much more complete inhibitions were shown. Figure 5.6 A shows the LasR-GFP to time combining AiiA and H9. Adding 10 μM H9 and 32 $\mu g/ml$ AiiA almost completely inhibit GFP. Similarly, AiiA combined with JUL1224 can reduce the LasR-GFP around 5 folds.

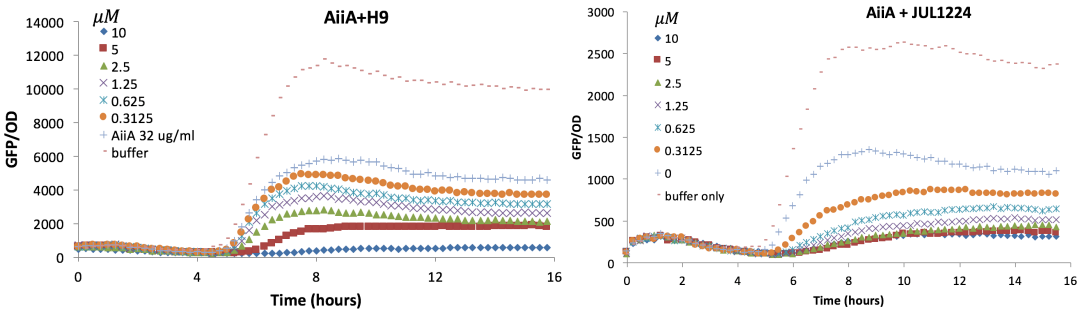

Figure 5.6: Inhibition effect of using both QQ alone and ajoene analogues. (A): LasR-GFP to time at different H9 concentrations with $32\mu g/ml$ AiiA. (B) LasR-GFP to time at different JUL1224 concentrations with 32 $\mu g/ml$ AiiA .

5.5 Concluding remarks

Effective inhibition of bacteria quorum sensing is significant in controlling membrane biofouling. In this chapter, two substances, QQ which degrades AHL/ BHL and QSI ajoene analogue which inhibits the translation of QS mRNAs have been studied. Their combined effect has been explored using cellular network models represented by ordinary differential equations. The results were acquired by stationary state analysis. The results showed that QQ and ajoene analogue has strong synergy in inhibiting both las and rhl circuits of *P.aeruginosa*. Ajoene analogue has stronger inhibition effect than competitive binding QSI G1 alone or combined with QQ. The result suggests a novel and more effective method of inhibiting bacteria QS which has the potential to reduce membrane biofouling.

Chapter 6

Population dynamics of small colony variants in *Pseudomonas aeruginosa* biofilms

6.1 Introduction

Bacterial cells can form colonies on biotic or abiotic surfaces, often including in EPS they produced and form biofilms. In nature, most bacterial cells live in biofilm state[41]. Cells in biofilms have slower growth rate but they are more resistant to unfavourable conditions like antibiotics and starvation[42]. Biofilms and EPS cause one of the serious problems in membrane technology, boifouling [16].

Three types of EPS were found in *P.aeruginosa* PAO1 biofilms, Alginate, Psl and Pel[2]. Alginate rich in mannuronic and guluronic acid residues was shown not important for biofilm structure[67]. Psl contains plenty of galactose and mannose and Pel mainly contains glucose [193]. Both Psl and Pel are important for biofilm formation. *P.aeruginosa* mutants not producing Psl or Pel could still form biofilm, but Psl and Pel double mutant could not form biofilm[2]. Psl was shown to be tightly

Table 6.1: Parameters in Chapter 6

Symbol	Definition
psl-	Strains that do not produce psl
psl+	Strains that produce normal amount of psl
psl++	Strains that produce excessive amount of psl
pel-	Strains that do not produce pel
pel+	Strains that produce normal amount of pel
pel++	Strains that produce excessive amount of pel
G	Concentration of growth substrate (glucose)
K_G	Concentration constant in growth dynamics
μ	Cell specific growth rate
μ_{max}	Cell maximum specific growth rate
P_S	Probability of shear detachment
K_S	Shear detach coefficient
h	Cell hight to the substratum
P_E	Probability of erosion detachment
K_{er}	Erosion detachment coefficient
n_+	Number of neighbouring psl+ cells
n_{++}	Number of neighbouring psl++ cells
η	Describes the effect of maximum Pel on erosion detachment
Pel_{max}	Maximum concentration of Pel
$f_e(n_+, n_{++})$	Describes the asdhesion between psl+ and psl++
$\mu_{max_{scv}}$	Maximum specific growth rate of SCV
ρ	Cell dry mass density
R_{div}	Cell division radius
H	Diffusion layer length
D_G	Diffusion coefficient of glucose
Y_G	Biomass Yield of substrate
f_c	Parameter describes the flow rate

bound with bacteria cells [194] and is cross linked in biofilm. Psl makes biofilm matrix more elastic[32]. Pel is viscous, deformable, reduces effective cross-linking of biofilm and tends to expand biofilm[32]. Pel also contributes to biofilm formation, but without Psl the biofilm is more flat and cannot form macrocolonies at later stages of biofilm development like PAO1 and mutant producing only Psl [2]. Psl is only shareable among Psl producing cells but Pel is shareable among all cells. Mutant only producing Psl form separate layer in biofilms with *S. aureus* but mutant producing only Pel can mix with *S. aureus* very well [2]. Adhesin CdrA specific to Psl might explain Psl is only shareable among Psl producing cells [195]. Psl appears at early stages of biofilm and Pel appears at relatively later stages, which explains why PAO1 biofilms decrease in cross-linking and elasticity with enhanced biofilm spreading when mature[2, 32].

Small colonies with autoaggregative properties were found in chronic cystic fibrosis patients. These small colony variants (SCVs) are more resistant to antibiotics and formed more stable biofilms[35]. Excessive production of Psl and Pel were found in these variants [193]. Overproduction of Psl and Pel might meditate the population dynamics of SCV and normal PAO1 cells in biofilm.

Shear affects biofilm physiologies and population dynamics [196] and privious experiments showed that large inflow rate will induce biofilm sloughing events. Experiments showed that at small flow rate, biofilm sloughing event was not observed. But when the flow rate is increased, biofilm sloughing events were obvious. The distinct properties of Psl and Pel are expected to response to shear differently in biofilms. The study in this chapter aim to incorporate Psl and Pel in biofilm individual based model (IBM), reproduce experimental results in reference [2] and predict the physiology and population dynamics of biofilms formed by SCV and PAO1 under shear.

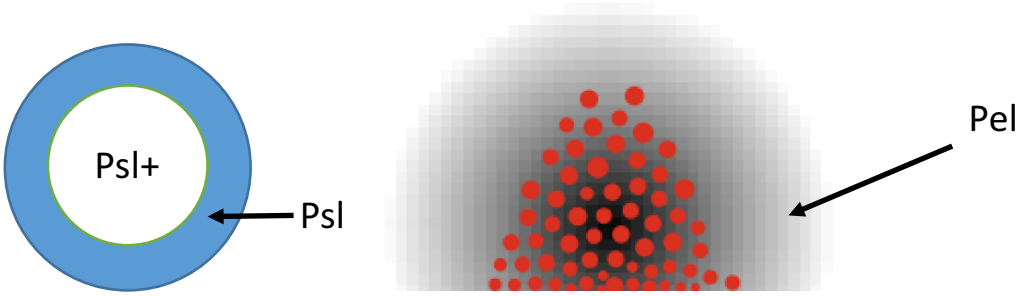

Figure 6.1: Psl and Pel in the model. Psl is tightly bound with cells and Pel is slowly diffusible. Psl+ represents strains that produce normal amount of psl, like psl+pel- and wt.

6.2 Methods

Biofilms are modelled using IBM similar with reference [33], with a few differences indicated below.

Psl- represent cells that do not produce any Psl; Psl+ represents cells that produce normal amount of Psl comparable with PAO1. Psl++ represents cells that produce excessive amount of Psl. The nomination also applies to Pel-, Pel+ and Pel++. In the model, Psl is thought to be tightly bound with individual cells, and not explicitly modelled but reflected by smaller cell-cell distance and lower erosion detachment rate of Psl+ and Psl++ cells. Pel is slowly diffusible as shown in figure 6.1.

Cells are treated as round disks in the 2D model. Cells have real radius R and effective radius. Cell-cell distance is reflected by effective radius: the minimum distance between two cells is the sum of their effective radii. They ratio of a cell's effective radius and real radius is called expansion ratio. Expansion ratio is proposed to be an linear function of local Pel for Psl-, Psl+ and Psl++ cells, as shown in figure 6.2.

Tessier kinetics (equation 6.1) is used to describe the growth of cells because Tessier kinetics best fits the experimental data of *P.aeruginosa* [197]. G represents the concentration of growth substrate and K_G is a concentration constant. The maximum specific growth rates of Pel-Psl-, Pel-Psl+, Pel+Psl- and PAO1 are the same [2] but

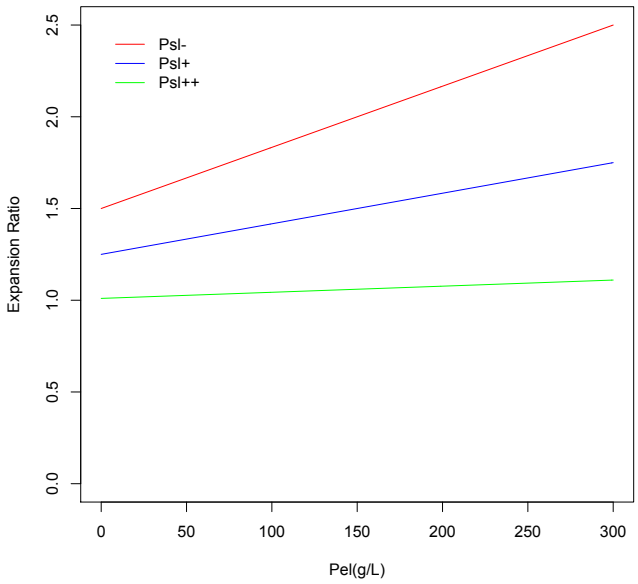

Figure 6.2: Expansion ratio of Psl-, Psl+ and Psl++ cells.

of Pel-Psl++, Pel++Psl++ and Pel++Psl- are smaller than that of PAO1 [35]. Nutrient gradient is ignored in this model, as the biofilm heights in experiments were only around $50\mu m$ [2] and flow can enhance the transportation inside biofilm.

$$\mu = \mu_{max}(1 - e^{-G/K_G}) \tag{6.1}$$

Cells in biofilms are subjected two kinds of detachments, shear detachment and erosion detachment. When flow rate is large, shear detachment is dominant and erosion detachment can be ignored. When flow rate is small, only erosion detachment exists. In shear detachment, cells experience higher shear at taller part of biofilms. The structure of a biofilm is often broken and cells are sloughed as aggregates. Thus not only cells at the surface but also cells in the internal part of biofilms can be shear detached. The shear detachment rate of a cell is proportional to the square of its height [196]. The probability of a cell is shear detached in time Δt is shown in equation 6.2.

$$P_S = K_S h^2 \Delta t \tag{6.2}$$

Where P_S is the probability that certain cell is shear detached, K_S is the shear detach coefficient and h is the height of this cell to the substratum.

Erosion detachment describes the process where cells at the biofilm surface are detached individually. Both local Pel and neighbouring Psl+ and Psl++ cells can reduce the probability that a cell is erosion detached [2, 196]. The probability that a cell is erosion detached within Δt is adapted from reference [196] and shown in equation 6.3.

$$P_E = K_{er}(1 - f_e(n_+, n_{++}) - \eta \frac{Pel}{Pel_{max}})\Delta t \tag{6.3}$$

Where n_+ is the number of neighbouring Psl+ cells and n_{++} is the number of neighbouring Psl++ cells. K_{er} is the erosion detachment coefficient and $\eta < 1$ which means that even with maximum local Pel, cells can still be detached. *Pel* represents the local concentration of Pel and Pel_{max} represents the maximum concentration of Pel. Two cells are neighbours if and only if their distance is smaller or equal than a fixed constant R_n. $f_e(n_+, n_{++})$ represents the adhesion between cells and is shown in equation 6.4. Substratum provides the same adhesion capability as Psl+ cells, and the overlap area of a cell's neighbouring area with the substratum is converted to n_+ while calculating $f_e(n_+, n_{++})$. n_{bmax} represents the maximum number of neighbouring cells within radius R_n.

$$f_e(n_+, n_{++}) = \begin{cases} 0 \text{ for Psl-} \\ \frac{(n_+ + n_{++})(n_{bmax} - 1) - n_{++})}{n_{bmax}(n_{bmax} - 1)} + \frac{n_{++}}{(n_+ + n_{++})(n_{bmax} - 1)} \text{ for Psl+} \\ \frac{(n_{bmax} - 2)(n_+ + n_{++}) - 2n_{++})}{n_{bmax}(n_{bmax} - 1)} + \frac{n_+ + 3n_{++}}{(n_+ + n_{++})(n_{bmax} - 1)} \text{ for Psl++} \end{cases} \tag{6.4}$$

The adaptation of equations 6.3 and 6.4 is based on the considerations that Pel is sharable among all *P.aeruginosa* mutants and can provide some level of adhesion to cells; Psl is only sharable among Psl producing mutants (Psl+ and Psl++) and neighbouring Psl++ provides stronger adhesion than Psl+ [2, 32]. From equation 6.3, $P_E < 0$ is equivalent to $P_E = 0$, meaning that the particular cell will not detach due to erosion.

The detachment rates should also be dependent on the geometry of the experimental setup and flow rate. The exact relationship of detachment rates and flow rate is

Table 6.2: Parameters used in the model

Symbol	Description	Value	Reference
μ_{max}	Maximum specific cell growth rate	$0.29h^{-1}$	[197]
$\mu_{max_{scv}}$	Maximum specific growth rate of SCV	$0.9\mu_{max}$	[35]
ρ	Cell biomass dry density	$0.3g/cm^3$	[198]
R_{div}	Cell division radius	$2\mu m$	[199]
H	Diffusion layer length	$20\mu m$	[82]
D_{pel}	Diffusion coefficient of Pel	$6\mu m^2/h$	[200]
D_G	Diffusion coefficient of glucose	$2.4\times10^6\mu m^2/h$	[201]
K_G	Parameter in Tessier kinetics	$0.027mg/cm^3$	[197]
Y_G	Biomass yield of substrate	0.628	[202]
Pel_{max}	maximum concentration of Pel	$0.5g/cm^3$	comparable with biomass density
η	Constant in erosion detach submodel, explained in text	0.9	assumed
K_{er0}	Base erosion detach coefficient	$0.05h^{-1}$	within range in ref [196]
K_{s0}	Base shear detach coefficient	$0.005h^{-1}$	within range in ref [196]
K_{spsl-0}	Base shear detach coefficient of Psl-	K_{s0}	assumed
K_{spsl+0}	Base shear detach coefficient of Psl+	$0.5K_{s0}$	assumed
$K_{spsl++0}$	Base shear detach coefficient of Psl++	$0.5K_{s0}$ or $0.25K_{s0}$	assumed
f_c	Flow coefficient explained in text	0.1-3.5	controlled in simulation experiment

unknown, but it is expected that higher flow leads to higher shear and erosion detachment rates. When flow rate is small, only erosion detachment exist, but when increasing the flow rate, sloughing event will occur. To simplify the problem in the model, base shear and erosion detachment coefficients are set for each mutants, and a parameter called flow coefficient f_c is applied. The shear or erosion detachment coefficient of any one mutant is its base coefficient multiplied by f_c. The parameters used in this model are listed in table 6.2. The outputs of the models are biofilm morphologies, mutants distribution inside biofilms and population percentages of mutants included in the simulations.

6.3 Results

6.3.1 Substrate gradients in biofilm

Substrates that are produced or consumed by bacteria cells in biofilms will have gradients inside biofilm [28]. When this gradient can be ignored in modelling and when it should be considered? This question can be answered by modeling one-dimensional biofilm. Figure 6.3 shows a homogeneous biofilm with thickness z_0. The maximum specific growth rate of the biomass is μ_{max}; density of the biofilm is ρ; half saturation constant of this substrate is K,supposing that there is only one rate-limiting substrate; substrate concentration at the bulk is c_b; and the diffusion layer length is H. The growth rate of biofilm at any point is shown is equation 6.5.

$$g(z) = u_{max}\frac{c}{K+c} \tag{6.5}$$

The substrate concentration $c(z)$ is determined by equation 6.6.

$$\frac{\partial c}{\partial t} = D\frac{\partial^2 c}{\partial z^2} - \frac{\rho}{Y}\frac{\mu_{max}c}{K+c} \tag{6.6}$$

Because the diffusion-reaction rate is much faster than the cell growth rate, the biomass distribution can be treated as constant at the time scale of substrate diffusion. Then the substrate will reach pseudo-steady state very soon. The steady-state substrate concentration profile is determined by equation 6.7.

$$\frac{\partial^2 c}{\partial z^2} = \frac{\rho}{YD}\frac{\mu_{max}c}{K+c} \tag{6.7}$$

We define a rule that if the growth rate at the top of biofilm is more than twice than the growth rate at the bottom ($g(0) \geq 2g(z_0)$), the the substrate gradient must be considered. Two conditions are considered separately: $c_0 \ll K$ and $c_0 \sim K$ or $c_0 \geq K$.

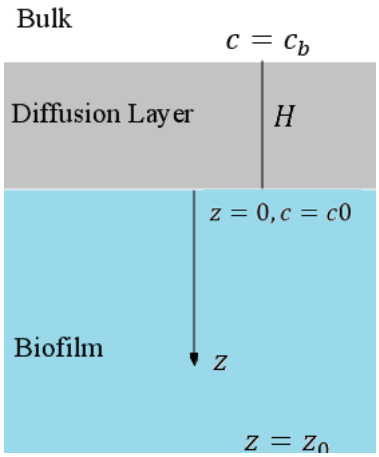

Figure 6.3: Biofilm with thickness z_0, density ρ and maximum specific growth rate μ_{max}. The system is 1D and separated into 3 layers: biofilm layer, diffusion layer and bulk layer. There is only one rate-limiting substrate and the concentration at $z = 0$ is c_0 (biofilm interface). The substrate concentration at the bulk is c_b.

1. $c_0 \ll K$

When $c_0 \ll K$, equation 6.7 becomes equation 6.8.

$$\frac{\partial^2 c}{\partial z^2} = \frac{\rho \mu_{max} c}{YDK}, (c(0) = c_0, c'(z_0) = 0) \tag{6.8}$$

The solution of equation 6.8 is

$$c = \frac{c_0}{1 + e^{-\frac{2z_0}{l}}} e^{-\frac{z}{l}} + \frac{c_0}{1 + e^{\frac{2z_0}{l}}} e^{\frac{z}{l}} \tag{6.9}$$

with $\frac{1}{l^2} = \frac{\rho \mu_{max}}{YDK}$. Under this condition $g(0) \geq 2g(z_0) \Leftrightarrow z_0 \geq 1.317l$. That means, if $z_0 \geq z_{limit}$, expressed in equation 6.10 substrate gradient must be considered.

$$z_{limit} = 1.317 \sqrt{\frac{DYK}{\rho \mu_{max}}} \tag{6.10}$$

2. $c_0 \sim K$ **or** $c_0 \geq K$

When $c_0 \sim K$ or $c_0 \geq K$, we deduce the relationship of z_0 and c_0 if substrate gradient does not need to be considered. If $g(0) \leq 2g(z_0)$, the inequation 6.11 will be valid.

$$c_{z_0} \geq \frac{Kc_0}{2K + c_0} \tag{6.11}$$

Because $c_{z_0} \leq c$ for $0 \leq z \leq z_0$, the inequation 6.12 will be valid.

$$\frac{\partial^2 c}{\partial z^2} = \frac{\rho}{YD}\frac{\mu_{max} c}{K+c} > \frac{\rho}{YD}\frac{\mu_{max} a}{K+a} \tag{6.12}$$

where, for convenience purpose, let $a = \frac{Kc_0}{2K+c_0}$. Thus, from inequation 6.12 and $c(0) = c_0, c'(z_0) = 0$, $z_0 < \sqrt{\frac{4DY}{\rho\mu_{max}}\frac{(K+c_0)^2}{(2K+c_0)}}$. That means, if $z_0 > z_{limit}$, expressed in equation 6.13, the substrate gradient must be considered.

$$z_{limit} = \sqrt{\frac{4DY}{\rho\mu_{max}}\frac{(K+c_0)^2}{(2K+c_0)}} \tag{6.13}$$

For low substrate concentration $c_0 \ll K$, equation 6.13 gets the results $z_{limit} = 2\sqrt{\frac{DYK}{\rho\mu_{max}}}$, a little larger than equation 6.10. For rough approximation, equation 6.13 is enough for all values of c_0.

For this experimental setup, the value of Z_{limit} is around 50 μm.

Calculate from bulk concentration c_b and diffusion layer length H

According to equation 6.7, the derivative of substrate concentration in biofilm can be expressed by equation 6.14 [203].

$$(\frac{dc}{dz})_f = \sqrt{\frac{2\mu_{max}\rho}{D_f Y}(c - K\ln\frac{K+c}{K})} \tag{6.14}$$

Because of the continuous substrate flux at the biofilm interface, we have equation 6.15.

$$D_f(\frac{dc}{dz})_f = D_w(\frac{dc}{dz})_w \tag{6.15}$$

where the subscript f means inside the biofilm and w means in the diffusion layer. When substrate concentration reaches a pseudo-steady profile, $(\frac{dc}{dz})_w$ is constant. Thus $(\frac{dc}{dz})_w = \frac{c_b - c_0}{H}$, where c_b is the bulk substrate concentration. So c_0 can be calculated from equation 6.16 numerically.

$$\sqrt{\frac{2D_f\mu_{max}\rho}{Y}(c_0 - K\ln\frac{K+c_0}{K})} = D_w\frac{c_b - c_0}{H} \tag{6.16}$$

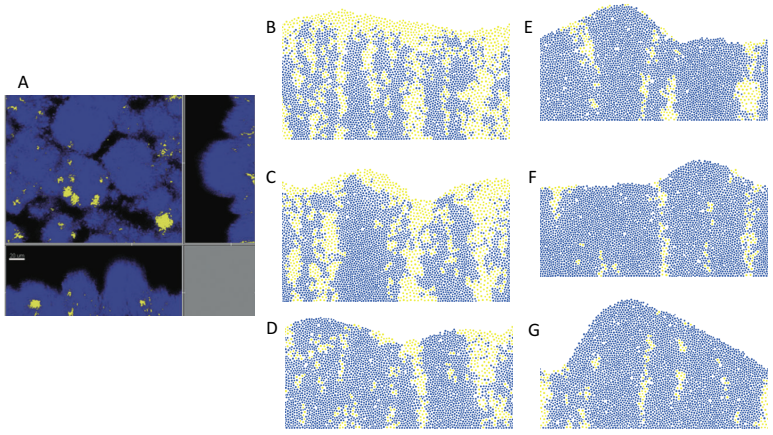

Figure 6.4: Morphologies of biofilm composed of Psl+Pel- (Blue) and Psl-Pel+(Yellow) mutants. (A) Experiments by Yang *et al*[2]. (B-G) Simulation morphologies with $K_{er} = 0.03, 0.06, 0.09, 0.12, 0.15, 0.18h^{-1}$, respectively.

6.3.2 Experimental morphology of Psl+Pel- and Psl-Pel+ reproduced by model

Figure 6.4 (B-G) show the morphologies of simulation results where Psl+Pel-(blue) and Psl-Pel+(yellow) mutants are mixed. In this simulation, only surface shear detachment is considered indicating no sloughing event because in the corresponding experiment of reference[2], the flow rate was small. At very low K_{er} ($0.03h^{-1}$), plenty Psl-Pel+ cells exist and they will enclose Psl+Pel-. When K_{er} increases, the number of Psl-Pel+ cells becomes less and they are gradually enclosed by Psl+Pel-. When $K_{er} = 0.18h^{-1}$ (figure 6.4 G), the morphology reproduces the experimental results by Yang *et al* [2] (figure 6.4 A).

The ratio of Psl-Pel+ in mixed biofilm composed of Psl-Pel+ and Psl+Pel- decreases with K_{er}, comparing at the same time (figure 6.5 A) or at the same total population (figure 6.5 B). The tendency of higher K_{er} decreasing Psl-Pel+ population ratio is clearly shown in figure 6.5 C (at time = 28h). Their relationship can be roughly described by linear relation and the linear regression line represented by the solid line in figure 6.5 C has negative slope.

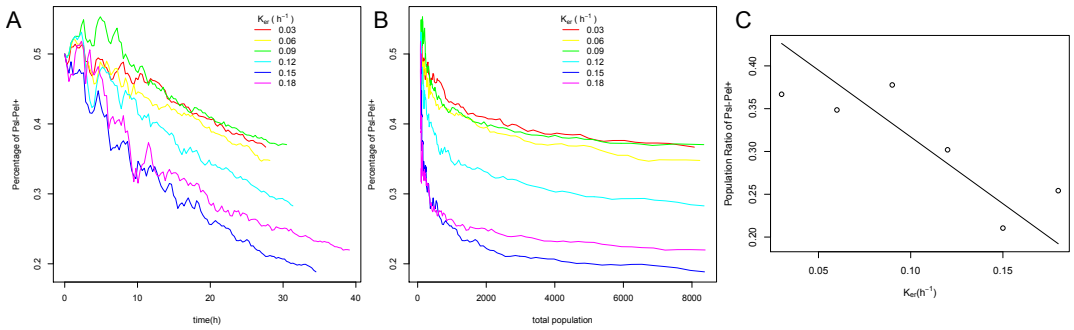

Figure 6.5: Population ratio of Psl-Pel+ in mixed biofilm composed of Psl-Pel+ and Psl+Pel-. (A) Psl-Pel+ population ratio to time at different K_{er} values. (B) Psl-Pel+ population ratio to total population at different K_{er} values. (C) Psl-Pel+ population ratio to K_{er} at 28h. The solid line is the linear regression of these points.

6.3.3 Psl++ mutant tends to aggregate when mixed with PAO1

When the flow rate in simulation is increased, shear detachment is included in the model. In biofilms formed by Psl++Pel++ and PAO1, initially, equal number of Psl++Pel++ and PAO1 cells are placed randomly at the substratum. Young biofilms are formed by small separated colonies, indicated by figure 6.6 A. Gradually, colonies formed by Psl++Pel++ start to merge. Four colony merging behaviours of Psl++Pel++ are pointed out by arrows of four different colors in figure 6.6.

The tendency of Psl++Pel++ colonies to merge still preserves when its shear detachment coefficient $K_{spsl++0}$ is changed from $0.5K_{s0}$ to $0.25K_{s0}$ (table 6.2), or when Psl++Pel++ is replaced by Psl++Pel- (scenario very similar to that indicated by figure 6.6 and not shown).

6.3.4 Percentage of Psl++ first increases and then decreases when mixed with PAO1

When one Psl++ mutant is mixed with PAO1, modelling results show that the percentage of Psl++ will first increase and then decrease overtime, as shown in figure

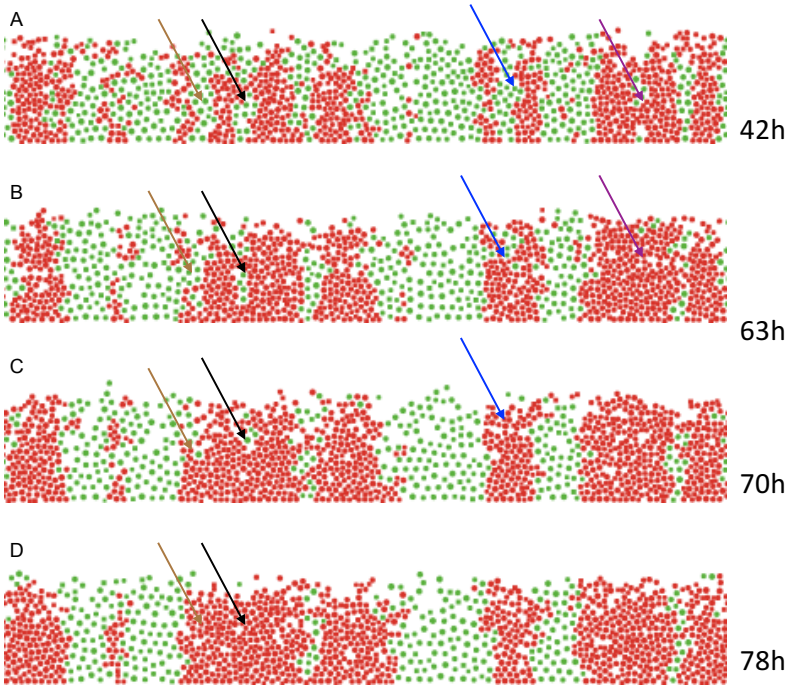

Figure 6.6: Biofilm formed by Psl++Pel++ (red) and PAO1 (green) at different times. Arrows of the same color indicate the merge of Psl++Pel++ colonies. In this simulation, $K_{spsl++0} = 0.5K_{s0}$.

6.7. Although randomly some curves deviate from this pattern, it holds good averagely for most f_c values. Figure 6.7 A represents biofilm composed by Psl++Pel++ and PAO1 with $K_{spsl++0} = 0.5K_{s0}$; figure 6.7 B represents biofilm of the same composition but with $K_{spsl++0} = 0.25K_{s0}$; figure 6.7 C and D represent biofilms composed by Psl++Pel- and PAO1 with $K_{spsl++0} = 0.5K_{s0}$ and $K_{spsl++0} = 0.25K_{s0}$, respectively. The phenomenon that the percentage of Psl++ population first increases and then decreases holds good for all the four conditions, which means that this phenomenon is independent of whether $K_{spsl++0}$ is equal to or smaller than K_{spsl+0} and whether Psl++ mutant produces Pel.

In biofilm composed by Psl++Pel++ (SCV) and PAO1 with $K_{spsl++0} = 0.5K_{s0}$, total population becomes pseudo-stationary after around 25h of growth (figure 6.8 C). However, the percentage of Psl++Pel++ continues to increase until 40-50h and then starts to decrease (figure 6.7 A).

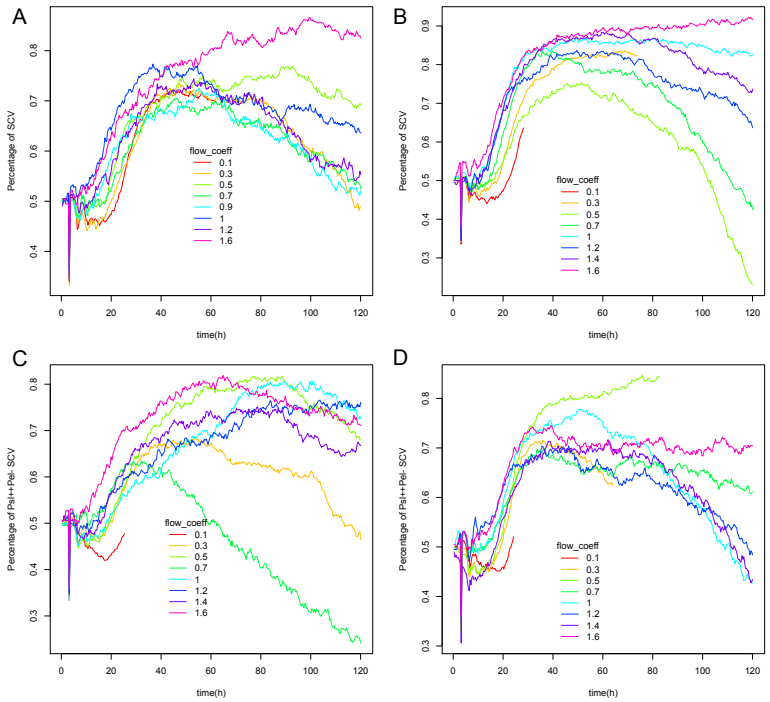

Figure 6.7: Percentage of Psl++ to time in biofilm composed of Psl++ and PAO1 (A): Biofilm composed of Psl++Pel++ and PAO1 with $K_{spsl++0} = 0.5K_{s0}$. (B): Biofilm composed of Psl++Pel++ and PAO1 with $K_{spsl++0} = 0.25K_{s0}$. (C): Biofilm composed of Psl++Pel- and PAO1 with $K_{spsl++0} = 0.5K_{s0}$. (D): Biofilm composed of Psl++Pel- and PAO1 with $K_{spsl++0} = 0.25K_{s0}$.

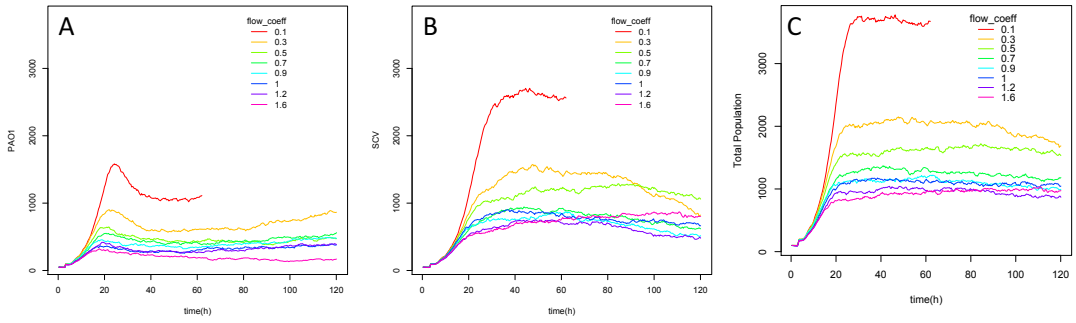

Figure 6.8: Population to time of biofilm composed by Psl++Pel++ and PAO1. In this simulation, $K_{spsl++0} = 0.5K_{s0}$. (A): Population of PAO1. (B): Population of Psl++Pel++. (C): Total population.

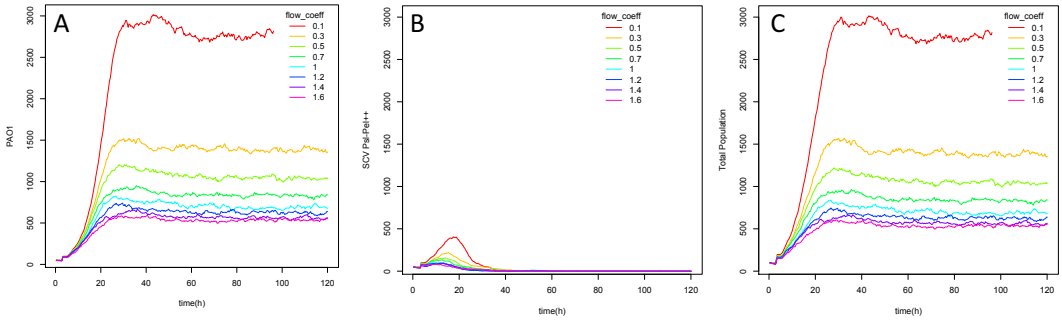

Figure 6.9: Population to time of biofilm composed of Psl-Pel++ and PAO1. (A): Population of PAO1. (B): Population of Psl-Pel++. (C): Total Population.

6.3.5 PAO1 out-competes Psl-Pel++

When Psl-Pel++ mutant is mixed with PAO1 with equal initial cell numbers, both strains started to grow in the initial period as shown in 6.9 A and B . After a short period, 5-20 hours in simulated environment depending on the flow rate, the population of Psl-Pel++ begins to decrease and finally disappear. PAO1 will finally exclude Psl-Pel++ and dominate the population.

As shown in figure 6.10, at the initial stage (time = 9h) of mixed biofilm composed by PAO1 and psl-pel++, psl-pel++ tends to occupy the top of biofilm. As the biofilm grows taller (time = 16h), the part biofilm occupied by psl-pel++ tends to be expanded and sparse, while the part occupied by PAO1 tends to be compressed and dense. At 22h, biofilm grows taller and most of the psl-pel++ cells are detached. Biofilm growth and detachment nearly reaches equilibrium at this stage. At the final equilibrium stage, psl-pel++ cells are gradually detached from the biofilm and all remaining cells are PAO1 cells (time = 54h).

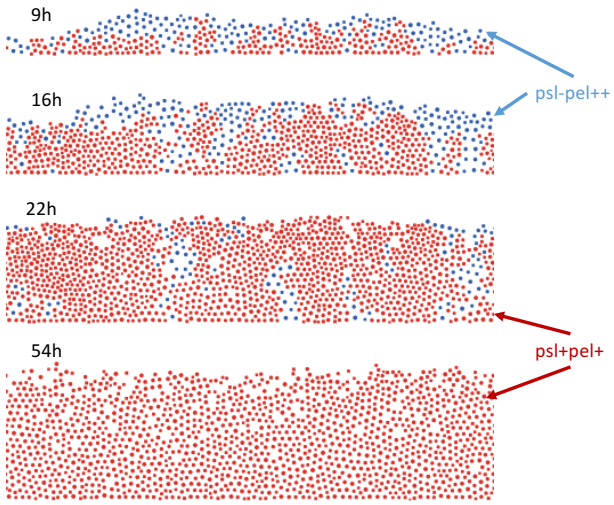

Figure 6.10: Morphologies of psl-pel++ and PAO1 (psl+pel+) mixed biofilm at different time of simulation.

6.4 Discussions

6.4.1 Incorporation of Psl and Pel in ABM biofilm model

According to experimental studies in references [2, 32], Psl is tightly bound with bacteria cells and provides crosslinking inside biofilm but Pel is deformable. Artificial particles of 0.5-1 μm can move inside biofilm containing only Pel EPS. It is assumed that cells inside Pel can also move. Psl tends to bind cells and shrink biofilm. Pel tends to expand biofilm. The maximum specific growth rates of Psl or Pel deletion mutants are the same as PAO1 but the growth rates of SCV (Psl++Pel++) is smaller [35]. Plenty of Psl appears at very early stage of biofilm. Psl is only shareable among Psl producing cells, but Pel is shareable among all *P.aeruginosa* mutants. In the ABM model of this study, Psl is bound with bacteria cells and moves with bacteria cells. Pel is slowly diffusible. Sufficient Psl is produced when cell is produced by division, and Pel is continuously produced. Psl decreases the expansion ratio of cells and thus decreases cell-cell distance. Pel increases cell cell distance by increasing expansion ratio. Crosslinking of Psl is modelled by smaller shear detachment coefficient of Psl producing cells and neighbouring Psl producing cells bind each other to prevent from

erosion detachment.

6.4.2 Surface roughness produced by model are strongly dependent on shoving algorithm

The shoving algorithm which reduces cell overlapping caused by cell growth and division is similar with that in references [34, 33], where overlapping cells are moved in opposite direction to reduce overlap. In this model, two algorithms are considered. The first algorithm is that, when two cells overlap, the distances they are shoved is anti-proportional to their mass, regardless of the direction of the movement. The second algorithm thinks that when two cells overlap, the shoving in horizontal direction is the same with the first algorithm, but in the vertical direction, upper cells moves up more than lower cells moves down. The first algorithm was used by references [34, 33], but the second algorithm is also reasonable, because when biofilm grows, top cells are easier to be pushed up than bottom cells to be pushed down. The results in this study are produced by mixing these two algorithms. However, separately, these two algorithms produce strikingly different surface shapes of biofilms. Thus surface roughness produced by model does not represent the real biofilm.

6.4.3 Shear and erosion detachments contribute differentially to biofilm morphology and percentage of Psl++ mutant

Shear detachment was shown to produce flat biofilms and erosion detachment was shown to produce towering like structures [196]. This phenomenon is reproduced by this work. Only shear or only erosion detachment is implemented separated in biofilm composed of Psl++Pel- and PAO1 to study how these two detachment mechanisms contribute to biofilm morphology and Psl++ percentage. When ignoring erosion detachment and only shear detachment is considered, the biofilms produced are flat, similar to that in figure 6.6. When only erosion detachment is considered,

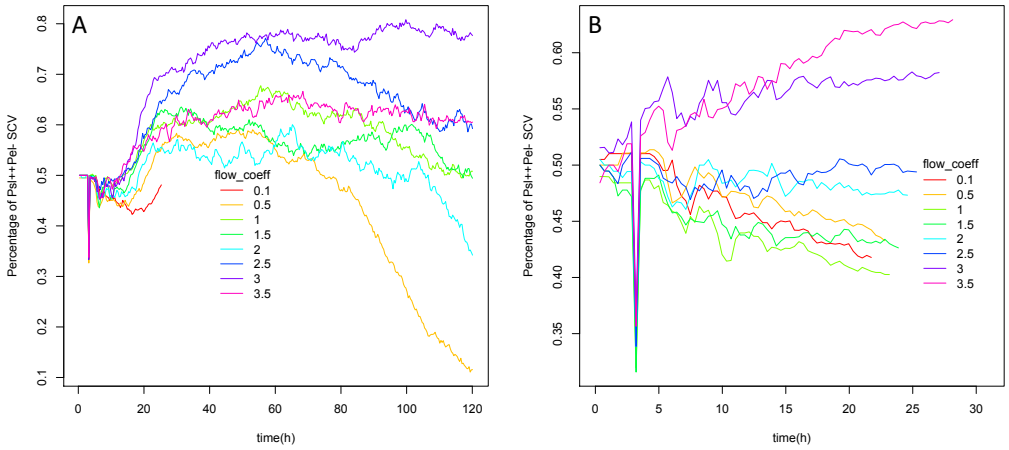

Figure 6.11: Percentage of Psl++Pel- when mixed with PAO1 when only shear detachment (A) or only erosion detachment (B) is implemented.

biofilms produced have rough surface, as shown in figure 6.12. The phenomenon that percentage of Psl++ first increases and then decreases is produced by only implementing shear detachment mechanism (figure 6.11A). When only erosion detachment is considered, shear obviously favours Psl++, as shown in figure 6.11B. At small f_c values, PAO1 dominates the population and at large f_c, Psl++ dominates the population. It is also observed in figure 6.12A and 6.12B. Tendency of Psl++ colonies to merge is also observed when implementing shear detachment only. But the time in simulations implementing erosion only was not large enough to observe whether Psl++ colonies tend to merge. Shear detachment and erosion detachment contribute differentially to biofilm morphology and percentage of Psl++. The sward-like shape in the Psl++ percentage curves at the initial stage is due to modelling artefact: initially equal number of cells with very small variation in size is located at the bottom of the substratum, but Psl++ grows slower and the first division time of Psl++ cells is a bit longer than PAO1 cells, thus producing this shape at first division. It can be safely ignored.

P.aeruginosa SCVs were shown to be autoaggregative[204, 205]. This autoaggregative property was explained by excessive production of Psl and Pel[79, 206]. In this study, the autoaggregative property of Psl++ is observed in the models. Excessive

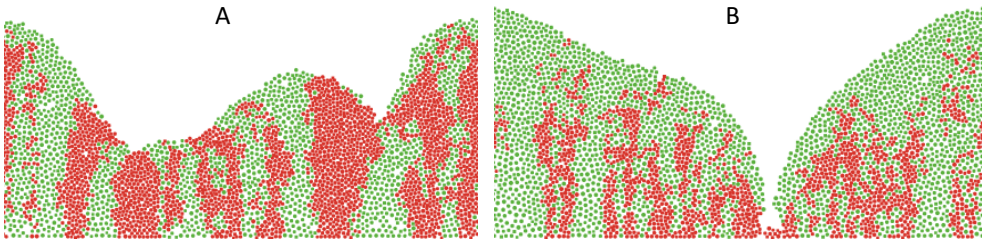

Figure 6.12: Morphologies of biofilm when only erosion detachment is implemented. (A): $f_c = 3.5$. (B): $f_c = 1$.

Psl tend to bind Psl++ cells tightly together. The PAO1 cells between two nearby Psl++ colonies are easily detached, and when the colonies grow larger then tend to merge, even when initial Psl++ and PAO1 cells are randomly located. The result is consistent with experimental observations that SCV form small colonies instead of being well mixed with wild type cells[79].

Psl++ cells are more stable in biofilms than PAO1 cells. However, this work predicts that the percentage of Psl++ cells will finally decrease with time and Psl++ will not dominate the population, as it grows slower than PAO1 cells. This is in agreement with experiments that SCV cells occupy only a small portion of population in *P.aeruginosas* biofilms [35].

6.5 Concluding remarks

This study uses the results and hypothesis of Psl and Pel properties from references[2, 32] to build an ABM of *P.aeruginosa* biofilm. The model successfully reproduced the experimental morphologies of Psl+Pel- and Psl-Pel+ mixed biofilm in reference[2]. This study also predicts the autoaggregative properties of SCV cells and that although SCV is more stable in biofilm than wild type cells, SCV cannot dominate the population. The predictions agrees with existing observations and can be further validated with experiments using continuous culture.

Chapter 7

Conclusion and future works

7.1 Concluding remarks

This thesis uses mathematical modelling to study QS, biofilm population dynamics and how EPS affect biofilm physiologies, which are important factors in membrane biofouling process.

Parameters of *V.fischeri* QS are fitted according to experimental data of various types using the least deviation score method which incorporates different data types and can be used to fit more accurate parameters when increasing experiment data has been accumulated. Different response curve topologies were found in reasonable parameter space. It demonstrates that the QS network response behaviour depends not only on network structure, but also parameter values and interaction strength. It also demonstrates that network properties can be regulated by changing parameters.

Noise caused by parameter heterogeneity is analysed and compared with network intrinsic noise. Combined with experimental data from literature, this analysis shows that both types of noise exist in QS network and their relative quantities are reversed between QS on and off states. A more clear picture of QS network noise is provided.

Table 7.1: Parameters in Chapter 7

Symbol	Definition
$\dot{\vec{r}}_i$	Location of i^{th} cell
$\vec{v}(\phi_i)$	Velocity of i^{th} cell
D_ϕ	Noise Density
$\zeta_i(t)$	Gaussian random noise with zero mean
α_{ij}	Angle of vector $\vec{r}_{ij}$
$\mu_\pm$	Describes the interaction between particles
z_n	Location of n^{th} dipole
U	Speed of a dipole
α_n	Orientation of dipole n
μ	Translation coefficient
ω	Fluid velocity represented by a complex number

QQ and competitive binding QSI combined show strong synergistic effect in inhibiting *P.aeruginosa* QS. This conclusion has been proved by mathematical models and experiments on AiiA as QQ and G1 as competitive binding QSI. Additionally, ajoene and its analogues, another kind of QSI inhibiting QS by interrupting translation of mRNAs, also show synergy with QQ and have stronger inhibition effect than competitive binding QSI like G1. Thus a more effective and cheaper way to inhibit QS and regulate biofouling has been proposed.

The study of population dynamics of SCV in *P.aeruginosa* biofilms is a specific example of how EPS regulate population dynamics and biofilm morphology. The results show that EPS produced by cells greatly affect biofilm morphologies and population dynamics in biofilms.

This thesis has provided deeper understandings QS network and dynamics of biofilm and EPS, which are closely related with biofouling, and proposed a more efficient and effective way of inhibiting QS. These studies contribute to regulating biofouling.

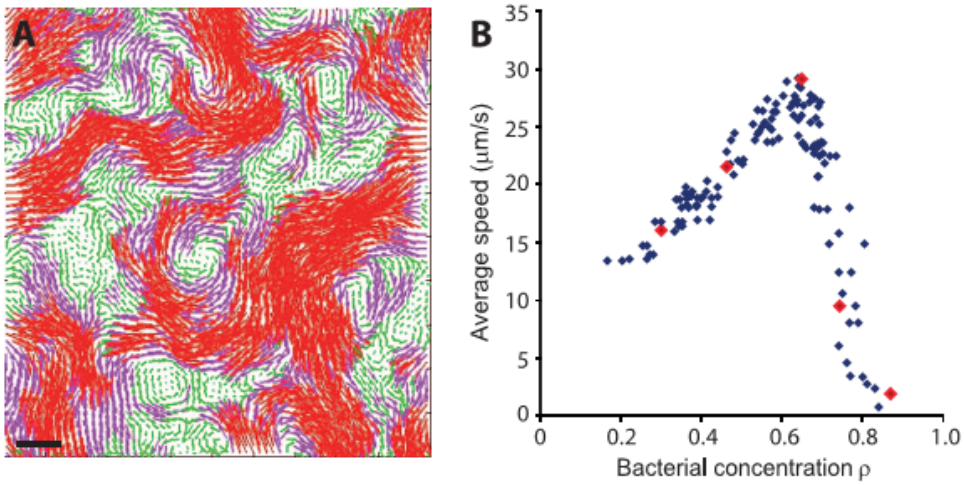

Figure 7.1: Collective motion of *Serratia marcescens*. (A): Velocity field of bacteria. green, <20$\mu m/s$; pink, 20-40 $\mu m/s$; red, >40$\mu m/s$. (B): Average speed to bacteria to bacteria surface coverage ρ. Image is from reference[3].

7.2 Recommendation for future work

The work in chapters 3, 4 and 5 studying bacterial QS structure and QS inhibition mainly focus on planktonic culture. Chapter 6 studies the population dynamics of *P.aeruginosa* SCV in biofilms. Planktonic and biofilm states are two ubiquitous living states for bacteria cells[207]. However, there exists transitional state between these two extreme states[208, 209, 3]. Many interesting questions can be asked about this transitional state. One of them is recommended here for future work.

Reference [3] observed the collective motion of a monolayer culture drop of spherical bacteria *Serratia marcescens* and found that the average speed of bacteria cells increases with cell surface coverage ρ when ρ is small (<0.67). After that, average speed will sharply decrease with cell density. The question is whether this increase in average velocity at small ρ is caused by increase of bacteria propagation power or by interaction of bacteria cells. Here it is proposed that interaction of bacteria cells leads to the increase of average velocity. Mathematical models and experiments are recommended to test this hypothesis. Validations of this hypothesis and methods of mathematical models are shown below.

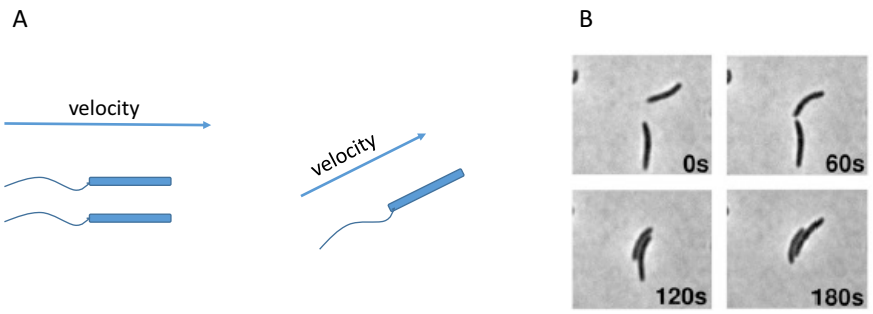

Figure 7.2: (A): Schematic drawing to show that nearby aligned bacteria cells swim faster than isolated cells. (B):Steric interaction of two *M.xanthus* cells leads to velocity alignment. figure B is from reference [4].

It was observed that nearby aligned *Bacillus subtilis* cells swim faster than isolated or mis-aligned cells[210]. This reference shows that the speed of cells in collective motion can reach $100\mu m/s$ but the speed of isolated cells is only 1-$10\mu m/s$ when *Bacillus subtilis* cell density is $10^9/cm^3$. The schematic drawing is shown in figure 7.2A. Experiments also show that the flagella of two nearby parallel cells are synchronized or anti-syncrhonized through hydrodynamic interaction[211]. Forces between two bacterial cells that don't touch each other were directly measured. The forces are mainly repulsive but the mechanisms are unknown. This force only affects nearby cells and is different from quorum sensing phenomenon[212]. From these results, it is probable that hydrodynamic interaction leads to increased velocity of aligned cells.

Many experiments show that in bacteria collective motion a cluster or group of nearby cells present very similar motion. cell velocities and alignments have correlations [3, 4, 213, 214]. This is in agreement with previous description that in cell collective motion, velocity is aligned and thus the average speed is increased.

Steric and hydrodynamic interactions were shown to lead to directional and velocity alignment. The simplest interaction is steric interaction, similar to collision, that cells will repulse each other when too close. Reference [4] shows that steric interaction *M. xanthus* cells can lead to velocity alignment (figure 7.2B). Hydrodynamic interactions can also lead to velocity alignment. Reference [213] proposed a model

with a set of equations for cell cell interaction through hydrodynamics which agrees with the experimental observation of vertex arrays. Hydrodynamic interactions of dipoles in confined space were analytically and numerically studied [215, 216, 217]. In reference [217], a dipole is comprised of a head and a tail connected by a rod of invariant length. Analysis shows that when the tail of the dipole is larger than the head, pursuit mode (one dipole follows another) is stable and when the head is larger than the tail, synchronization mode (dipoles swim in parallel) is stable. For most bacterial cells with only one flagellum, or with multiple flagella but pointing to the same direction while swimming, they resembles hydrodynamic dipoles with head larger than tail and thus velocity alignment is the stable mode with hydrodynamic interaction.

From the above analysis, the picture of the hypothesis is quite clear here: cell cell interactions like steric and hydrodynamic interactions can lead to cell alignment. When cells are aligned, hydrodynamic interactions lead to increased average swimming speed. However, further models are needed to validate this hypothesis. Here 3 methods of cell cell hydrodynamic interactions are provided.

The first method is proposed by reference [213], as shown by equations 7.1-7.4.

$$\dot{\vec{r}}_i = \vec{v}(\phi_i) \tag{7.1}$$

$$\dot{\phi}_i = \sum_{j\neq i}^{N} T_\phi(\vec{r}_{ij}, \phi_i, \phi_j) + \sqrt{2D_\phi}\zeta_i(t) \tag{7.2}$$

$$T_\phi(\vec{r}_{ji}, \phi_i, \phi_j) = \mu(r_{ji})\sin(\phi_j - \phi_i) - \kappa\sin(\alpha_{ji} - \phi_i)\Theta(\xi_r - r_{ji}) \tag{7.3}$$

$$\mu(r_{ji}) = \begin{cases} \mu_+(1-(r_{ji}/\xi_a)^2) \text{ for } 0 \leq r_{ji} \leq \xi_a \\ -\mu_- \frac{4(r_{ij}-\xi_a)(1-r_{ji})}{(1-\xi_a)^2} \text{ for } \xi_a < r_{ji} < 1 \end{cases} \tag{7.4}$$

$\vec{r}_i$ is the location of ith cell; $\vec{v}(\phi_i)$ is the velocity. D_ϕ is the noise density; $\zeta_i(t)$ is Gaussian random noise with zero mean. α_{ij} is the angle of vector $\vec{r}_{ij}$. $\mu_\pm$ describes the interaction between particles. The model in this reference reproduced directional alignment observed in bacteria collective motion[218, 219]. This method can be used to modelling how hydrodynamic and steric interactions lead to cell directional

alignment. But as it assumes cell speed is constant, adjustments are needed to model how cell alignments can lead to increased swimming speed.

The second method is proposed by reference [217], as shown in equations 7.5. In this work, bacteria cell is represented by a hydrodynamic dipole with head and tail connected with a rod with invariable length.

$$\begin{cases} \dot{\bar{z}}_n = U e^{-i\alpha_n} + \mu \bar{\omega}(z_n) \\ \alpha_n = \mathrm{Re}[\nu_1 \frac{d\bar{\omega}}{dz} i e^{2i\alpha_n} + \nu_2 \bar{\omega} i e^{i\alpha_n}] \\ \bar{\omega}(z_n) = \sum_{j \neq n} \sigma \frac{e^{i\alpha_j}}{(z_n - z_j)^2} \end{cases} \tag{7.5}$$

z_n is the location of n^{th} dipole, represented by a complex number; U is the speed of a dipole; α_n is orientation of n^{th} dipole; μ is the translation coefficient; ω is the fluid velocity represented by a complex number; $\nu_1 = \frac{(\lambda_h \mu_h + \lambda_t \mu_t}{\lambda_h + \lambda_t}$, $\nu_2 = (\mu_h - \mu_t)/l$; subscript h means head and t means tail; λ_h and λ_t are parameters that enforce the distance between head and tail of the dipole is constant l. Reference [217] used this model and concluded that for swimmers like bacteria with larger head and smaller tail, alignment is the stable mode of hydrodynamic interactions, thus proving that hydrodynamic interaction leads to cell cell alignment. Similar with method 1, this model assumes constant swimming speed of the dipole, which should be adjusted to address how alignment increases average speed.

The third one is adapted from Kirkwood hydrodynamic interaction approximation. Kirkwood approximation of hydrodynamic interaction between nodes in polymer chain was used to calculate the diffusion coefficient of polymers[220]. $\vec{v}_i$ is the fluid velocity at the location of i^{th} chain node if node i doesn't exist and $\vec{u}_i$ is its velocity. The force node i exerts on the fluid $\vec{F}_i$ is expressed in equation 7.6.

$$\vec{F}_i = -\zeta(\vec{v}_i - \vec{u}_i) \tag{7.6}$$

If a force $\vec{F}$ is exerted on fluid at location 0, the perturbation of fluid velocity $\vec{v'}$ at location $\vec{r}$ is calculated by Oseen tensor $\vec{v'}(\vec{r}) = \overleftrightarrow{T}(\vec{r}) \cdot \vec{F}$ with $\overleftrightarrow{T}(\vec{r}) = (1/8\pi\eta_0 r)[\overleftrightarrow{I} +$

$(\vec{r}\vec{r}/r^2)]$ [221].

$$\vec{v'}(\vec{r}) = (1/8\pi\eta_0 r)[\vec{F} + \vec{r}(\vec{r}\cdot\vec{F})/r^2] \tag{7.7}$$

where $r = |\vec{r}|$ and η_0 is the viscosity coefficient of the fluid. Supposing the background velocity of the fluid is $\vec{v}_0(\vec{r})$ and the velocity of every node $\vec{u}_i$ is known, $\vec{v}_i$ can be expressed as

$$\vec{v}_i = \vec{v}_0(\vec{r}_i) + \sum_{j\neq i} \overleftrightarrow{T}_{ij}\vec{F}_j \tag{7.8}$$

$\overleftrightarrow{T}_{ij} = \overleftrightarrow{T}(\vec{r}_i - \vec{r}_j)$. Combing equation 7.6 and equation 7.8, we can get equation .

$$\vec{F}_i = -\zeta(\vec{v}_0(\vec{r}_i) - \vec{u}_i) - \zeta\sum_{j\neq i} \overleftrightarrow{T}_{ij}\vec{F}_j \tag{7.9}$$

If there are n nodes, there will be n equations and n unknown $\vec{F}_i$ in equation 7.9. Thus the hydrodynamic interactions between these nodes represented by n $\vec{F}_i$s can be numerically solved. Bacteria cells are active swimming agents. The force exerted on fluid by bacterial cell i contains two parts, the force of hydrodynamic interaction $\vec{F}_{1i}$ and the active propagation force $\vec{F}_{2i}$ (equation 7.10).

$$\vec{F}_i = \vec{F}_{1i} + \vec{F}_{2i} \tag{7.10}$$

Equation 7.8 still holds and equation 7.9 is updated to equation

$$\vec{F}_{1i} = -\zeta(\vec{v}_0(\vec{r}_i) - \vec{u}_i) - \zeta\sum_{j\neq i} \overleftrightarrow{T}_{ij}(\vec{F}_{1j} + \vec{F}_{2j}) \tag{7.11}$$

In a model where bacteria propagation force $-\vec{F}_{2i}$, location $\vec{r}_i$ and velocity $\vec{u}_i$ of every bacteria cell is known, the hydrodynamic interaction $\vec{F}_{1i}$s can be solved numerically from equation 7.11. This method can be used to study whether velocity alignment leads to increased swimming speed.

This recommendation of future work has proposed a hypothesis with clear picture that in bacteria collective motion, steric and hydrodynamic interactions lead to bacteria velocity alignment and hydrodynamic interaction in turn increases the swimming speed of bacteria cells in alignment, thus explaining the experimental phenomenon in reference[3]. This hypothesis has strong literature support. 3 methods are proposed to model cell interactions to validate this hypothesis.

Bibliography

[1] Sean Yang-Yi Tan, Song-Lin Chua, Yicai Chen, Scott A Rice, Staffan Kjelleberg, Thomas E Nielsen, Liang Yang, and Michael Givskov. Identification of five structurally unrelated quorum-sensing inhibitors of pseudomonas aeruginosa from a natural-derivative database. *Antimicrobial agents and chemotherapy*, 57(11):5629–5641, 2013.

[2] Liang Yang, Yifan Hu, Yang Liu, Jingdong Zhang, Jens Ulstrup, and Søren Molin. Distinct roles of extracellular polymeric substances in pseudomonas aeruginosa biofilm development. *Environmental microbiology*, 13(7):1705–1717, 2011.

[3] Amit Rabani, Gil Ariel, and Avraham Be'er. Collective motion of spherical bacteria. *PloS one*, 8(12):e83760, 2013.

[4] Fernando Peruani, Jörn Starruß, Vladimir Jakovljevic, Lotte Søgaard-Andersen, Andreas Deutsch, and Markus Bär. Collective motion and nonequilibrium cluster formation in colonies of gliding bacteria. *Physical review letters*, 108(9):098102, 2012.

[5] David Seckler, Randolph Barker, and Upali Amarasinghe. Water scarcity in the twenty-first century. *International Journal of Water Resources Development*, 15(1-2):29–42, 1999.

[6] Klaus Kümmerer. The presence of pharmaceuticals in the environment due to human use–present knowledge and future challenges. *Journal of environmental management*, 90(8):2354–2366, 2009.

[7] Ignasi Sirés and Enric Brillas. Remediation of water pollution caused by pharmaceutical residues based on electrochemical separation and degradation technologies: a review. *Environment international*, 40:212–229, 2012.

[8] B Jefferson, A Laine, S Parsons, T Stephenson, and S Judd. Technologies for domestic wastewater recycling. *Urban water*, 1(4):285–292, 2000.

[9] Simon Judd. *The MBR book: principles and applications of membrane bioreactors for water and wastewater treatment*. Elsevier, 2010.

[10] TorOve Leiknes and Hallvard Ødegaard. The development of a biofilm membrane bioreactor. *Desalination*, 202(1):135–143, 2007.

[11] S Jamal Khan, Shazia Ilyas, Sadaf Javid, C Visvanathan, and V Jegatheesan. Performance of suspended and attached growth mbr systems in treating high strength synthetic wastewater. *Bioresource technology*, 102(9):5331–5336, 2011.

[12] Shuai Yang, Fenglin Yang, Zhimin Fu, and Ruibo Lei. Comparison between a moving bed membrane bioreactor and a conventional membrane bioreactor on organic carbon and nitrogen removal. *Bioresource Technology*, 100(8):2369–2374, 2009.

[13] Zhimin Fu, Fenglin Yang, Yingyu An, and Yuan Xue. Simultaneous nitrification and denitrification coupled with phosphorus removal in an modified anoxic/oxic-membrane bioreactor (a/o-mbr). *Biochemical Engineering Journal*, 43(2):191–196, 2009.

[14] I Ivanovic and TO Leiknes. The biofilm membrane bioreactor (bf-mbr)—a review. *Desalination and Water Treatment*, 37(1-3):288–295, 2012.

[15] Joshua D Shrout and Robert Nerenberg. Monitoring bacterial twitter: does quorum sensing determine the behavior of water and wastewater treatment biofilms? *Environmental science and technology*, 46(4):1995–2005, 2012.

[16] Wenbo Yang, Nazim Cicek, and John Ilg. State-of-the-art of membrane bioreactors: Worldwide research and commercial applications in north america. *Journal of membrane Science*, 270(1):201–211, 2006.

[17] Kyung-Min Yeon, Won-Seok Cheong, Hyun-Suk Oh, Woo-Nyoung Lee, Byung-Kook Hwang, Chung-Hak Lee, Haluk Beyenal, and Zbigniew Lewandowski. Quorum sensing: a new biofouling control paradigm in a membrane bioreactor for advanced wastewater treatment. *Environmental science and technology*, 43(2):380–385, 2008.

[18] H Lade, D Paul, and J. H. Kweon. N-acyl homoserine lactone-mediated quorum sensing with special reference to use of quorum quenching bacteria in membrane biofouling control. *Biomed Research International*, 2014:1–25, 2014.

[19] Hee Yoon Kim, Kyung-Min Yeon, Chung-Hak Lee, Sangho Lee, and Tyagarajan Swaminathan. Biofilm structure and extracellular polymeric substances in low and high dissolved oxygen membrane bioreactors. *Separation Science and Technology*, 41(7):1213–1230, 2006.

[20] K. M. Yeon, C. H. Lee, and J Kim. Magnetic enzyme carrier for effective biofouling control in the membrane bioreactor based on enzymatic quorum quenching. *Environmental Science and Technology*, 43(19):7403–9, 2009.

[21] Kavitha M., Akila A., Nandhini A., and Shakunthala P. Quorum sensing: A review. *Indian Journal of Multidisciplinary Dentistry*, 2014.

[22] Pablo Delfino Pérez and Stephen J Hagen. Heterogeneous response to a quorum-sensing signal in the luminescence of individual vibrio fischeri. *PLoS One*, 5(11):e15473, 2010.

[23] Irena Kuzmanovska, Andreas Milias-Argeitis, Christoph Zechner, and Mustafa Khammash. Parameter inference method for stochastic single-cell dynamics from tree-structured data. *arXiv preprint arXiv:1605.05517*, 2016.

[24] S Fetzner. Quorum quenching enzymes. *Journal of Biotechnology*, 201:2, 2015.

[25] Tim Holm Jakobsen, Maria van Gennip, Richard Kerry Phipps, Meenakshi Sundaram Shanmugham, Louise Dahl Christensen, Morten Alhede, Mette Eline Skindersoe, Thomas Bovbjerg Rasmussen, Karlheinz Friedrich, Friedrich Uthe, et al. Ajoene, a sulfur-rich molecule from garlic, inhibits genes controlled by quorum sensing. *Antimicrobial agents and chemotherapy*, 56(5):2314–2325, 2012.

[26] July Fong, Mingjun Yuan, Tim Holm Jakobsen, Kim T Mortensen, May Margarette Salido Delos Santos, Song Lin Chua, Liang Yang, Choon Hong Tan, Thomas E Nielsen, and Michael Givskov. Disulfide bond-containing ajoene analogues as novel quorum sensing inhibitors of pseudomonas aeruginosa. *Journal of medicinal chemistry*, 60(1):215–227, 2016.

[27] Satoshi Tsuneda, Hirotoshi Aikawa, Hiroshi Hayashi, Atsushi Yuasa, and Akira Hirata. Extracellular polymeric substances responsible for bacterial adhesion onto solid surface. *FEMS microbiology letters*, 223(2):287–292, 2003.

[28] Hans-Curt Flemming and Jost Wingender. The biofilm matrix. *Nature Reviews Microbiology*, 8(9):623–633, 2010.

[29] Carla CCR de Carvalho and M Manuela R da Fonseca. Principal component analysis applied to bacterial cell behaviour in the presence of organic solvents. *Biocatalysis and Biotransformation*, 22(3):203–214, 2004.

[30] Morten Ernebjerg and Roy Kishony. Distinct growth strategies of soil bacteria as revealed by large-scale colony tracking. *Applied and environmental microbiology*, 78(5):1345–1352, 2012.

[31] Gary Dorken, Gail P Ferguson, Chris E French, and Wilson CK Poon. Aggregation by depletion attraction in cultures of bacteria producing exopolysaccharide. *Journal of The Royal Society Interface*, 9(77):3490–3502, 2012.

[32] Su Chuen Chew, Binu Kundukad, Thomas Seviour, Johan RC van der Maarel, Liang Yang, Scott A Rice, Patrick Doyle, and Staffan Kjelleberg. Dynamic remodeling of microbial biofilms by functionally distinct exopolysaccharides. *MBio*, 5(4):e01536–14, 2014.

[33] Laurent A Lardon, Brian V Merkey, Sónia Martins, Andreas Dötsch, Cristian Picioreanu, Jan-Ulrich Kreft, and Barth F Smets. idynomics: next-generation individual-based modelling of biofilms. *Environmental Microbiology*, 13(9):2416–2434, 2011.

[34] Sara Mitri, João B Xavier, and Kevin R Foster. Social evolution in multispecies biofilms. *Proceedings of the National Academy of Sciences*, 108(Supplement 2):10839–10846, 2011.

[35] Jacob G Malone. Role of small colony variants in persistence of pseudomonas aeruginosa infections in cystic fibrosis lungs. *Infection and drug resistance*, 8:237, 2015.

[36] Henry A Fremont. Activated sludge treatment, March 17 1981. US Patent 4,256,630.

[37] George Tchobanoglous and Franklin L Burton. Wastewater engineering. *Management*, 7:1–4, 1991.

[38] Xiaohui Wang, Xianghua Wen, Craig Criddle, George Wells, Jie Zhang, and Yin Zhao. Community analysis of ammonia-oxidizing bacteria in activated sludge of eight wastewater treatment systems. *Journal of Environmental Sciences*, 22(4):627–634, 2010.

[39] Andreas Schramm, Dirk de Beer, Michael Wagner, and Rudolf Amann. Identification and activities in situ of nitrosospiraand nitrospira spp. as dominant populations in a nitrifying fluidized bed reactor. *Applied and environmental microbiology*, 64(9):3480–3485, 1998.

[40] Sofia Andersson. Characterization of bacterial biofilms for wastewater treatment. 2009.

[41] J-M Monier and SE Lindow. Frequency, size, and localization of bacterial aggregates on bean leaf surfaces. *Applied and environmental microbiology*, 70(1):346–355, 2004.

[42] Ece Karatan and Paula Watnick. Signals, regulatory networks, and materials that build and break bacterial biofilms. *Microbiology and Molecular Biology Reviews*, 73(2):310–347, 2009.

[43] M-F Dignac, V Urbain, D Rybacki, A Bruchet, D Snidaro, and P Scribe. Chemical description of extracellular polymers: implication on activated sludge floc structure. *Water Science and Technology*, 38(8):45–53, 1998.

[44] Cristiano Nicolella, Mark CM van Loosdrecht, and Sef J Heijnen. Particle-based biofilm reactor technology. *Trends in Biotechnology*, 18(7):312–320, 2000.

[45] Tian C Zhang and Paul L Bishop. Density, porosity, and pore structure of biofilms. *Water Research*, 28(11):2267–2277, 1994.

[46] Maysam Sodagari, Hua Wang, Bi-min Zhang Newby, and Lu-Kwang Ju. Effect of rhamnolipids on initial attachment of bacteria on glass and octadecyltrichlorosilane-modified glass. *Colloids and Surfaces B: Biointerfaces*, 103:121–128, 2013.

[47] WG Characklis. Bioengineering report: fouling biofilm development: a process analysis. *Biotechnology and Bioengineering*, 23(9):1923–1960, 1981.

[48] Diane McDougald, Scott A Rice, Nicolas Barraud, Peter D Steinberg, and Staffan Kjelleberg. Should we stay or should we go: mechanisms and ecological consequences for biofilm dispersal. *Nature Reviews Microbiology*, 10(1):39–50, 2012.

[49] Don Monroe. Looking for chinks in the armor of bacterial biofilms. *PLoS biology*, 5(11), 2007.

[50] Philip S Stewart and Michael J Franklin. Physiological heterogeneity in biofilms. *Nature Reviews Microbiology*, 6(3):199–210, 2008.

[51] Konstantinos P Koutsoumanis and Alexandra Lianou. Stochasticity in colonial growth dynamics of individual bacterial cells. *Applied and environmental microbiology*, 79(7):2294–2301, 2013.

[52] David S Holmes and Michael Quigley. A rapid boiling method for the preparation of bacterial plasmids. *Analytical biochemistry*, 114(1):193–197, 1981.

[53] Fred E Hahn. Modes of action of antimicrobial agents. In *Medicinal Chemistry*, pages 1–19. Springer, 1977.

[54] David Davies. Understanding biofilm resistance to antibacterial agents. *Nature reviews Drug discovery*, 2(2):114–122, 2003.

[55] Rodney M Donlan. Biofilms and device-associated infections. *Emerging infectious diseases*, 7(2):277, 2001.

[56] CR Kokare, S Chakraborty, AN Khopade, and KR Mahadik. Biofilm: Importance and applications. *Indian Journal of Biotechnology*, 8(2):159–168, 2009.

[57] Vinay Kumar, Abul K Abbas, and Jon C Aster. *Robbins basic pathology*. Elsevier Health Sciences, 2012.

[58] Xianming Shi and Xinna Zhu. Biofilm formation and food safety in food industries. *Trends in Food Science & Technology*, 20(9):407–413, 2009.

[59] Kwang Y Kim and Joseph F Frank. Effect of nutrients on biofilm formation by listeria monocytogenes on stainless steel. *Journal of Food Protection®*, 58(1):24–28, 1995.

[60] Youssef Salama, Mohammed Chennaoui, Aboubacar Sylla, Mohammed Mountadar, Mohammed Rihani, and Omar Assobhei. Characterization, structure, and function of extracellular polymeric substances (eps) of microbial biofilm in biological wastewater treatment systems: a review. *Desalination and Water Treatment*, pages 1–18, 2015.

[61] TT More, JSS Yadav, S Yan, RD Tyagi, and RY Surampalli. Extracellular polymeric substances of bacteria and their potential environmental applications. *Journal of environmental management*, 144:1–25, 2014.

[62] Christian Mayer, Ralf Moritz, Carolin Kirschner, Werner Borchard, Ralf Maibaum, Jost Wingender, and Hans-Curt Flemming. The role of intermolecular interactions: studies on model systems for bacterial biofilms. *International journal of biological macromolecules*, 26(1):3–16, 1999.

[63] Guo-Ping Sheng, Han-Qing Yu, and Xiao-Yan Li. Extracellular polymeric substances (eps) of microbial aggregates in biological wastewater treatment systems: a review. *Biotechnology advances*, 28(6):882–894, 2010.

[64] Davide Marenduzzo, Kieran Finan, and Peter R Cook. The depletion attraction: an underappreciated force driving cellular organization. *The Journal of cell biology*, 175(5):681–686, 2006.

[65] Xiaoqi Zhang and Paul L Bishop. Biodegradability of biofilm extracellular polymeric substances. *Chemosphere*, 50(1):63–69, 2003.

[66] R Späth, H-C Flemming, and S Wuertz. Sorption properties of biofilms. *Water Science and Technology*, 37(4):207–210, 1998.

[67] Daniel J. Wozniak, Timna J. O. Wyckoff, Melissa Starkey, Rebecca Keyser, Parastoo Azadi, George A. O'Toole, and Matthew R. Parsek. Alginate is not a significant component of the extracellular polysaccharide matrix of pa14 and pao1 pseudomonas aeruginosa biofilms. *Proceedings of the National Academy of Sciences*, 100(13):7907–7912, 2003.

[68] Pierre Guyon, Annik Petit, Jacques Tempe, and Yves Dessaux. Transformed plants producing opines specifically promote growth of opine-degrading agrobacteria. *MOLECULAR PLANT MICROBE INTERACTIONS*, 6:92–92, 1993.

[69] Steven D Allison and Julie D Jastrow. Activities of extracellular enzymes in physically isolated fractions of restored grassland soils. *Soil Biology and Biochemistry*, 38(11):3245–3256, 2006.

[70] Jirí Chaloupka. *Extracellular enzymes of microorganisms*. Springer Science & Business Media, 2012.

[71] Melissa B Miller and Bonnie L Bassler. Quorum sensing in bacteria. *Annual Reviews in Microbiology*, 55(1):165–199, 2001.

[72] Jan-Willem Veening, Oleg A Igoshin, Robyn T Eijlander, Reindert Nijland, Leendert W Hamoen, and Oscar P Kuipers. Transient heterogeneity in extracellular protease production by bacillus subtilis. *Molecular systems biology*, 4(1):184, 2008.

[73] Martin Ackermann. A functional perspective on phenotypic heterogeneity in microorganisms. *Nature Reviews Microbiology*, 13(8):497–508, 2015.

[74] Martin E Kolewe, Michael A Henson, and Susan C Roberts. Characterization of aggregate size in taxus suspension cell culture. *Plant cell reports*, 29(5):485–494, 2010.

[75] Holger Daims, Sebastian Lücker, and Michael Wagner. Daime, a novel image analysis program for microbial ecology and biofilm research. *Environmental microbiology*, 8(2):200–213, 2006.

[76] J-M Monier and SE Lindow. Differential survival of solitary and aggregated bacterial cells promotes aggregate formation on leaf surfaces. *Proceedings of the National Academy of Sciences*, 100(26):15977–15982, 2003.

[77] Blaženka Kos, Jagoda Šušković, Snježana Vuković, Miljenko Šimpraga, Jadranka Frece, and Srećko Matošić. Adhesion and aggregation ability of probiotic strain lactobacillus acidophilus m92. *Journal of applied microbiology*, 94(6):981–987, 2003.

[78] ELLIS E Golub, JOSEPH Cheruka, B Boosz, C Davis, and D Malamud. A comparison of bacterial aggregation induced by saliva, lysozyme, and zinc. *Infection and immunity*, 48(1):204–210, 1985.

[79] Jacob G Malone, Tina Jaeger, Christian Spangler, Daniel Ritz, Anne Spang, Cécile Arrieumerlou, Volkhard Kaever, Regine Landmann, and Urs Jenal. Yfibnr mediates cyclic di-gmp dependent small colony variant formation and persistence in pseudomonas aeruginosa. *PLoS Pathog*, 6(3):e1000804, 2010.

[80] Jan-Ulrich Kreft, Ginger Booth, and Julian WT Wimpenny. Bacsim, a simulator for individual-based modelling of bacterial colony growth. *Microbiology*, 144(12):3275–3287, 1998.

[81] Kenneth Williamson and Perry L McCarty. A model of substrate utilization by bacterial films. *Journal (Water Pollution Control Federation)*, pages 9–24, 1976.

[82] Harald Horn and Susanne Lackner. Modeling of biofilm systems: a review. In *Productive Biofilms*, pages 53–76. Springer, 2014.

[83] Makram T Suidan, Joseph RV Flora, Pratim Biswas, and Gregory D Sayles. Optimization modelling of anaerobic biofilm reactors. *Water Science and Technology*, 30(12):347–355, 1994.

[84] Nicholas Paul Harris and GS Hansford. A study of substrate removal in a microbial film reactor. *Water Research*, 10(11):935–943, 1976.

[85] HJ Eberl, MCM van Loosdrecht, E Morgenroth, DR Noguera, J Perez, C Picioreanu, Bruce E Rittmann, AO Schwarz, and O Wanner. Modelling a spa-

tially heterogeneous biofilm and the bulk fluid: Selected results from benchmark problem 2(bm 2). *Water Science & Technology*, 49(11):155–162, 2004.

[86] Herman J Eberl, David F Parker, and Mark Van Loosdrecht. A new deterministic spatio-temporal continuum model for biofilm development. *Computational and Mathematical Methods in Medicine*, 3(3):161–175, 2001.

[87] Harald Horn and Dietmar C Hempel. Growth and decay in an auto-/heterotrophic biofilm. *Water Research*, 31(9):2243–2252, 1997.

[88] Ravindra Duddu, David L Chopp, and Brian Moran. A two-dimensional continuum model of biofilm growth incorporating fluid flow and shear stress based detachment. *Biotechnology and bioengineering*, 103(1):92–104, 2009.

[89] James N Wilking, Thomas E Angelini, Agnese Seminara, Michael P Brenner, and David A Weitz. Biofilms as complex fluids. *MRS bulletin*, 36(05):385–391, 2011.

[90] NG Cogan. Two-fluid model of biofilm disinfection. *Bulletin of mathematical biology*, 70(3):800–819, 2008.

[91] O Wanner and E Morgenroth. Biofilm modeling with aquasim. *Water Science & Technology*, 49(11):137–144, 2004.

[92] Cristian Picioreanu, Mark CM van Loosdrecht, Joseph J Heijnen, et al. A new combined differential-discrete cellular automaton approach for biofilm modeling: application for growth in gel beads. *Biotechnology and bioengineering*, 57(6):718–731, 1998.

[93] Magnus G Fagerlind, Jeremy S Webb, Nicolas Barraud, Diane McDougald, Andreas Jansson, Patric Nilsson, Mikael Harlén, Staffan Kjelleberg, and Scott A Rice. Dynamic modelling of cell death during biofilm development. *Journal of theoretical biology*, 295:23–36, 2012.

[94] Leah R Johnson. Microcolony and biofilm formation as a survival strategy for bacteria. *Journal of Theoretical Biology*, 251(1):24–34, 2008.

[95] Brian V Merkey, Laurent A Lardon, Jose M Seoane, Jan-Ulrich Kreft, and Barth F Smets. Growth dependence of conjugation explains limited plasmid invasion in biofilms: an individual-based modelling study. *Environmental microbiology*, 13(9):2435–2452, 2011.

[96] Silja Heilmann, Kim Sneppen, and Sandeep Krishna. Coexistence of phage and bacteria on the boundary of self-organized refuges. *Proceedings of the National Academy of Sciences*, 109(31):12828–12833, 2012.

[97] DA Head. Linear surface roughness growth and flow smoothening in a three-dimensional biofilm model. *Physical Review E*, 88(3):032702, 2013.

[98] Gavin Melaugh, Jaime Hutchison, Kasper Nørskov Kragh, Yasuhiko Irie, Aled Roberts, Thomas Bjarnsholt, Steve P Diggle, Vernita Gordon, and Rosalind J Allen. Shaping the growth behaviour of bacterial aggregates in biofilms. *arXiv preprint arXiv:1506.08168*, 2015.

[99] Uri Wilensky. {NetLogo}. 1999.

[100] Matthew B Biggs and Jason A Papin. Novel multiscale modeling tool applied to pseudomonas aeruginosa biofilm formation. *PloS one*, 8(10):e78011, 2013.

[101] Thomas E Gorochowski, Antoni Matyjaszkiewicz, Thomas Todd, Neeraj Oak, Kira Kowalska, Stephen Reid, Krasimira T Tsaneva-Atanasova, Nigel J Savery, Claire S Grierson, and Mario di Bernardo. Bsim: an agent-based tool for modeling bacterial populations in systems and synthetic biology. *PloS one*, 7(8):e42790, 2012.

[102] David W Adams and Jeff Errington. Bacterial cell division: assembly, maintenance and disassembly of the z ring. *Nature Reviews Microbiology*, 7(9):642–653, 2009.

[103] DW Tempest, John Robert Norris, and MH Richmond. *Dynamics of microbial growth*. John Wiley and Sons, 1978.

[104] Stephen Cooper. Bacterial growth and division. *Encyclopedia of Molecular Cell Biology and Molecular Medicine*, 2006.

[105] GC Okpokwasili and CO Nweke. Microbial growth and substrate utilization kinetics. 2006.

[106] Yunhu Tan, Zhi-Xin Wang, and Kevin C Marshall. Modeling substrate inhibition of microbial growth. *Biotechnology and bioengineering*, 52(5):602–608, 1996.

[107] Iqbal Kabir Jahid, Na-Young Lee, Anna Kim, and Sang-Do Ha. Influence of glucose concentrations on biofilm formation, motility, exoprotease production, and quorum sensing in aeromonas hydrophila. *Journal of Food Protection®*, 76(2):239–247, 2013.

[108] Astha Agarwal and Amita Jain. Glucose & sodium chloride induced biofilm production & ica operon in clinical isolates of staphylococci. *The Indian journal of medical research*, 138(2):262, 2013.

[109] Omar M El-Halfawy and Miguel A Valvano. Chemical communication of antibiotic resistance by a highly resistant subpopulation of bacterial cells. *PloS one*, 8(7):e68874, 2013.

[110] Arthur Prindle, Jintao Liu, Munehiro Asally, San Ly, Jordi Garcia-Ojalvo, and Gürol M Süel. Ion channels enable electrical communication in bacterial communities. *Nature*, 527(7576):59–63, 2015.

[111] Alexander R Horswill, Paul Stoodley, Philip S Stewart, and Matthew R Parsek. The effect of the chemical, biological, and physical environment on quorum sensing in structured microbial communities. *Analytical and bioanalytical chemistry*, 387(2):371–380, 2007.

[112] Christopher M Waters and Bonnie L Bassler. Quorum sensing: cell-to-cell communication in bacteria. *Annu. Rev. Cell Dev. Biol.*, 21:319–346, 2005.

[113] Ann M Stevens and EP Greenberg. Quorum sensing in vibrio fischeri: essential elements for activation of the luminescence genes. *Journal of Bacteriology*, 179(2):557–562, 1997.

[114] Everett C Pesci, James P Pearson, Patrick C Seed, and Barbara H Iglewski. Regulation of las and rhl quorum sensing in pseudomonas aeruginosa. *Journal of bacteriology*, 179(10):3127–3132, 1997.

[115] Roger S Smith, Sarah G Harris, Richard Phipps, and Barbara Iglewski. The pseudomonas aeruginosa quorum-sensing molecule n-(3-oxododecanoyl) homoserine lactone contributes to virulence and induces inflammation in vivo. *Journal of bacteriology*, 184(4):1132–1139, 2002.

[116] Jasmine Lee and Lianhui Zhang. The hierarchy quorum sensing network in pseudomonas aeruginosa. *Protein & cell*, 6(1):26–41, 2015.

[117] Martin Schuster, C Phoebe Lostroh, Tomoo Ogi, and EP Greenberg. Identification, timing, and signal specificity of pseudomonas aeruginosa quorum-controlled genes: a transcriptome analysis. *Journal of bacteriology*, 185(7):2066–2079, 2003.

[118] Arul Jayaraman and Thomas K Wood. Bacterial quorum sensing: signals, circuits, and implications for biofilms and disease. *Annu. Rev. Biomed. Eng.*, 10:145–167, 2008.

[119] Ty A Gould, Jake Herman, Jessica Krank, Robert C Murphy, and Mair EA Churchill. Specificity of acyl-homoserine lactone synthases examined by mass spectrometry. *Journal of bacteriology*, 188(2):773–783, 2006.

[120] Steven T Rutherford and Bonnie L Bassler. Bacterial quorum sensing: its role in virulence and possibilities for its control. *Cold Spring Harbor Perspectives in Medicine*, 2(11):a012427, 2012.

[121] Kathrin Riedel, Morten Hentzer, Otto Geisenberger, Birgit Huber, Anette Steidle, Hong Wu, Niels Høiby, Michael Givskov, Søren Molin, and Leo

Eberl. N-acylhomoserine-lactone-mediated communication between pseudomonas aeruginosa and burkholderia cepacia in mixed biofilms. *Microbiology*, 147(12):3249–3262, 2001.

[122] Neville Firth, Peter D Fink, Luke Johnson, and Ronald A Skurray. A lipoprotein signal peptide encoded by the staphylococcal conjugative plasmid psk41 exhibits an activity resembling that of enterococcus faecalis pheromone cad1. *Journal of bacteriology*, 176(18):5871–5873, 1994.

[123] Michael G Surette, Melissa B Miller, and Bonnie L Bassler. Quorum sensing in escherichia coli, salmonella typhimurium, and vibrio harveyi: a new family of genes responsible for autoinducer production. *Proceedings of the National Academy of Sciences*, 96(4):1639–1644, 1999.

[124] Roderick McNab, Suzannah K Ford, Azza El-Sabaeny, Bruno Barbieri, Guy S Cook, and Richard J Lamont. Luxs-based signaling in streptococcus gordonii: autoinducer 2 controls carbohydrate metabolism and biofilm formation with porphyromonas gingivalis. *Journal of Bacteriology*, 185(1):274–284, 2003.

[125] HEIDI B Kaplan and EP Greenberg. Diffusion of autoinducer is involved in regulation of the vibrio fischeri luminescence system. *Journal of bacteriology*, 163(3):1210–1214, 1985.

[126] Jack D Dockery and James P Keener. A mathematical model for quorum sensing in pseudomonas aeruginosa. *Bulletin of mathematical biology*, 63(1):95–116, 2001.

[127] Marc Weber and Javier Buceta. Dynamics of the quorum sensing switch: stochastic and non-stationary effects. *BMC systems biology*, 7(1):1, 2013.

[128] AB Goryachev, DJ Toh, and T Lee. Systems analysis of a quorum sensing network: design constraints imposed by the functional requirements, network topology and kinetic constants. *Biosystems*, 83(2):178–187, 2006.

[129] Laura R Hmelo and Benjamin AS Van Mooy. Kinetic constraints on acylated homoserine lactone-based quorum sensing in marine environments. 2009.

[130] Agnes Fekete, Christina Kuttler, Michael Rothballer, Burkhard A Hense, Doreen Fischer, Katharina Buddrus-Schiemann, Marianna Lucio, Johannes Müller, Philippe Schmitt-Kopplin, and Anton Hartmann. Dynamic regulation of n-acyl-homoserine lactone production and degradation in pseudomonas putida isof. *FEMS microbiology ecology*, 72(1):22–34, 2010.

[131] Gunnar F Kaufmann, Rafaella Sartorio, Sang-Hyeup Lee, Claude J Rogers, Michael M Meijler, Jason A Moss, Bruce Clapham, Andrew P Brogan, Tobin J Dickerson, and Kim D Janda. Revisiting quorum sensing: discovery of additional chemical and biological functions for 3-oxo-n-acylhomoserine lactones. *Proceedings of the National Academy of Sciences of the United States of America*, 102(2):309–314, 2005.

[132] Subhayu Basu, Yoram Gerchman, Cynthia H Collins, Frances H Arnold, and Ron Weiss. A synthetic multicellular system for programmed pattern formation. *Nature*, 434(7037):1130–1134, 2005.

[133] Shu-Wen Teng, Yufang Wang, Kimberly C Tu, Tao Long, Pankaj Mehta, Ned S Wingreen, Bonnie L Bassler, and NP Ong. Measurement of the copy number of the master quorum-sensing regulator of a bacterial cell. *Biophysical journal*, 98(9):2024–2031, 2010.

[134] Wiep Klaas Smits, Jan-Willem Veening, and Oscar P Kuipers. Phenotypic variation and bistable switching in bacteria. In *Bacterial Physiology*, pages 339–365. Springer, 2008.

[135] Peter T McKenney, Adam Driks, and Patrick Eichenberger. The bacillus subtilis endospore: assembly and functions of the multilayered coat. *Nature Reviews Microbiology*, 11(1):33–44, 2013.

[136] Daniel B Kearns and Richard Losick. Cell population heterogeneity during growth of bacillus subtilis. *Genes & development*, 19(24):3083–3094, 2005.

[137] J Vidal-Mas, O Resina-Pelfort, E Haba, J Comas, A Manresa, and J Vives-Rego. Rapid flow cytometry–nile red assessment of pha cellular content and heterogeneity in cultures of pseudomonas aeruginosa 47t2 (ncib 40044) grown in waste frying oil. *Antonie Van Leeuwenhoek*, 80(1):57–63, 2001.

[138] Francoise Russo-Marie, Mario Roederer, Brian Sager, Leonard A Herzenberg, and Dale Kaiser. Beta-galactosidase activity in single differentiating bacterial cells. *Proceedings of the National Academy of Sciences*, 90(17):8194–8198, 1993.

[139] AEJ Van Merode, DC Pothoven, HC Van Der Mei, HJ Busscher, and BP Krom. Surface charge influences enterococcal prevalence in mixed-species biofilms. *Journal of applied microbiology*, 102(5):1254–1260, 2007.

[140] Annet EJ Van Merode, Henny C Van der Mei, Henk J Busscher, Karola Waar, and Bastiaan P Krom. Enterococcus faecalis strains show culture heterogeneity in cell surface charge. *Microbiology*, 152(3):807–814, 2006.

[141] Muhammad Tariq, Chissa Bruijs, Jan Kok, and Bastiaan P Krom. Link between culture zeta potential homogeneity and ebp in enterococcus faecalis. *Applied and environmental microbiology*, 78(7):2282–2288, 2012.

[142] Ido Golding, Johan Paulsson, Scott M Zawilski, and Edward C Cox. Real-time kinetics of gene activity in individual bacteria. *Cell*, 123(6):1025–1036, 2005.

[143] Peter S Swain, Michael B Elowitz, and Eric D Siggia. Intrinsic and extrinsic contributions to stochasticity in gene expression. *Proceedings of the National Academy of Sciences*, 99(20):12795–12800, 2002.

[144] Vipin Chandra Kalia. Quorum sensing inhibitors: an overview. *Biotechnology advances*, 31(2):224–245, 2013.

[145] Lin Feng, Zhuoying Wu, and Xin Yu. Quorum sensing in water and wastewater treatment biofilms. *Journal of Environmental Biology*, 34(2 suppl):437, 2013.

[146] M Worth Calfee, James P Coleman, and Everett C Pesci. Interference with pseudomonas quinolone signal synthesis inhibits virulence factor expression by pseudomonas aeruginosa. *Proceedings of the National Academy of Sciences*, 98(20):11633–11637, 2001.

[147] Margaret E Teasdale, Jiayuan Liu, Joselynn Wallace, Fatemeh Akhlaghi, and David C Rowley. Secondary metabolites produced by the marine bacterium halobacillus salinus that inhibit quorum sensing-controlled phenotypes in gram-negative bacteria. *Applied and environmental microbiology*, 75(3):567–572, 2009.

[148] Hui Fan, Yihu Dong, Donghui Wu, Matthew W Bowler, Lianhui Zhang, and Haiwei Song. Qsia disrupts lasr dimerization in antiactivation of bacterial quorum sensing. *Proceedings of the National Academy of Sciences*, 110(51):20765–20770, 2013.

[149] Michael Manefield, Thomas Bovbjerg Rasmussen, Morten Henzter, Jens Bo Andersen, Peter Steinberg, Staffan Kjelleberg, and Michael Givskov. Halogenated furanones inhibit quorum sensing through accelerated luxr turnover. *Microbiology*, 148(4):1119–1127, 2002.

[150] Elisabeth Kay, Bérénice Humair, Valérie Dénervaud, Kathrin Riedel, Stéphanie Spahr, Leo Eberl, Claudio Valverde, and Dieter Haas. Two gaca-dependent small rnas modulate the quorum-sensing response in pseudomonas aeruginosa. *Journal of bacteriology*, 188(16):6026–6033, 2006.

[151] Ursula N Broder, Tina Jaeger, and Urs Jenal. Lads is a calcium-responsive kinase that induces acute-to-chronic virulence switch in pseudomonas aeruginosa. *Nature microbiology*, 2:16184, 2016.

[152] Farren J Isaacs, Jeff Hasty, Charles R Cantor, and James J Collins. Prediction and measurement of an autoregulatory genetic module. *Proceedings of the National Academy of Sciences*, 100(13):7714–7719, 2003.

[153] James E Ferrell. Self-perpetuating states in signal transduction: positive feedback, double-negative feedback and bistability. *Current opinion in cell biology*, 14(2):140–148, 2002.

[154] Sara Hooshangi, Stephan Thiberge, and Ron Weiss. Ultrasensitivity and noise propagation in a synthetic transcriptional cascade. *Proceedings of the National Academy of Sciences of the United States of America*, 102(10):3581–3586, 2005.

[155] Ertugrul M Ozbudak, Mukund Thattai, Iren Kurtser, Alan D Grossman, and Alexander Van Oudenaarden. Regulation of noise in the expression of a single gene. *Nature genetics*, 31(1):69–73, 2002.

[156] Mads Kærn, Timothy C Elston, William J Blake, and James J Collins. Stochasticity in gene expression: from theories to phenotypes. *Nature Reviews Genetics*, 6(6):451–464, 2005.

[157] Sally James, Patric Nilsson, Geoffrey James, Staffan Kjelleberg, and Torbjörn Fagerström. Luminescence control in the marine bacterium vibrio fischeri: an analysis of the dynamics of lux regulation. *Journal of molecular biology*, 296(4):1127–1137, 2000.

[158] Wai-Leung Ng and Bonnie L Bassler. Bacterial quorum-sensing network architectures. *Annual review of genetics*, 43:197, 2009.

[159] Anand Pai and Lingchong You. Optimal tuning of bacterial sensing potential. *Molecular systems biology*, 5(1):286, 2009.

[160] Suvi Flagan, Weng-Ki Ching, and Jared R Leadbetter. Arthrobacter strain vai-a utilizes acyl-homoserine lactone inactivation products and stimulates quo-

rum signal biodegradation by variovorax paradoxus. *Applied and environmental microbiology*, 69(2):909–916, 2003.

[161] Lorenzo Pasotti, Susanna Zucca, Michela Casanova, Giuseppina Micoli, Maria Gabriella Cusella De Angelis, Paolo Magni, et al. Half-life measurements of chemical inducers for recombinant gene expression. *Journal of biological engineering*, 8(1):1, 2014.

[162] Juan M Pedraza and Alexander van Oudenaarden. Noise propagation in gene networks. *Science*, 307(5717):1965–1969, 2005.

[163] Daniel J Sayut, Pavan Kumar Reddy Kambam, and Lianhong Sun. Noise and kinetics of luxr positive feedback loops. *Biochemical and biophysical research communications*, 363(3):667–673, 2007.

[164] Tae-Hyuk Ahn, Yang Cao, and Layne T Watson. Stochastic simulation algorithms for chemical reactions. In *BIOCOMP*, pages 431–436, 2008.

[165] Lihui Feng, Steven T Rutherford, Kai Papenfort, John D Bagert, Julia C van Kessel, David A Tirrell, Ned S Wingreen, and Bonnie L Bassler. A qrr noncoding rna deploys four different regulatory mechanisms to optimize quorum-sensing dynamics. *Cell*, 160(1):228–240, 2015.

[166] D Herbert, R Elsworth, and RC Telling. The continuous culture of bacteria; a theoretical and experimental study. *Microbiology*, 14(3):601–622, 1956.

[167] Philippe Régnier and Cecilia Maria Arraiano. Degradation of mrna in bacteria: emergence of ubiquitous features. *Bioessays*, 22(3):235–244, 2000.

[168] Reinhard Rauhut and Gabriele Klug. mrna degradation in bacteria. *FEMS microbiology reviews*, 23(3):353–370, 1999.

[169] Kamalendu Nath and Arthur L Koch. Protein degradation in escherichia coli ii. strain differences in the degradation of protein and nucleic acid resulting from starvation. *Journal of Biological Chemistry*, 246(22):6956–6967, 1971.

[170] Ertugrul M Ozbudak, Mukund Thattai, Han N Lim, Boris I Shraiman, and Alexander Van Oudenaarden. Multistability in the lactose utilization network of escherichia coli. *Nature*, 427(6976):737–740, 2004.

[171] Jonathan A Bernstein, Arkady B Khodursky, Pei-Hsun Lin, Sue Lin-Chao, and Stanley N Cohen. Global analysis of mrna decay and abundance in escherichia coli at single-gene resolution using two-color fluorescent dna microarrays. *Proceedings of the National Academy of Sciences*, 99(15):9697–9702, 2002.

[172] Samuel O Skinner, Leonardo A Sepúlveda, Heng Xu, and Ido Golding. Measuring mrna copy number in individual escherichia coli cells using single-molecule fluorescent in situ hybridization. *Nature protocols*, 8(6):1100–1113, 2013.

[173] Artémis Llamosi, Andres M Gonzalez-Vargas, Cristian Versari, Eugenio Cinquemani, Giancarlo Ferrari-Trecate, Pascal Hersen, and Gregory Batt. What population reveals about individual cell identity: Single-cell parameter estimation of models of gene expression in yeast. *PLoS Comput Biol*, 12(2):e1004706, 2016.

[174] Sui Huang. Non-genetic heterogeneity of cells in development: more than just noise. *Development*, 136(23):3853–3862, 2009.

[175] Zhonghua Zhang, Yaohong Suo, and Juan Zhang. Stability and sensitive analysis of a model with delay quorum sensing. In *Abstract and Applied Analysis*, volume 2015. Hindawi Publishing Corporation, 2015.

[176] Joshua D Shrout, David L Chopp, Collin L Just, Morten Hentzer, Michael Givskov, and Matthew R Parsek. The impact of quorum sensing and swarming motility on pseudomonas aeruginosa biofilm formation is nutritionally conditional. *Molecular microbiology*, 62(5):1264–1277, 2006.

[177] Jeremy M Yarwood and Patrick M Schlievert. Quorum sensing in staphylococcus infections. *The Journal of clinical investigation*, 112(11):1620–1625, 2003.

[178] Brian K Hammer and Bonnie L Bassler. Quorum sensing controls biofilm formation in vibrio cholerae. *Molecular microbiology*, 50(1):101–104, 2003.

[179] Diby Paul, Young Sam Kim, Kannan Ponnusamy, and Ji Hyang Kweon. Application of quorum quenching to inhibit biofilm formation. *Environmental Engineering Science*, 26(8):1319–1324, 2009.

[180] Yi-Hu Dong, Lian-Hui Wang, and Lian-Hui Zhang. Quorum-quenching microbial infections: mechanisms and implications. *Philosophical Transactions of the Royal Society of London B: Biological Sciences*, 362(1483):1201–1211, 2007.

[181] Anne M Albus, Everett C Pesci, Laura J Runyen-Janecky, SE West, and Barbara H Iglewski. Vfr controls quorum sensing in pseudomonas aeruginosa. *Journal of Bacteriology*, 179(12):3928–3935, 1997.

[182] Pattarachai Kiratisin, Kenneth D Tucker, and Luciano Passador. Lasr, a transcriptional activator of pseudomonas aeruginosa virulence genes, functions as a multimer. *Journal of bacteriology*, 184(17):4912–4919, 2002.

[183] Magnus G Fagerlind, Scott A Rice, Patric Nilsson, Mikael Harlén, Sally James, Timothy Charlton, and Staffan Kjelleberg. The role of regulators in the expression of quorum-sensing signals in pseudomonas aeruginosa. *Journal of molecular microbiology and biotechnology*, 6(2):88–100, 2004.

[184] Kai Papenfort and Bonnie L Bassler. Quorum sensing signal-response systems in gram-negative bacteria. *Nature Reviews Microbiology*, 14(9):576–588, 2016.

[185] P.aeruginosa. *Microwiki*, 2016.

[186] Pontus Melke, Patrik Sahlin, Andre Levchenko, and Henrik Jönsson. A cell-based model for quorum sensing in heterogeneous bacterial colonies. *PLoS Comput Biol*, 6(6):e1000819, 2010.

[187] S Loewe. The problem of synergism and antagonism of combined drugs. *Arzneimittelforschung*, 3:285–290, 1953.

[188] Athel Cornish-Bowden, Athel Cornish-Bowden, et al. Fundamentals of enzyme kinetics. 2012.

[189] Eric J Stewart, Richard Madden, Gregory Paul, and François Taddei. Aging and death in an organism that reproduces by morphologically symmetric division. *PLoS Biol*, 3(2):e45, 2005.

[190] Gisela Storz, Jörg Vogel, and Karen M Wassarman. Regulation by small rnas in bacteria: expanding frontiers. *Molecular cell*, 43(6):880–891, 2011.

[191] Ron Milo and Rob Phillips. *Cell biology by the numbers*. Garland Science, 2015.

[192] Su-Jin Park, Sun-Yang Park, Choong-Min Ryu, Seung-Hwan Park, Jung-Kee Lee, et al. The role of aiia, a quorum-quenching enzyme from bacillus thuringiensis, on the rhizosphere competence. *J. Microbiol. Biotechnol*, 18(9):1518–1521, 2008.

[193] L Friedman and R Kolter. Two genetic loci produce distinct carbohydrate-rich structural components of the pseudomonas aeruginosa biofilm matrix. *Journal of Bacteriology*, 186(14):4457–4465, 2004.

[194] L. Ma, M Conover, H. Lu, M. R. Parsek, K Bayles, and D. J. Wozniak. Assembly and development of the pseudomonas aeruginosa biofilm matrix. *Plos Pathogens*, 5(3):: e1000354., 2009.

[195] B. R. Borlee, A. D. Goldman, K Murakami, R Samudrala, D. J. Wozniak, and M. R. Parsek. Pseudomonas aeruginosa uses a cyclic-di-gmp-regulated

adhesin to reinforce the biofilm extracellular matrix. *Molecular Microbiology*, 75(4):827–842, 2010.

[196] Jason D Chambless and Philip S Stewart. A three-dimensional computer model analysis of three hypothetical biofilm detachment mechanisms. *Biotechnology and bioengineering*, 97(6):1573–1584, 2007.

[197] Haluk Beyenal, Suet Nee Chen, and Zbigniew Lewandowski. The double substrate growth kinetics of pseudomonas aeruginosa. *Enzyme and Microbial Technology*, 32(1):92–98, 2003.

[198] Lars R Bakken and Rolf A Olsen. Buoyant densities and dry-matter contents of microorganisms: conversion of a measured biovolume into biomass. *Applied and Environmental Microbiology*, 45(4):1188–1195, 1983.

[199] Silke Ehrich, Doris Behrens, Elena Lebedeva, Wolfgang Ludwig, and Eberhard Bock. A new obligately chemolithoautotrophic, nitrite-oxidizing bacterium, nitrospira moscoviensis sp. nov. and its phylogenetic relationship. *Archives of Microbiology*, 164(1):16–23, 1995.

[200] Nabil Mabrouk, Guillaume Deffuant, Tim Tolker-Nielsen, and Claude Lobry. Bacteria can form interconnected microcolonies when a self-excreted product reduces their surface motility: evidence from individual-based model simulations. *Theory in Biosciences*, 129(1):1–13, 2010.

[201] Ping Han and David M Bartels. Temperature dependence of oxygen diffusion in h 2 o and d 2 o. *The Journal of Physical Chemistry*, 100(13):5597–5602, 1996.

[202] Dong-Jin Kim and Sun-Hee Kim. Effect of nitrite concentration on the distribution and competition of nitrite-oxidizing bacteria in nitratation reactor systems and their kinetic characteristics. *Water research*, 40(5):887–894, 2006.

[203] David Al'bertovich Frank-Kamenetskii. *Diffusion and heat transfer in chemical kinetics*. Plenum Press, 1969.

[204] Susanne Häußler, Burkhard Tümmler, Hartmut Weißbrodt, Manfred Rohde, and Ivo Steinmetz. Small-colony variants of pseudomonas aeruginosa in cystic fibrosis. *Clinical infectious diseases*, 29(3):621–625, 1999.

[205] Jason W Hickman and Caroline S Harwood. Identification of fleq from pseudomonas aeruginosa as ac-di-gmp-responsive transcription factor. *Molecular microbiology*, 69(2):376–389, 2008.

[206] Melissa Starkey, Jason H Hickman, Luyan Ma, Niu Zhang, Susan De Long, Aaron Hinz, Sergio Palacios, Colin Manoil, Mary Jo Kirisits, Timothy D Starner, et al. Pseudomonas aeruginosa rugose small-colony variants have adaptations that likely promote persistence in the cystic fibrosis lung. *Journal of bacteriology*, 191(11):3492–3503, 2009.

[207] Enrique Hernández-Jiménez, Rosa del Campo, Victor Toledano, Maria Teresa Vallejo-Cremades, Aurora Muñoz, Carlota Largo, Francisco Arnalich, Francisco García-Rio, Carolina Cubillos-Zapata, and Eduardo López-Collazo. Biofilm vs. planktonic bacterial mode of growth: Which do human macrophages prefer? *Biochemical and biophysical research communications*, 441(4):947–952, 2013.

[208] Natalie Verstraeten, Kristien Braeken, Bachaspatimayum Debkumari, Maarten Fauvart, Jan Fransaer, Jan Vermant, and Jan Michiels. Living on a surface: swarming and biofilm formation. *Trends in microbiology*, 16(10):496–506, 2008.

[209] Song Lin Chua, Yang Liu, Joey Kuok Hoong Yam, Yicai Chen, Rebecca Munk Vejborg, Bryan Giin Chyuan Tan, Staffan Kjelleberg, Tim Tolker-Nielsen, Michael Givskov, and Liang Yang. Dispersed cells represent a distinct stage in the transition from bacterial biofilm to planktonic lifestyles. *Nature communications*, 5, 2014.

[210] Christopher Dombrowski, Luis Cisneros, Sunita Chatkaew, Raymond E Goldstein, and John O Kessler. Self-concentration and large-scale coherence in bacterial dynamics. *Physical Review Letters*, 93(9):098103, 2004.

[211] Douglas R Brumley, Kirsty Y Wan, Marco Polin, and Raymond E Goldstein. Flagellar synchronization through direct hydrodynamic interactions. *Elife*, 3:e02750, 2014.

[212] Maria Dienerowitz, Laura V Cowan, Graham M Gibson, Rebecca Hay, Miles J Padgett, and Vernon R Phoenix. Optically trapped bacteria pairs reveal discrete motile response to control aggregation upon cell–cell approach. *Current microbiology*, 69(5):669–674, 2014.

[213] Robert Großmann, Pawel Romanczuk, Markus Bär, and Lutz Schimansky-Geier. Vortex arrays and mesoscale turbulence of self-propelled particles. *Physical review letters*, 113(25):258104, 2014.

[214] Xiao Chen, Xu Dong, Avraham Be'er, Harry L Swinney, and HP Zhang. Scale-invariant correlations in dynamic bacterial clusters. *Physical review letters*, 108(14):148101, 2012.

[215] Tommaso Brotto, Jean-Baptiste Caussin, Eric Lauga, and Denis Bartolo. Hydrodynamics of confined active fluids. *Physical review letters*, 110(3):038101, 2013.

[216] Tsevi Beatus, Roy H Bar-Ziv, and Tsvi Tlusty. The physics of 2d microfluidic droplet ensembles. *Physics reports*, 516(3):103–145, 2012.

[217] Eva Kanso and Alan Cheng Hou Tsang. Pursuit and synchronization in hydrodynamic dipoles. *Journal of Nonlinear Science*, 25(5):1141–1152, 2015.

[218] Andrey Sokolov, Raymond E Goldstein, Felix I Feldchtein, and Igor S Aranson. Enhanced mixing and spatial instability in concentrated bacterial suspensions. *Physical Review E*, 80(3):031903, 2009.

[219] HP Zhang, Avraham Be'Er, Rachel S Smith, E-L Florin, and Harry L Swinney. Swarming dynamics in bacterial colonies. *EPL (Europhysics Letters)*, 87(4):48011, 2009.

[220] John G Kirkwood and Jacob Riseman. The intrinsic viscosities and diffusion constants of flexible macromolecules in solution. *The Journal of Chemical Physics*, 16(6):565–573, 1948.

[221] Horace Lamb. *Hydrodynamics*. Cambridge university press, 1932.